Assessment of structural diversity of β-amyloid with genetically engineered antibody fragments

---

Dissertation

zur Erlangung des akademischen Grades
doctor rerum naturalium (Dr. rer. nat.)

vorgelegt dem Rat der Biologisch-Pharmazeutischen Fakultät
der Friedrich-Schiller-Universität Jena

von M. Sc. Magdalena Bereza
geboren am 07. August 1980 in Warschau

---

1. Gutachter: Prof. Dr. Stephan Diekmann, Universität Jena, Deutschland

2. Gutachter: Prof. Dr. Marcus Fändrich, Universität Ulm, Deutschland

3. Gutachter: Prof. Dr. Vittorio Bellotti, Universität Pavia, Italy

Tag der öffentlichen Verteidigung / Rigorosum: 28. Januar 2013

Contents

Chapter 1

Introduction

1.1 Molecular basis of protein conformational diseases

1.1.1 Conformational diseases

Conformational diseases, also termed misfolding diseases, are associated with aberrant protein metabolism in terms of the aggregation and extracellular deposition of otherwise soluble proteins (Sunde and Blake 1998, Chiti and Dobson 2006). In these conditions amyloidogenic proteins escape the chaperon-assisted folding process and convert from their native conformational state into diverse structures (Dobson 2001, Maltsev et al. 2011). Misfolded proteins have an increased tendency to accumulate as thread-like, highly ordered aggregates called amyloid fibrils. Diseases associated with amyloid deposits are termed 'amyloidoses' (Table 1.1). Amyloidoses are generally classified according to the location of amyloid deposition. Hence, an amyloid occurring in one site or one type of tissue is associated with localised amyloid deposition, e.g., β-amyloid (Aβ), α-synuclein or prion protein. When an amyloid is distributed in multiple tissues or organs, usually outside the brain, like in case of transthyretin or β_2-microglobulin deposition, we speak of systemic amyloidosis (Westermark et al. 2007). What all amyloidoses have in common is the intra- or extracellular deposition of fibrillar material. Although polypeptide precursors of fibrils do not share sequence identity or structural homology, the resulted fibrils display features typical of amyloid.

According to the Nomenclature Committee of the International Society of Amyloidosis, amyloid fibrils are defined as 'an insoluble protein fibril that is deposited, mainly, in the extracellular spaces of organs and tissues as a result of a sequence of changes in protein folding that results in a condition known as amyloidosis' (Sipe et al. 2010). The features of fibrils include distinctive appearance in electron microscopy (EM), typical cross-β X-ray diffraction pattern, and binding of Congo red (CR) with a characteristic green birefringence (Westermark et al. 2005). For distinction purposes, synthetic protein fibrils displaying some

amyloid characteristics are being referred to as 'amyloid-like' fibrils (Sipe et al. 2010).

Table 1.1. Diseases associated with the amyloidogenic aggregation and deposition

Disease	Precursor polypeptide chain	Native structure
Alzheimer's disease	Aβ-protein precursor (AβPP)	*IUPC*
Spongiform encephalopathies	Prion protein	*IUPC* (residues 1–120) α-helical (residues 121–230)
Parkinson's disease	α-Synuclein	*IUPC*
Frontotemporal dementia with Parkinsonism	Tau	*IUPC*
Huntington's disease	Huntingtin	Mainly *IUPC*
British familial dementia	ABriPP	*IUPC*
Danish familial dementia	ADanPP	*IUPC*
Systemic AL amyloidosis	Ig light chains or fragments	All-β, Ig-like
Systemic AA amyloidosis	Serum amyloid A protein	All-α, unknown fold
Dialysis-related amyloidosis	β_2-microglobulin	*IUPC*
Medullary carcinoma of the thyroid	Calcitonin	*IUPC*
Finnish hereditary amyloidosis	Gelsolin	*IUPC*
Type II diabetes	Islet amyloid polypeptide	*IUPC*
Insulin-related amyloidosis	Insulin A Insulin B	All-α, insulin-like
Aortic medial amyloidosis	Lactadherin	Unknown
Lysozyme amyloidosis	Lysozyme	α+β, lysozyme fold
Icelandic hereditary cerebral amyloid angiopathy	Cystatin C	α+β, cystatin-like

IUPC: intrinsically unfolded polypeptide chain. Sources: Fändrich (2007), Chiti and Dobson (2006), Sunde and Blake (1998)

1.1.2 Onset and epidemiology of Alzheimer's disease

Alzheimer's disease (AD) has been first described by Alois Alzheimer in 1906. He reported presence of extracellular clumps ('senile plaques') and intracellular tangled bundles of fibres ('neurofibrillary tangles') in the *post-mortem* brain tissue of a woman who suffered from very severe cognitive impairment (Alzheimer 1906).

AD is nowadays the most prevalent cause of dementia, and one of the major health concerns of ageing societies (Jakob-Roetne and Jacobsen 2009). In 2005, the estimated number of people with AD was 24.3 millions. It is predicted that 42.3 millions will have developed AD symptoms by 2020, and 81.1 million will be afflicted by 2040 (Ferri et al.

2006). Currently, 10% of the individuals over 65 years, and 40% of 85 years old are estimated to be affected with AD (Morgan 2011).

Two forms of this neurodegenerative disease are usually referred to in the literature: very rare, early-onset and late-onset AD (Myers and Goate 2001). The late onset is generally sporadic and by far the dominating form of AD, while the early onset is rare (5% of the cases) and mainly found to be familial. Mutation in presenilin 1 (PS1), presenilin 2 (PS2), and β-amyloid precursor protein (AβPP) genes are typically associated with the early onset AD (Suh and Checler 2002). PS1 and PS2 genes are part of the large proteolytic machinery, which processes AβPP (Jakob-Roetne and Jacobsen 2009). Mutations in the AβPP gene, located on chromosome 21, lead to the increased production of Aβ peptides, while PS1 (chromosome 14) and PS2 (chromosome 1) point mutations can result in the enhanced proteolytic cleavage of AβPP (Selkoe 2001). The late onset AD is mainly age-related and usually develops after the age of 60, but the exact cause of the appearance of this form of dementia is a matter of debate. Several genetic risk factors are potentially involved, among which apolipoprotein E4 gene may play the most prominent role (Maltsev et al. 2011). Recently discovered clusterin and complement receptor 1 are also thought to be AD risk factors (Eisenstein 2011). However, also environmental factors, such as decreased physical, mental, and social activity or high cholesterol diet, were suggested to be correlated with the development of this most common form of dementia (DeWeerdt 2011).

1.1.3 Molecular background of AD

The β-amyloid plays a pivotal role in the pathogenesis of AD. This small 4 kDa peptide is formed due to the proteolytic processing of the bigger transmembrane protein—AβPP. The physiological role of AβPP is still to be elucidated, but putatively AβPP may act as a cell surface receptor, and could be involved in synapse formation and neuronal iron transport (Zheng and Koo 2011). AβPP undergoes several post-translational modifications, one of which is a proteolytic cleavage with α-, β- and γ-secretases (Hardy and Selkoe 2002). α-secretase cleavage does not play a pathological role in AD (as it cleaves AβPP within the Aβ sequence), and is frequently suggested to be protective (Lichtenthaler and Haass 2004). The action of β- and γ-secretases releases 37–42 amino acid Aβ peptide fragments. β-secretase cleaves the extracellular, hydrophilic N-terminal part of AβPP, and γ-secretase releases the hydrophobic, membrane-inserted C-terminal fragment (Figure 1.1). Aβ40 is the most abundant form in the brain, but Aβ42 shows a stronger correlation with the neurological symptoms of Alzheimer's disease (Selkoe 2001).

Aβ peptide undergoes several chemical modifications. The N-terminal truncation at

positions 3 or 11, as well as the modification with pyroglutamate appear most relevant pathologically (Jakob-Roetne and Jacobsen 2009).

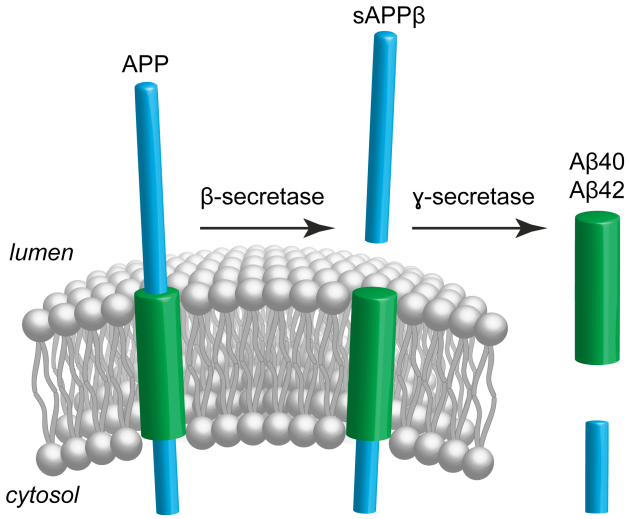

Figure 1.1. Processing of AβPP. Sequential cleavage of APP by β- and γ-secretases leads to the production of Aβ40 or Aβ42 peptides, and subsequent release into extracellular space.

1.1.4 Amyloid hypothesis

Despite intensive research to date, AD is still not curable. Definite diagnosis requires *post-mortem* analysis of the brain (Williams 2011); up to date physical and mental exercises are considered as most effective preventive measures (DeWeerdt 2011), and only symptomatic treatment is applied. The exact cause of the AD is still under debate. However, the amyloid hypothesis formulated by Hardy and Allsop (1991) is compelling. This hypothesis states that aggregating and accumulating cerebral Aβ peptide is the driving force of the AD pathogenesis. Remaining disease processes, like tau hyperphosphorylation and neurofibrillary tangle formation, could be secondary events, resulting from the imbalance between Aβ formation and clearance (Figure 1.2; Hardy and Selkoe 2002). Recent study of Jakob-Roetne and Jacobsen (2009) also showed that the Aβ40:Aβ42 ratio, shifted in favour of the latter, positively correlates with the occurrence of dementia symptoms. Growing evidence indicates that small soluble Aβ oligomers, but not the monomers or amyloid fibrils, are the main culprits of the neurodegeneration in AD (Lambert et al. 1998). The extracellular deposition of the insoluble amyloid plaques in the brain was suggested to constitute an inactive reservoir, not contributing to the disease pathology (Hardy and Selkoe 2002).

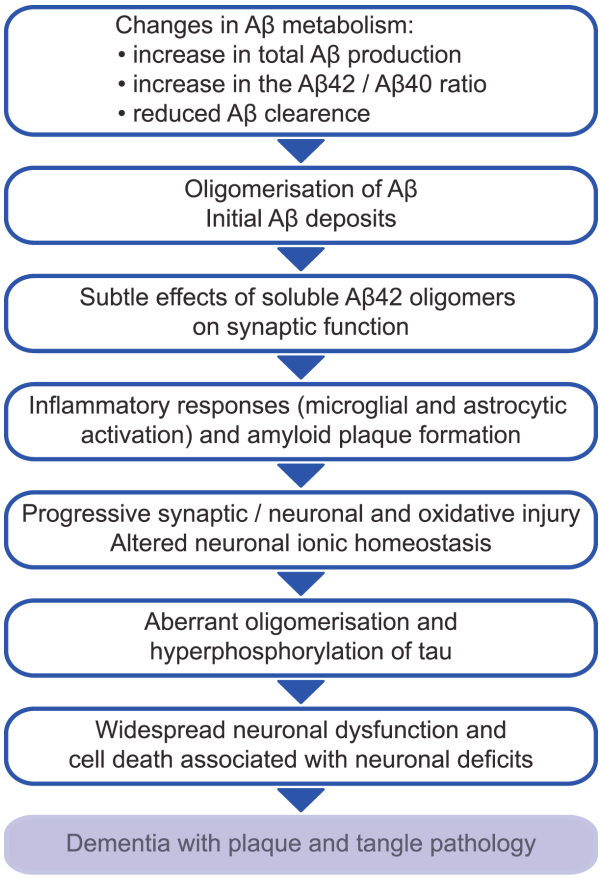

Figure 1.2. Amyloid cascade hypothesis.
Adapted from Haass and Selkoe (2007).

1.1.5 Role of Aβ aggregation in AD aetiology

It is well established that the aggregation of Aβ peptide is central to the pathology of AD. The aggregation of Aβ is a nucleation-dependent process, with two well-resolved phases. The first phase – the lag phase – is concentration-dependent, and involves Aβ nuclei formation. The second phase – the exponential growth phase – includes rapid association of Aβ molecules with the nucleus (Chiti and Dobson 2006). The extracellular deposition of amyloid fibrils as plaques represents the final stadium of the Aβ aggregation. Among few Aβ isoforms, the Aβ40 and Aβ42 fibrils are pathologically the most relevant. Even though Aβ42 fibrils better correlate with the symptoms of AD, Aβ40 fibrils constitute a major component of the amyloid plaques. Dense core amyloid plaques are a hallmark of AD, but the pathway of Aβ assembly also includes several on- or off- pathway intermediates. A simplified Aβ peptide aggregation pathway is presented in Figure 1.3. The Aβ intermediates include many structurally diverse species, described under different names (Bitan et al. 2005). The general terms ‘oligomers’ and ‘protofibrils’ have been coined to categorise the two most distinct groups. Spherically shaped oligomers precede appearance of protofibrils, which are the next

stage in Aβ assembly cascade – the intermediate step between oligomers and fibrils. The protofibrils are curvilinear aggregates – structurally similar to oligomers, but morphologically resemble fibrils (Scheidt et al. 2011).

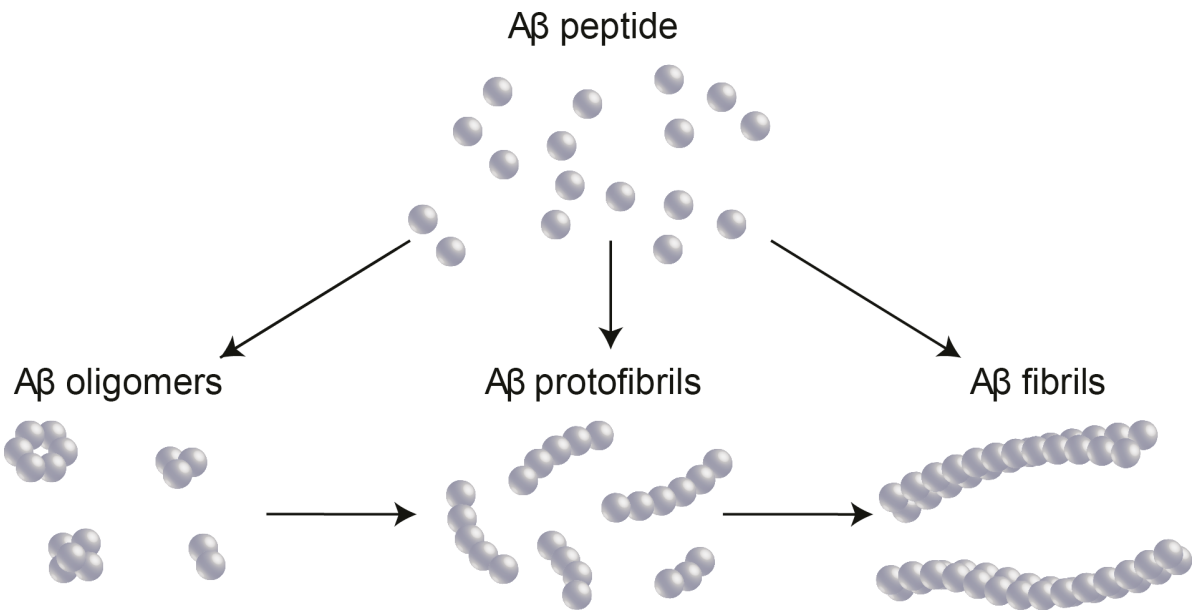

Figure 1.3. Aggregation of Aβ peptide. Schematic illustration of the Aβ peptide assembly shows two intermediate states, i.e., oligomers and protofibrils, as well as the final aggregation state – mature fibrils.

1.2 Structure and properties of amyloid fibrils

1.2.1 Morphological appearance

Aβ40 fibrils have a typical appearance on transmission electron microscopy (TEM) images. They represent long, linear structures with diameter of 10–25 nm, and a length of 1 μm (Fändrich et al. 2011). Another typical feature of mature Aβ fibrils are cross-over distances, which represent apparent constrictions of the fibril width, as observed with TEM projections (Figure 1.4; Meinhardt et al. 2009). Aβ40 fibrils are similar to the other amyloid fibrils: the width, cross-over distances or cross-sectional structures vary between single fibrils prepared under identical conditions, or even derived from the same sample (Meinhardt et al. 2009). As suggested by Pedersen and Otzen (2008), the distinct appearance of fibrils might result from the absence of structure controlling mechanisms in case of non-functional protein conformations.

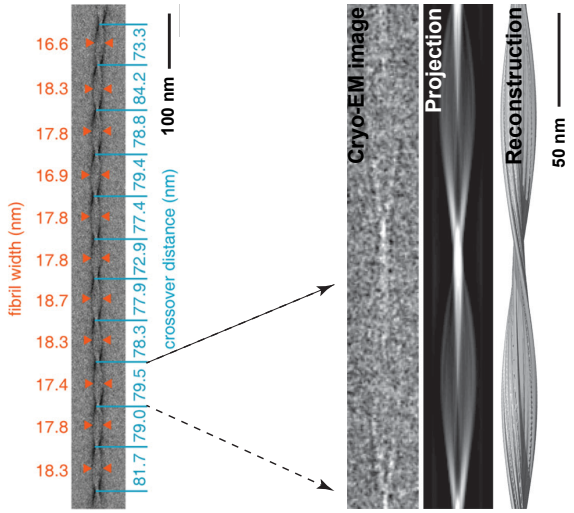

Figure 1.4. Negatively stained and cryo-EM images of Aβ40 fibrils. Cross-over distances and fibril width measurements are demonstrated on the same fibril (left panel). 3D reconstruction of the Aβ40 fibril obtained from the cryo-EM image (right panels). Images after Meinhardt et al. (2009) and Sachse et al. (2008), modified.

1.2.2 Structural characteristics

For the last two decades, the structure of amyloid fibrils has been a matter of intense investigation. Aβ fibrils are composed of insoluble, and thus non-crystalline material. Naturally occurring fibrillar polymorphism makes their examination more difficult (Meinhardt et al. 2009). However, due to recent development of high resolution techniques, like solid state nuclear magnetic resonance (ssNMR), or cryo-EM, several structural models of Aβ fibrils at near-atomic resolution have been proposed (Lührs et al. 2005, Petkova et al. 2006, Sachse et al. 2006, Sawaya et al. 2007, Sachse et al. 2008). Initially, the structure of the fibrils was based on X-ray diffraction measurements (Sunde et al. 1997). The cross-β conformation, reflected in regular main chain spacing of 4.7 Å (Marshall and Serpell 2009), and variable distances in fibril cross-section of 5–12 Å (Fändrich 2007), is a well-established structural motif of amyloid fibrils. The cross-β conformation consists of β-strands running perpendicular to the main fibril axis. Recent cryo-EM study revealed an improved fibril structure at 8 Å resolution (Figure 1.5a; Sachse et al. 2008). 3D reconstruction of Aβ40 fibrils showed that mature fibrils consist of two partially overlapping protofilaments (Figure 1.5b; Sachse et al. 2008). According to this reconstruction, each protofilament encompasses juxtaposed paired β-sheet structures. These findings are in good agreement with the steric zipper structure, demonstrated earlier by Sawaya et al. (2007).

In comparison, cryo-EM structure of Aβ42 fibrils revealed a slightly different arrangement (Figure 1.5c). Mature Aβ42 fibril comprises only one protofilament, and the β-sheet packing is tighter (Schmidt et al. 2009). Schmidt et al. (2009) also showed that protofilament structures of Aβ40 and Aβ42 fibrils are very similar, and that each cross-β repeat contains an equal number of Aβ molecules.

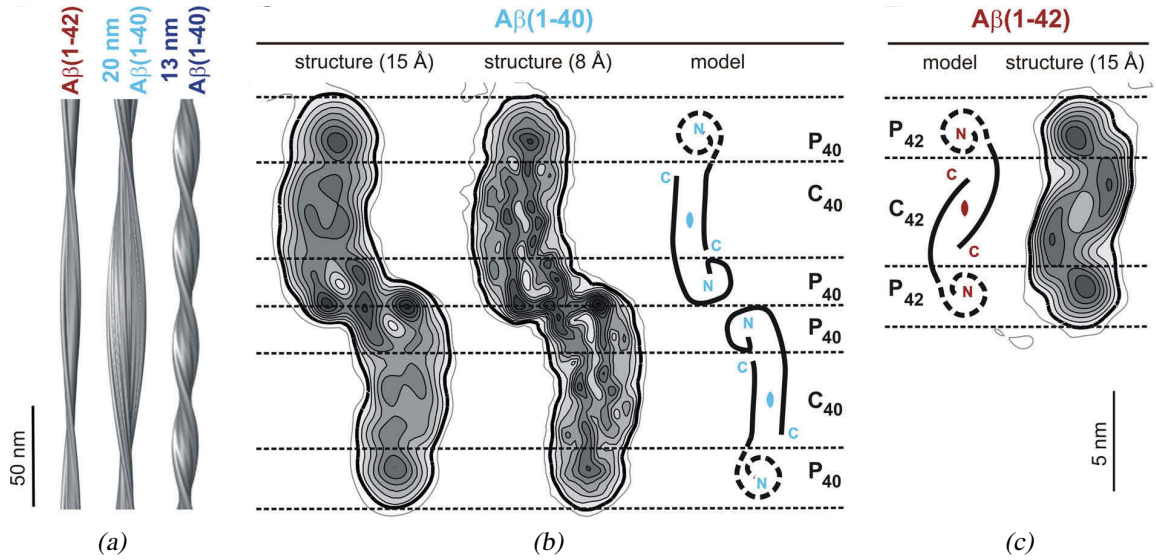

Figure 1.5. Comparison of Aβ40 and Aβ42 fibrils structure. Three distinct fibril morphologies are based on reconstructions of Aβ40 and Aβ42 fibrils *(a)*. Aβ40 fibril consists of two protofilaments (structure) with the similar organisation of Aβ molecules (model) as in Aβ42 fibril *(b)*. Cross-section of Aβ42 fibril shows presence of one protofilament (structure) and possible peptide position (model) *(c)*. Images after Schmidt et al. (2009).

1.2.3 Tinctorial characteristics

An elongated and regular structural pattern implies an additional distinct fibril characteristic, namely high affinity for amyloid-dyes: CR and Thioflavin T (ThT) (Figures 1.6a and 1.6b). This affinity allows easy detection of amyloid fibrils. This methods, however, are not free from limitations – such as sensitivity to the solution and staining conditions (Westermark et al. 2005, Fändrich 2007). The mechanism of binding of mature fibrils with these dyes is not fully elucidated, but in the case of ThT binding, it may be based on the interaction with aromatic and aliphatic side chains of amyloid fibrils (Biancalana and Koide 2010). CR binding probably relies on the interaction with charged and hydrophobic residues on amyloid fibrils (Frid et al. 2007). However, a previous study on insulin fibrils suggests that aromatic residues could also be involved in amyloid deposits-CR binding (Turnell and Finch 1992).

Aβ oligomers show decreased affinity for amyloid ligands like ThT or CR (compared to fibrils), but they strongly interact with 1-anilino-8-naphthalene sulfonate (ANS; Figure 1.6c), a fluorescent dye (Haupt et al. 2012). ANS binds to hydrophobic surfaces of proteins (Matulis et al. 1999). In contrast, Aβ fibrils do not show a significant interaction with ANS (Figure 1.6d).

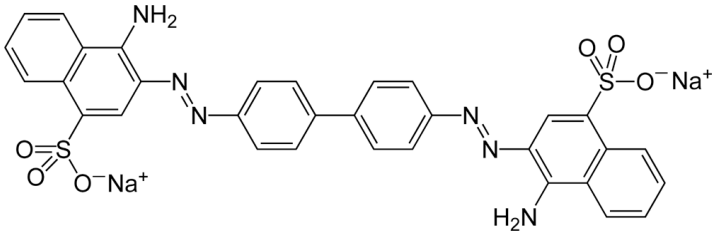

(a) Congo red

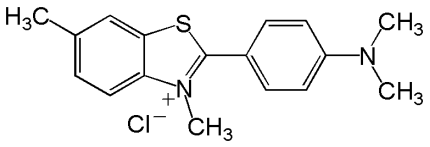

(b) Thioflavin T

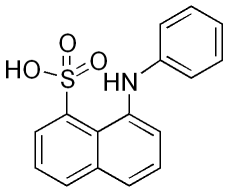

(c) 1-anilino-8-naphthalene sulfonate

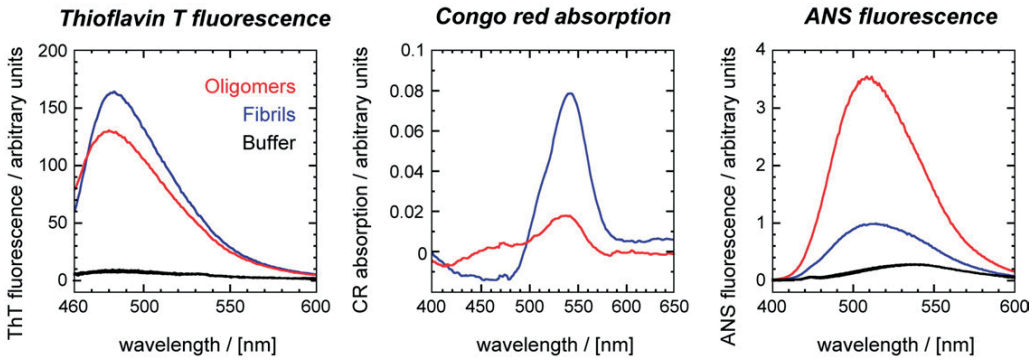

(d) Absorption and fluorescence

Figure 1.6. Structure of amyloid-binding dyes and their interaction with amyloid conformers. Strong ThT fluorescence signal was obtained with Aβ fibrils (a); CR absorption difference was high for fibrils but low for oligomers *(b)*; high fluorescence signal indicates strong interaction of oligomers with ANS *(c)*. Images after Haupt et al. (2012) and Fändrich (2012), modified.

1.2.4 Amyloid fibrils in AD: inert or protective deposits – or a potent toxin?

A strong correlation between the level of soluble Aβ and the deterioration of neuronal functions has been reported in many studies (McLean et al. 1999, Dahlgren et al. 2002, Lue et al. 1999, Selkoe 2008, Shankar and Walsh 2009, O'Nuallain et al. 2010). Even though soluble oligomers are the putative cause of AD (Kirkitadze et al. 2002), cytotoxic effects of Aβ fibrils were also observed. Initially, their toxic impact on cultured primary hippocampal neurones was shown by Lorenzo and Yankner (1994) and, more recently, by Petkova et al. (2005). Results obtained from two different populations of Aβ fibrils indicate that at least some fibril morphologies may be pathologically relevant (Figure 1.7; Petkova et al. 2005, Schmitz et al. 2004). Geula et al. (1998) found that Aβ fibrils cause the activation of microglia

and neuronal loss in primate brains. In contrast, some indication exists that accumulation of Aβ peptide in form of insoluble deposits performs a protective function. Holmes et al. (2008) showed that targeting of the Aβ deposits by vaccination did not prevent progressive neurodegeneration, but instead led to undesirable side effects i.e., meningoencephalitis and leukoencephalopathy (Orgogozo et al. 2003).

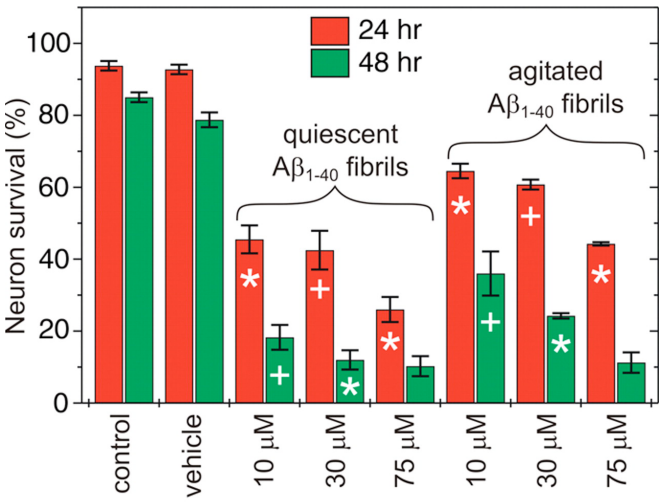

Figure 1.7. Toxicity of Aβ40 fibrils on cultured primary embryonic rat hippocampal neurones. Two different populations of fibrils were examined: one growing in the quiescent and second subjected to agitation. Viability of the cultured neurones was measured after 24 h or 48 h exposure to Aβ40 fibrils. Image after Petkova et al. (2005).

Whether harmless or toxic, the effect of fibrils in the demented brain needs to be elucidated. It is well known that they constitute the most abundant amyloid aggregates in the brain of people with AD; hence, Aβ fibrils are the matters of comprehensive structural and functional investigations.

1.2.5 Common structure of amyloid fibrils derived from various polypeptides

It has been demonstrated that amyloid fibrils derived from different polypeptide precursors display similar structural characteristics (Chiti and Dobson 2006, Fändrich et al. 2009). Fibrils formed from insulin, glucagon, yeast prion protein Ure2p or β_2-microglobulin provide good examples. These fibrils have been grown from different polypeptides and differ morphologically (short or long, straight or curvilinear). Nonetheless, all of them posses the β-sheet amyloid-like structure (Haupt et al. 2011a) and bind ThT and CR dyes, along with a shared ability to produce the characteristic reflection pattern in X-ray diffraction. Remarkably, not all amyloid aggregates are associated with a disease, for instance glucagon (Pedersen and Otzen 2008) and apomyoglobin fibrils (Fändrich et al. 2006) are pathologically irrelevant.

1.3 Characterisation of Aβ oligomers

1.3.1 Diversity of oligomeric Aβ aggregates

Accumulating evidence suggests that the Aβ oligomeric aggregates are primary toxic species that causes AD. A number of on- or off-pathway Aβ intermediates have been described in the literature. However, acquisition of homogeneous batches of Aβ peptides, and establishing of a reproducible protocol for oligomer preparation pose major challenges. Metastable character of oligomeric aggregates, and their vulnerability to solution conditions make them prone to aggregation. Hence, in order to examine the properties of oligomeric aggregates, it is necessary to subject them to a temporary arrest. This may be achieved with various methods, e.g., by lyophilisation, or by ligand binding.

Oligomeric species described in the literature differ in size, shape, aggregation pathways, and mechanism of toxicity (Bitan et al. 2005). In addition, the vague nomenclature of the oligomeric species is confusing: a given entity is described under different names (Bitan et al. 2005). Commonly described intermediate Aβ species include protofibrils, annular protofibrils, and oligomers (see Table 1.2 for a summary). Protofibrils are structurally similar to mature Aβ fibrils, but they can be distinguished by their curvilinear shape and weaker binding affinity to amyloid ligands, i.e., ThT and CR (Walsh et al. 1999, Goldsbury et al. 2000). Annular protofibrils are characterised by a pore-like shape. Disruption of the cell-membrane, the putative toxicity mechanism of this species, is attributable to this property (Lashuel et al. 2002). While morphological properties of protofibrils and annular protofibrils allow their differentiation, the group called 'oligomers' includes species displaying a whole repertoire of shapes and structures. This diverse group contains species such as Aβ*56 oligomers, amyloid-derived diffusible ligands (ADDL), and globulomers, to name but a few.

Aβ oligomers are generally defined as partially soluble, metastable conformers derived from Aβ peptides, varying in diameter from 2 to 50 nm. Oligomers include species ranging in size two (dimers) and several hundreds of monomers per unit. Species of up to 50 kDa are often referred to as low molecular weight (LMW) oligomers (Bitan et al. 2003); those above 50 kDa are referred to as non-fibrillar, high molecular weight (HMW) oligomers.

Most oligomeric species described in the literature were prepared from synthetic Aβ peptides, according to established protocols. The remaining ones originated from naturally occurring Aβ species, detected and isolated *post-mortem* from AD brains (Haass and Selkoe 2007). For example, 70 kDa or larger aggregates, containing Aβ dimers, have been isolated from human brain tissues (Shankar et al. 2008). Aβ*56 oligomers were purified from brains of AD transgenic mice (Lesne et al. 2006). Oligomeric species prepared *in vitro* from synthetic

Table 1.2. Oligomeric Aβ species

Oligomeric species	Aβ isoform	Characteristics
Protofibrils	Aβ40, Aβ42	Curvilinear, soluble assemblies; diameter: 6–8 nm and length up to 200 nm (derived from AFM and TEM); MW: >100 kDa (according to SEC) (Harper et al. 1997, Walsh et al. 1997, Broersen et al. 2010); bind to CR and ThT (Habicht et al. 2007); high level β-sheet content (as stated with CD and X-ray diffraction) (Walsh et al. 1999, Habicht et al. 2007)
Annular protofibrils (APF)	Aβ42	Ring-like shape with central opening; diameter: 8–25 nm; substantial β-sheet structure (as stated with CD) (Kayed et al. 2009); 36-mers (out of 6 hexamers) (Lasagna-Reeves et al. 2011)
Aβ-derived diffusible ligands (ADDL)	Aβ42	Soluble, globular structure; diameter: 4.8–5.7 nm; MW: 17–42 kDa (derived from AFM); disrupt LTP in rats (Lambert et al. 1998, Chromy et al. 2003, Lacor et al. 2004)
Aβ*56	Aβ42	Dodecamer isolated from the brains of AβPP transgenic mice; MW: 56 kDa (Lesne et al. 2006)
Globulomers	Aβ42	Diameter: 1–5 nm; MW: 16–64 kDa (Barghorn et al. 2005); rich in β-sheet structure (as stated with ATR-FTIR)(Eckert et al. 2008)
Low n-oligomers	Aβ40, Aβ42	SDS resistant dimers and trimers; diameter: 2–7 nm; MW: 8–12 kDa; significant β-sheet content (as stated with CD) (Walsh et al. 2002, Bitan et al. 2003, Ono et al. 2009)

Modified after Haass and Selkoe (2007) and Meinhardt (2010); MW: molecular weight

or recombinant Aβ peptide include ADDL, globulomers or annular protofibrils (Lambert et al. 1998, Gellermann et al. 2008, Caughey and Lansbury 2003).

Because some entities have been described by different investigators, it is necessary to verify their identity. For some oligomeric intermediates, it also needs to be established whether or not they share a common aggregation pathway. Finally, toxic and non-toxic Aβ species need to be identified and categorised. Small ligands, such as Aβ-specific antibodies, may prove particularly helpful in fulfilling these tasks.

1.3.2 Structure of Aβ oligomers

The structural study of Aβ oligomers has been hindered by difficulties in obtaining homogeneous populations that are free from monomers or fibrils. Furthermore, the inability to acquire atomic-level structural information about different types of Aβ oligomers is due to their small size, metastable nature, and structural sensitivity to the conditions of preparation.

Access to oligomer structure would allow better understanding of Aβ toxicity, mediated by assembly process. The most common methods used for determination of oligomers' size and weight are the polyacrylamide gel electrophoresis (PAGE) with presence of sodium dodecyl sulphate (SDS), or native PAGE, as well as size exclusion chromatography (SEC) (Bitan et al. 2003, 2005, Sandberg et al. 2010). However, these techniques are not free from limitations. For instance, SDS can promotes aggregation of the amphipathic molecules and thus SDS-PAGE may produce false results in terms of size of the Aβ oligomers (Bitan et al. 2005). The main drawback of the SEC is a relatively low resolution, compared to SDS-PAGE (Bitan et al. 2005). Morphological assessment of various oligomeric forms is usually performed with TEM or atomic force microscopy (AFM) (Bitan et al. 2005, Glabe 2008, Mastrangelo et al. 2006). Current structural studies of Aβ intermediates are based on spectroscopic methods, of which ssNMR provides the best resolution (Ahmed et al. 2010). Presence of the antiparallel β-sheet structure in Aβ oligomeric species was suggested by several attenuated total reflectance (ATR) Fourier transform infrared spectroscopy (FTIR) studies (Habicht et al. 2007, Eckert et al. 2008, Cerf et al. 2009). Aβ42 oligomers investigated by Ahmed et al. (2010) with ssNMR also showed significant content of β-sheet structure, but organised in different, antiparallel and less ordered manner than in Aβ40 oligomers or Aβ42 fibrils. Indication of antiparallel β-sheet structure in certain oligomer types are intermolecular hydrogen bonds (Sandberg et al. 2010). However, ssNMR study conducted by Chimon et al. (2007) revealed that Aβ40 spherical oligomers possess amyloid-like parallel β-sheet structure.

1.3.3 Impact of Aβ oligomers on the aetiology of AD

The original Aβ hypothesis, formulated by Hardy and Higgins (1992); was based on the assumption that AD is caused by extracellular deposition of fibrils in amyloid plaques. However, several more recent reports have indicated that neurodegeneration begins before fibrillar aggregates appear, and that it might be independent of the number of deposited plaques (Hsia et al. 1999, McLean et al. 1999). This discovery has shifted the attention of the scientists to soluble species, and revealed the need for the invention of therapeutic solutions directed against prefibrillar species. Currently, soluble oligomers are seen as the most important mediators of amyloid toxicity (Jakob-Roetne and Jacobsen 2009). Compared with fibrils, the correlation of oligomers with occurrence of AD symptoms is stronger (McLean et al. 1999, Dahlgren et al. 2002, Lue et al. 1999, Selkoe 2008, Shankar and Walsh 2009, O'Nuallain et al. 2010). Such effects of oligomers as inhibition of long-term potentiation (LTP; Walsh et al. 2002), neuronal loss, or synaptic plasticity deterioration has been shown in AD mouse models (Lesne et al. 2006).

Many oligomeric structures (e.g. ADDL) have been reported to be toxic in neuronal cell cultures (Lambert et al. 1998). Aβ42 globulomers have been detected in amyloid deposits in AβPP Tg2576 transgenic mice, as well as acquired *in vitro* by incubation under established conditions (Barghorn et al. 2005). Neurotoxic, soluble Aβ dimers and trimers have been shown to inhibit LTP in rats (Walsh et al. 2002) and Aβ*56 oligomers were also reported to impair memory (Lesne et al. 2006). However, the correlation between neurotoxicity and structure of oligomeric conformers derived from the AD brain tissues, and those formed by the incubation of the synthetic Aβ peptide, remains unclear. Nonetheless, the neurotoxic impact of both synthetic a and wild-type oligomers on neurones is well-documented (McLean et al. 1999, Hsia et al. 1999). The neuronal membrane permeabilisation has been put forth as a putative mechanism of destruction of neurones by annular protofibrils (Lasagna-Reeves et al. 2011). Impairment of mitochondria by Aβ42 oligomers was observed in tau transgenic mice (Eckert et al. 2008). However, the exact mechanism of how oligomers exert the toxic effect is poorly known.

1.4 Toxicity mechanism and therapeutic approaches in AD

Despite the controversy about the impact of Aβ fibrils and oligomers on the neuronal toxicity and some contradicting data on this topic, the key role of Aβ aggregation in AD pathology is well documented. Therefore, all Aβ aggregates are targeted therapeutically. While Aβ toxicity might be mediated in several ways, the exact mechanism remains unknown. Aβ aggregates may interact with cellular components like membranes, mitochondria or other macromolecules (Eckert et al. 2008). In consequence, this may lead to oxidative stress, disruption of important cellular functions like efflux of calcium ions, impairment of axonal transport or synaptic communication (reviewed by Chiti and Dobson 2006). Currently, neither definitive diagnostic markers, nor effective therapeutic tools for AD are available. In this context, anti-Aβ antibodies are gaining attention. They may reveal some pharmacological potential, or may prove useful for structural Aβ studies.

1.4.1 Immunotherapeutic strategies to combat Aβ toxicity

Prevailing evidence indicates that, among several therapeutic strategies against toxicity of Aβ, immunotherapeutic approaches are the most promising. Both active and passive immunotherapy have been demonstrated to be effective in reducing amyloid burden in animal models (Lombardo et al. 2003, Schenk et al. 2005). Active immunotherapy uses antigen stimulation of the host immune system to produce antibodies against applied antigens. It

has been proven useful in improving the cognitive decline by reducing the amyloid plaque load in transgenic mouse models (Morgan et al. 2000, Lemere et al. 2000, Weiner et al. 2000, McLaurin et al. 2002) and elevating the Aβ level in the periphery (Lemere et al. 2003). However, the first clinical trials with the active vaccine AN1792 (ELAN / Wyeth) have been halted, because 6% of patients developed meningoencephalitis (Schenk 2002). Currently, several Aβ vaccines are undergoing clinical trials (Lemere and Masliah 2010, Delrieu et al. 2011). These include second-generation vaccines like ACC-001, CAD-105 or V950, which were designed to avoid stimulation of the adverse immune responses (Lemere and Masliah 2010, Delrieu et al. 2011).

In passive immunotherapy, antibodies or antibody fragments specific against certain Aβ epitopes are provided externally. This eliminates the need of host immune response development, which is often problematic in elderly patients. Beneficial effects of passive vaccination, including disintegration of pre-existing Aβ deposits (Bard et al. 2000) and improvement of cognitive functions (Wilcock et al. 2004), have been demonstrated in AD transgenic mice. Due to the complexity of the topic, and the relevance for this dissertation, I will further focus only on the passive vaccination solutions.

1.4.2 Putative mechanisms underlying the Aβ clearance by antibodies

Although the question how passive vaccination might rescue cognitive functions in AD brain remains unanswered, some mechanisms describing antibody-mediated Aβ clearance have been proposed (Figure 1.8). The peripheral sink mechanism hypothesis is based on the observation made by DeMattos et al. (2001). Peripheral injection of the 266 monoclonal antibody, which binds with picomolar affinity to soluble Aβ, reduced the amyloid load in the brains of transgenic mice. Thus, peripheral injection of the anti-Aβ antibodies may cause efflux of the parenchymal Aβ, by shifting the Aβ ratio between blood plasma and the central nervous system (CNS).

Fc receptor-mediated phagocytosis by activated microglia is the second proposed mechanism (Istrin et al. 2006). It has been demonstrated that a small amount of peripherally administrated antibodies reaches the brain parenchyma of PDAβPP transgenic mice and triggers the microglia-dependent phagocytosis of amyloid deposits (Bard et al. 2000).

Proponents of the third mechanism, the direct resolution hypothesis, suggested that the antibodies against the N-terminal part of Aβ are able to directly resolve the Aβ fibrils and remove the Aβ deposits (Frenkel et al. 2001, Solomon et al. 1997, McLaurin et al. 2002). Hence, this mechanism could also constitute the base for the therapeutic effect.

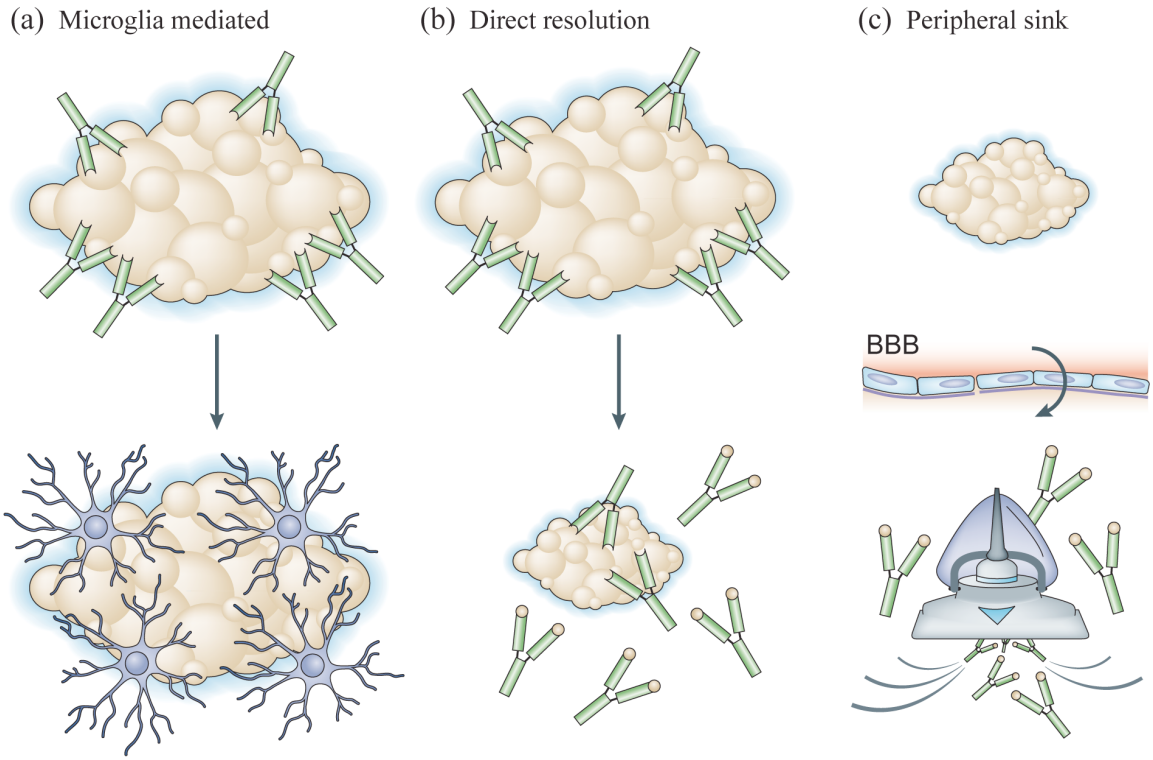

Figure 1.8. Schematic illustrations presenting putative mechanisms of Aβ clearance by antibodies. Microglia mediated Aβ clearance *(a)*, direct resolution mechanism *(b)*, peripheral sink hypothesis *(c)*. Images after Citron (2004). BBB: blood–brain barrier.

1.4.3 Existing antibodies against Aβ

A whole set of polyclonal sera and monoclonal antibodies have emerged against different Aβ conformers. Anti-Aβ antibodies can be roughly grouped into two categories – sequence-specific and conformation-specific binders. The first group includes the antibodies which bind to the polypeptide sequence of Aβ; their specificity is broader. For instance, 3D6 and 82E1 monoclonal antibodies bind the N-terminal part of Aβ, and were also effective in the reduction of the amyloid deposits in human brain (Shankar et al. 2008). Aβ C-terminal (2G3, 21F12) and mid-region (266) specific antibodies were unsuccessful in Aβ precipitation and preventing neuronal deterioration (Shankar et al. 2008).

The second group of antibodies recognises a certain structural motif on proteins, which is independent of the amino acid sequence. Kayed and coworkers isolated polyclonal sera (A11, OC and α-APF) specific to several soluble Aβ conformers (Kayed et al. 2003, 2007, 2009). These polyclonal antibodies are specific to three different types of Aβ oligomers: prefibrillar oligomers, fibrillar oligomers and annular protofibrils (Kayed et al. 2010). The other example of conformation-specific binders constitute WO1 and WO2 monoclonal antibodies generated by immunisation, which bind to Aβ fibrils (O'Nuallain and Wetzel 2002).

1.4.4 Conventional antibodies versus recombinant antibodies

The previous examples constitute but a few out of many Aβ binders reported in the literature. However, their mechanism of binding is poorly understood. Most of the currently available Aβ binders have been obtained by means of animal immunisation, which is often an expensive and time-consuming approach. Additionally, the generation of monoclonal antibodies by immunisation requires special cell culture systems and involves exploitation of animals (Donzeau and Knappik 2007).

Recombinant antibodies constitute a different class of amyloid binders. They are generated from synthetic antibody gene libraries. Their production eliminates many disadvantages associated with generation of antibodies by immunisation. First of all, the generation of antibodies *in vitro* circumvents the problem of animal use. Second, all reagents are monoclonal, making them suitable for high-throughput screening (Krebs et al. 2001). Moreover, recombinant antibodies are easy to express in large quantities with the use of the same expression system (Habicht 2002). Finally, the accessibility of DNA sequences of recombinant antibodies facilitates genetic manipulations, thus giving way to the generation of novel downstream reagents with modified properties (Plückthun and Pack 1997, Plückthun 1992).

This thesis will cover selection of conformation-specific binders directed against β-amyloid from a synthetic phage library and their mode of action.

1.5 Selection of antibody fragments from a recombinant DNA library

1.5.1 Display technologies

Naive and recombinant libraries were constructed to enable *in vitro* or *in vivo* selection of antibodies (Sergeeva et al. 2006). Several different display approaches have been successfully implemented to generate recombinant antibodies directed against a variety of antigens (Sergeeva et al. 2006). These include bacterial, yeast and mammalian cell surface display, as well as ribosome and phage display. Besides the possibility of generation of highly specific binders, display technologies facilitate the improvement of antibody properties, like affinity or stability. The main advantages of the displaying methods include: the possibility of application against a vast range of antigens, and the ability of adjusting the selection's conditions to particular needs (Ponsel et al. 2011). Among aforementioned techniques, ribosome and phage display earned most attention.

Phage display has been established by Smith in 1985 (Smith 1985). Nowadays, it is the most commonly applied display method used for read out of combinatorial antibody libraries

(Ponsel et al. 2011). Phage display involves cloning the DNA coding for a peptide or a protein to the M13 bacteriophage genome. Fusion of a gene fragment coding for an antibody to the coat protein of M13 phage facilitates the expression of the antibody on the surface of the phage as the coat-fusion protein; hence, provides a physical link between the genotype and phenotype of the protein. As a result, recombinant proteins are displayed on the surface of the M13 bacteriophage – usually as a fusion with phage coat protein III. M13 is a single strand filamentous bacteriophage, which consists of 10 genes (Figure 1.9; Arap 2005). The major capsid protein, pVIII, exists in approximately 2700 copies (Arap 2005). The minor capsid pIII protein, used for the protein fusion, is present in 5 copies (Sergeeva et al. 2006). Assembly of the phages and expression of the antibodies takes place in the periplasmic space of *Escherichia coli* (*E. coli*). The phage display system, used to generate antibodies directed against β-amyloid – which are the matter of this thesis – consists of two components: phagemid vector and helper phage. The monovalent expression of the antibodies on the phage surface and their small size are the major advantages of the phagemid use. It enables the construction of larger libraries. However, the overall size of libraries displayed on phages is limited by the efficiency of *E. coli* transformation (Vaughan et al. 1996). Phage display selection of antibodies proves to be a very fast and effective method of antibody generation, in comparison to animal immunisation (Habicht et al. 2007, Lafaye et al. 2009). Competitive selection conditions limit unsolicited cross-reactivity and the selection just sequence–specific binders.

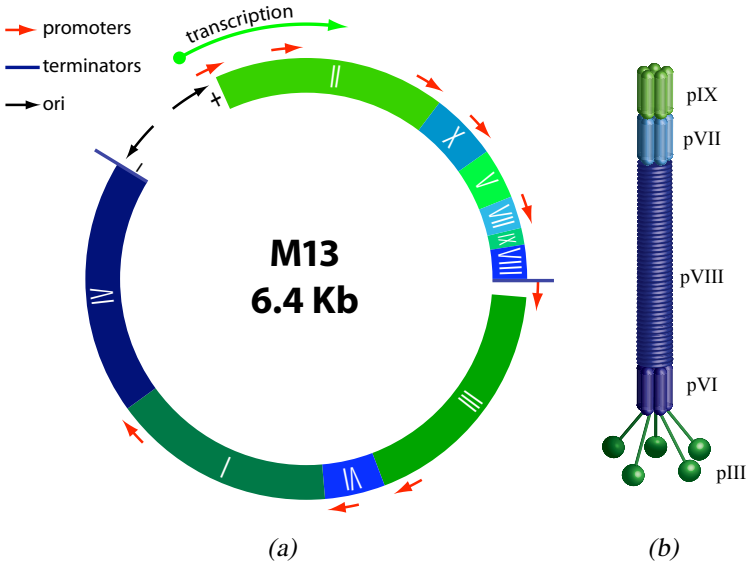

Figure 1.9. Schematic representation of the M13 phage. Genome of the M13 phage consists of ten genes *(a)*. Structure of the M13 phage with marked capsid proteins (pIX, pVII, pVIII, pVI, pIII) *(b)*. Image after http://viralzone.expasy.org and Arap (2005), modified.

1.5.2 Synthetic antibody library based on the Camelidae *immunoglobulin (Ig)*

The subject of my dissertation are *Camelidae* variable heavy chain domain (VHH) antibodies and their interaction with Aβ conformers. The phage display library generated at the Hans Knöll Institute (HKI; Jena, Germany) was used for the selection of the antibody fragments directed against β-amyloid conformers. The fully synthetic, combinatorial HKI phage library consists of VHHs of camelid heavy chain antibodies (HCAb) (Habicht 2002). *Camelidae* contain two distinct classes of the antibodies, conventional and HCAb. HCAb significantly differ from conventional antibodies, because they are devoid of the light chain (Figure 1.10); thus, the whole specificity of the camelid antibody is encoded within the heavy chain (Hamers-Casterman et al. 1993). VHHs of the HCAb, referred also as 'nanobodies', are the smallest possible antigen-binding fragments, which can be generated in nature (Huang et al. 2010). The small size of this antibody fragment is its great advantage. It penetrates tissues better, thus providing easier access to the antigens. Furthermore, the increased stability of the VHH domain is caused by the replacement of the hydrophobic regions in framework 2, and by the presence of the intramolecular disulphide bond (Ewert et al. 2002, Van der Linden et al. 1999). In addition, the intramolecular disulphide bond makes it functionally suited for the expression in periplasm of *E. coli*. VHH antibodies are gaining increasing attention among amyloid researchers. They have proved to be effective in the elucidation of the mechanism of Aβ aggregation and were demonstrated to ameliorate amyloid-mediated cytotoxicity (Habicht et al. 2007, Lafaye et al. 2009, Kasturirangan et al. 2010b,a, Streltsov et al. 2011).

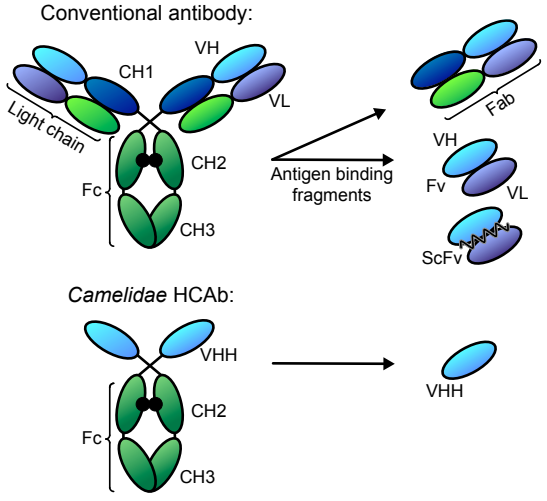

Figure 1.10. Comparison of the conventional and *Camelidae* HCAb. Fc: crystallisable fragment; Fab: antigen binding fragment; CH: constant region; VH: heavy chain variable region; VL: light chain variable region; ScFv: single chain variable fragment. Image after Muyldermans (2001), modified.

Construction of the HKI VHH antibody library was based on the alignment of the 59 llama VHH sequences, and involved a three-step polymerase chain reaction (PCR) assembly of randomised oligonucleotides coding for the framework and complementary determining fragments. The big diversity of the HKI camelid library is due to the full randomisation of the

complementarity determining region (CDR) positions, the length variations of the CDR3, as well as some naturally occurring framework polymorphism (Habicht 2002).

1.6 Relevance of the B10 antibody fragment for the structural study of amyloid fibrils

1.6.1 Selection of the B10 antibody fragment

Habicht et al. (2007) developed an approach to select a binder to Aβ40 fibrils. This approach is based on the recombinant library of VHH domains. The selection of the VHH antibody against Aβ40 fibrils has been performed in a competitive environment. Aβ40 fibrils served as bait for the phage display; a surplus of disaggregated, primarily monomeric, Aβ40 peptide was applied to prevent selection of sequence-specific binders. This phage display selection generated an antibody fragment termed B10 (Habicht et al. 2007). B10 binds in a conformation-specific manner to Aβ40 fibrils, but it reacts neither with disaggregated Aβ peptides, nor with Aβ oligomers. The apparent dissociation constant (aK_D) of B10 binding to the fibrils, measured with surface plasmon resonance (SPR), was 475 ± 54 nM. Genetic fusion of the B10 VHH domain to alkaline phosphatase (AP) yielded a dimeric protein formation (termed B10AP). B10AP has an increased binding affinity to fibrils (K_D = 7.22 $\pm$ 0.97 nM; Habicht et al. 2007). The fusion of B10 with AP enables its detection in immunoassays, and eliminates a need for a secondary antibody. The presence of the AP moiety facilitated immunohistological staining of *post-mortem* AD brain slices; eleven of twelve confirmed Alzheimer's cases showed positive staining with B10AP, thus providing evidence for the binding of B10AP to *in vivo* amyloid tissue deposits (Habicht et al. 2007).

1.6.2 Stabilisation of Aβ40 protofibrils by B10AP

B10AP recognises prefibrillar aggregates: a kinetic study of Aβ40 monitored with ThT fluorescence and B10AP immunoblot staining revealed that the formation of the B10-epitope precedes the appearance of ThT-positive fibrils (Habicht et al. 2007). Furthermore, B10AP not only binds to prefibrillar aggregates, but also inhibits further aggregation. The monitoring of the Aβ40 aggregation with ThT has shown that mature Aβ40 fibrils are formed only in absence of B10AP, while presence of B10AP inhibits their formation. Finally, it was confirmed with TEM imaging that B10AP prevents fibril formation by stabilising protofibrils (Figure 1.11).

The ability to interact with protofibrils has been described for the WO1 anti-fibril antibody (Williams et al. 2005), suggesting that protofibrils and fibrils share a common structure. A recent ssNMR protofibril study also indicated this similarity (Scheidt et al. 2011). Even

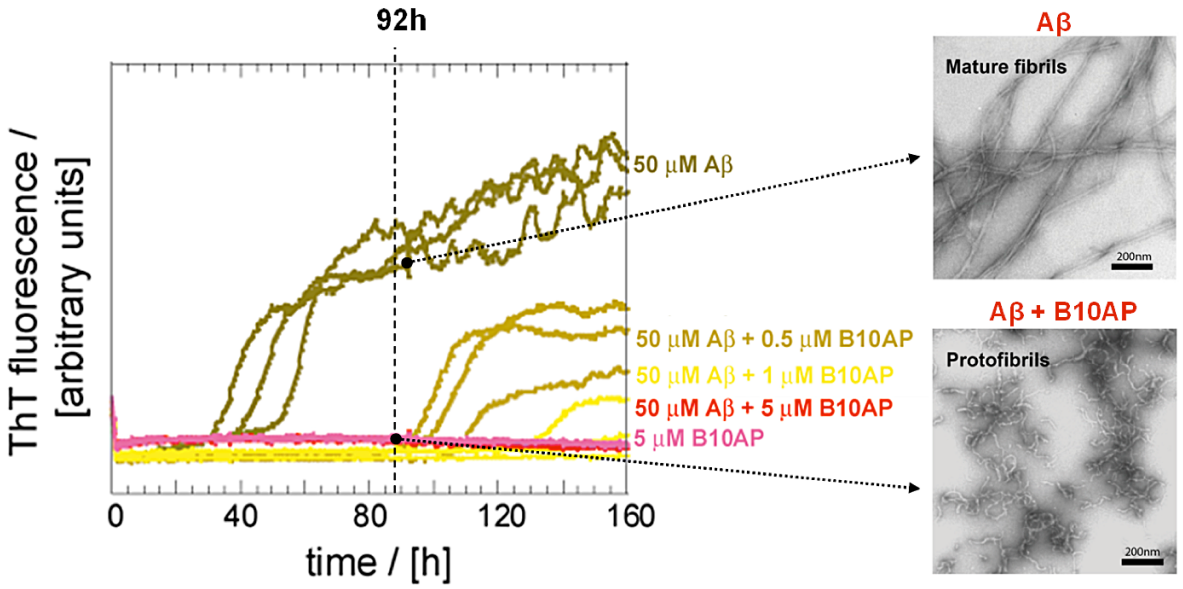

Figure 1.11. Aβ40 aggregation in presence or absence of B10AP. Formation of the ThT–positive Aβ40 structures was potently inhibited by B10AP. Fibril formation was monitored with ThT fluorescence (left) and TEM (right). No ThT–positive Aβ40 fibrils were formed upon Aβ incubation with B10AP presence. Analysis of the TEM images revealed that B10AP stabilises the protofibril stage. Image after Habicht et al. (2007), modified.

though the structures of protofibrils and oligomers are similar, protofibrils encompass a considerable part of β-sheet which recruits similar residues as fibrils (Scheidt et al. 2011, Kheterpal et al. 2006). Hence, there may exist a similarity in how B10 recognises Aβ fibrils and protofibrils.

1.6.3 Crystal structure of B10 implies the mechanism of recognition

The crystal structure of B10 (Figure 1.12a; Haupt et al. 2011b) has been resolved with X-ray crystallography at 1.8 Å resolution by Isabel Morgado and her coworkers at the Max Planck Research Unit (MPRU) in Halle. The antigen-binding surface of the conformation-specific B10 antibody fragment was found to be completely flat, and thus structurally compatible with the even surface of the Aβ40 fibril. In comparison, sequence-specific antibodies recognising the Aβ peptide usually contain a deep antigen-binding pocket which encompasses the extended polypeptide chain (Basi et al. 2010).

The analysis of the B10 amino acid sequence has revealed that the CDRs are rich in positively charged amino acids, while negatively charged amino acids are absent; the analysis of the electrostatic surface confirmed that the binding site of B10 is strongly cationic, with basic residues distributed throughout (Figure 1.12b; Haupt et al. 2011b). The peculiar characteristics of B10 suggest that electrostatic interactions are involved in Aβ40 recognition, but the actual mechanism requires to be elucidated.

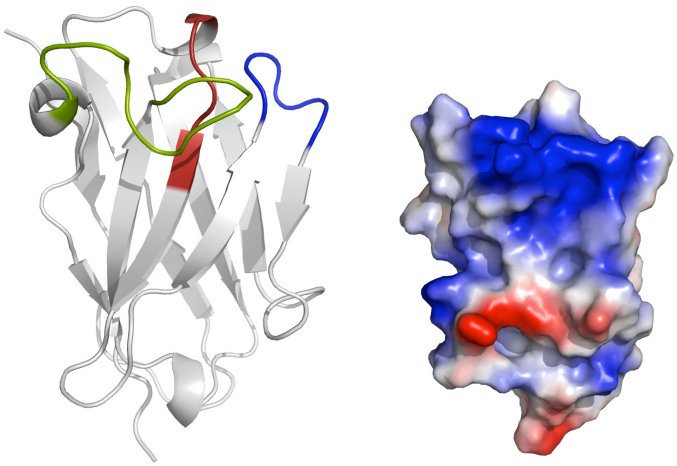

(a) *(b)*

Figure 1.12. B10 crystal structure and electrostatic surface. Ribbon diagram of the B10 crystal structure; green: CDR1; red: CDR2; blue: CDR3 *(a)*. Presentation of the B10 electrostatic surface; blue: basic region; red: acidic region *(b)*. Images after Haupt et al. (2011b), modified.

1.6.4 Specificity of B10 binding to other amyloid fibrils

B10 has initially been demonstrated to bind to several amyloid fibrils, e.g., serum amyloid A fibrils, or AL amyloid fibrils (derived from the Ig light chain; Habicht et al. 2007). These fibrils do not share a similar sequence with Aβ40 fibrils. Nonetheless, they display some typical amyloid characteristics. A further study of B10 specificity has shown that it recognises neither globular β-sheet proteins, nor intrinsically disordered polypeptides (Haupt et al. 2011b). These data are in agreement with the finding that B10 does not significantly react with β-sheet-rich oligomers (Habicht et al. 2007). A better understanding of the B10 interaction with amyloid fibrils is necessary. It may facilitate the application of B10 as a diagnostic tool in amyloid diseases. The detailed mechanism of B10 recognition will be the matter of my thesis.

1.7 Selection of antibody fragments directed against Aβ40 oligomers

Further antibody fragments directed against Aβ conformers were isolated from the HKI VHH library by Karin Wieligmann (HKI, Jena). Here, Aβ40 oligomers were used as an immobilised target; freshly dissolved Aβ40 peptide in surplus served as a competitor in the solution phase. Four rounds of selection were performed to generate three antibodies (termed KW1, KW2, and KW3). The initial characterisation of the selected VHH domains has shown a strong and selective interaction between KW1 and Aβ40 oligomers (Morgado et al. 2012). The crystal structure of KW1, determined at 1.9 Å resolution, revealed a β-sandwich fold structure with a hydrophobic binding region (Figure 1.13), encompassing an aromatic benzamidine molecule from the crystallisation buffer (Morgado et al. 2012). None

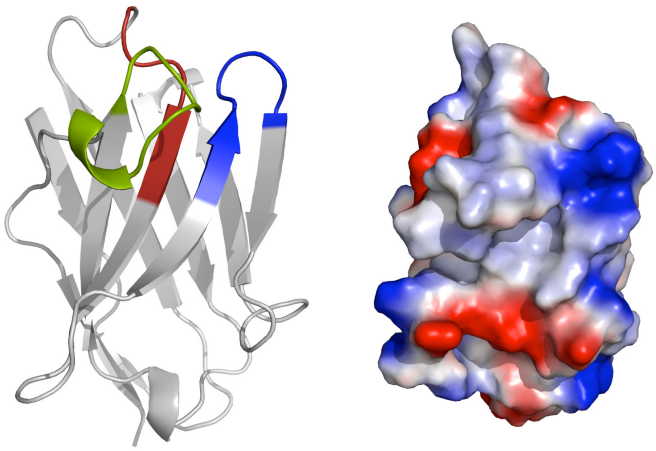

(a) *(b)*

Figure 1.13. Crystal structure and electrostatic surface of KW1. Ribbon diagram of the KW1 crystal structure; green: CDR1; red: CDR2; blue: CDR3 *(a)*. Electrostatic surface potential of the KW1 crystal structure. Blue: basic region, red: acidic region *(b)*. Images after Morgado et al. (2012), modified.

of the selected binders interacted considerably with more than one type of Aβ40 conformers; all three antibody domains are thus conformationally specific: KW1 is specific to Aβ40 oligomers, while KW2 and KW3 are specific to Aβ40 fibrils (K. Wieligmann, unpublished data).

Accumulating evidence indicates that Aβ conformers, particularly oligomers, cause Alzheimer's disease. Understanding the mode of action of KW domains may help clarify the structural differences between Aβ aggregates. In the future, this knowledge may facilitate design of disease modifying strategies. The binding characteristics of KW1, KW2, and KW3 domains will be considered in further sections of this dissertation.

Aβ40 oligomers are not the only toxic spherical conformers involved in neurodegeneration. Pathogenic relevance of Aβ42 oligomers is widely documented (e.g., Roher et al. 1996, Bernstein et al. 2009, Upadhaya et al. 2011). However, VHH domains specific to Aβ42 oligomers are lacking. Therefore, I attempted to select a VHH domain specific to Aβ42 oligomers in the course of my project.

1.8 Aims

Aβ peptide aggregation plays an important role in Alzheimer's disease. The exact assembly mechanism of Aβ, as well as the structure of the involved Aβ aggregates, is not fully understood. Accumulating evidence indicates that Aβ conformers, particularly oligomers, are the pathological agent in Alzheimer's disease. Therefore, highly specific antibodies capable of detecting, eliminating, or neutralising toxic Aβ aggregates would be extremely useful in AD diagnostics and therapy.

The aim of this thesis is to elucidate the mechanism of Aβ-antibody recognition by analysing the mode of action of selected VHH antibodies. To meet this aim, and to provide further information on the intricate structure of Aβ aggregates, I will study conformation-specific antibodies generated by means of phage display from a library of camelid VHH domains.

I will devise a method of selection for a VHH antibody directed against Aβ42 oligomers. Such an antibody will potentially be used to discriminate between different types of oligomers; it may also reveal some potential to alleviate Aβ-mediated neurotoxicity.

Furthermore, I aim to resolve the molecular basis of fibril binding by the existing VHH antibody domains. To identify the fibril-binding properties of VHH antibodies, B10, KW2 and KW3 antibodies will be analysed with a set of biochemical and biophysical methods. I will also characterise the KW1 antibody fragment to determine whether its epitope is specific to a certain oligomer type (e.g., Aβ40 or Aβ42). Molecular characterisation of Aβ specific binders will enable a comparison of their modes of action, and will supply information about surface structure of their respective Aβ ligands.

Chapter 2

Materials and methods

2.1 Basic microbiological solutions and reagents

E. coli cells were cultivated in LB or 2xYT liquid media. Propagation of the plasmids in *E. coli* cells was performed in 2xYT medium. Solid plate *E. coli* cell cultures were grown on 2% LB agar or 1.5% LB agar (Petri plates). When necessary antibiotics were added, as selection markers. Kanamycin (30 μg/ml) was used for *E. coli* cells infected with M13 helper phages; tetracycline (15 μg/ml) for *E. coli XL-1 Blue* growth, ampicillin (100 μg/ml) for growth of *E. coli* cells transformed with *p41_6His* vector or chloramphenicol (30 μg/ml) for growth of *E. coli* cells transformed with *ptetpA6H* vector. SOC medium was used for the transformation of *E. coli* cells.

TB broth was used for the cultivation and protein expression of *E. coli RV308* carrying the plasmids: *ptetpA6H_B10glu* and *ptetpA6H_B10scr*. Expression of the remaining antibody domains (i.e., B10, B10AP, KW1, KW1AP, KW2, KW2AP, KW3, KW3AP) was performed in M9 minimal media, supplemented with trace elements. Additionally, thiamine (vitamin B1) was supplemented for growth of *E. coli RV308* in M9 minimal medium. Detailed components of particular media are listed in Table 2.1.

Table 2.1. Microbiological media and their application

Medium	Medium components (per 1 L)	Application
LB	10 g tryptone, 5 g yeast extract, 10 g NaCl	*E. coli* growth
LB-agar	10 g tryptone, 5 g yeast extract, 10 g NaCl, 15 or 20 g agar	*E. coli* growth
2×YT	16 g peptone, 10 g yeast extract, 5 g NaCl	Plasmid and phage propagation
TB	12 g peptone, 24 g yeast extract, 72 mM K_2HPO_4, 17 mM KH_2PO_4	Plasmid propagation and protein expression in *E. coli*
SOB	20 g peptone, 5 g yeast extract, 10 mM NaCl, 2.5 mM KCl, 10 mM $MgCl_2$, 10 mM $MgSO_4$	Preparation of *E. coli* competent cells
SOC	20 g peptone, 5 g yeast extract, 10 mM NaCl, 2.5 mM KCl, 10 mM $MgCl_2$, 10 mM $MgSO_4$, 20 mM glucose	Plasmid transformation and growth of *E. coli*
M9	8.6 g $Na_2HPO_4{\cdot}12H_2O$, 0.5 g NaCl, 3 g KH_2PO_4, 1 g NH_4Cl, 10 ml Fe-citrate (0.023 M), 0.1 ml EDTA (0.2 M), 0.1 ml $CoCl_2{\cdot}6H_2O$ (0.1 M), 0.1 ml $MnCl_2{\cdot}4H_2O$ (0.75 M), 0.1 ml $CuCl_2{\cdot}4H_2O$ (0.1 M), 0.1 ml H_3BO_3 (0.5 M), 0.1 ml $Na_2MoO_4{\cdot}2H_2O$ (0.1 M), 2ml $Zn(CH_3COO)_2{\cdot}2H_2O$ (0.018 M), after autoclaving added: 5 ml $MgSO_4$ (1M), 20 ml glucose (2.5 M)	High yield protein expression in *E. coli*

2.2 Strains, plasmids and oligonucleotides

E. coli strains and phages used for phage display and protein expression are listed in Table 2.2. Relevant plasmids are shown in Table 2.3.

Table 2.2. *Escherichia coli* strains and phages

Strain	Genotype	Source
K12-TG1	*supE thi-1* Δ(*lac-proAB*) Δ(*mcrB-hsdSM*)5, ($r_K^-m_K^-$) F' [*traD36 proAB*$^+$ *lacI*^{q} *lacZ*Δ*M15*]	Stratagene
K12-RV308	*lac*74, *gal*IS II::OP308, *strA*	ATCC 31608
K12-XL1-Blue	*endA*1 gyrA96(nal^R) *thi*-1 *recA*1 *relA*1 *lac glnV*44 F'[::Tn10 proAB$^+$ *lacI*^{q} Δ(*lacZ*)M15] *hsdR*17(r_K^- m_K^+)	Stratagene
BL21(DE3)	F-, dcm, ompT, hsdS_B(r_B^- m_B^-), gal λ(DE3), [pLysS Camr]	Novagen
K12-ER2738	F'proA+B+ lacIq Δ(lacZ)M15 zzf::Tn10(Tet^R)/fhuA2 glnV Δ(lac-proAB) Δ(hsdS-mcrB)5 [r–kmk–McrBC–]	New England Biolab
M13KE phages	M13mp19 derivative, male-specific coliphage, peptide display as a fusion with pIII	New England Biolab
VCSM13	Helper Phage, derived from M13-K07 mutant, Kan^R	Stratagene

Table 2.3. Plasmids

Plasmid	Expressed construct	Reference
pAK 200	phagemid, VHH domains fused to gene III for presentation on M13 surface, Cm^R	Plückthun et al. (1996)
p41_6His	monovalent VHH domains, PelB signal sequence, Amp^R, Tet^R	Plückthun et al. (1996)
p41_B10_6His	B10 VHH domain, Amp^R	Habicht et al. (2007)
p41_KW1_6His	KW1 VHH domain, Amp^R	this study
p41_KW2_6His	KW2 VHH domain, Amp^R	this study
p41_KW3_6His	KW3 VHH domain, Amp^R	this study
ptetpA6H	bivalent VHH domains as PhoA fusion, PelB signal sequence, Cm^R, Tet^R	Plückthun et al. (1996)
ptet_B10_pA6H	B10 AP VHH domain, Cm^R	Habicht et al. (2007)
ptet_KW1_pA6H	KW1AP VHH domain, Cm^R	this study
ptet_KW2_pA6H	KW2AP VHH domain, Cm^R	this study
ptet_KW3_pA6H	KW3AP VHH domain, Cm^R	this study
ptet_B10glu_pA6H	B10glu_AP VHH domain, Cm^R	this study
ptet_B10scr_pA6H	B10scr_AP VHH domain, Cm^R	this study

Table 2.4 lists the oligonucleotides used in the mutation of 'amber' codon in KW2 and KW3 antibody domains.

Table 2.4. Oligonucleotides used for the replacement of 'amber' mutation

Oligonucleotide	Sequence 5' → 3'
KW3mut_fw	CTTTAGCGGTCGTCAAACTTGGTGGTTTC
KW3mut_bw	GAAACCACCAAGTTTGACGACCGCTAAAG
KW2mut_fw	GATTAATGTGGTTACTCAACGGACCTATTATGCG
KW2mut_bw	CGCATAATAGGTCCGTTGAGTAACCACATTAATC
Sfi_fw	CGCATTTCTAGATAACGAGGGCAAATCATGAAATACC
Sfi_bw	GGTTTTCCAGAACAGGCATTTCCGG

'bw': backward primer; 'fw': forward primer; oligonucleotides were provided by MWG Biotech

2.3 Standard microbiological and biochemical techniques

2.3.1 Isolation of DNA and preparation of agarose gel

DNA plasmid was isolated from *E. coli* cells with QIAprep Spin Miniprep Kit (Qiagen), according to the manufacturer instructions. DNA from the M13 phages was isolated fol-

lowing the protocol provided by the manufacturer (New England Biolab). Concentration and purity of DNA was measured with NanoDrop (Thermo Scientific). DNA fragments were electrophoretically separated on 1% agarose gel and subsequently stained with ethidium bromide. Subsequently, they were analysed with the gel imaging and documentation system (Bio Imaging System, Chemi Genius^2, Syngene). DNA fragments were extracted from the agarose gel with QIAquick Gel Extraction Kit (Qiagen).

2.3.2 Cloning, ligation and transformation

Isolated DNA plasmid was processed by digestion with *SfiI* restriction enzyme purchased from New England Biolabs GmbH. Digested DNA fragments were extracted from the agarose gel and inserted to the expression plasmids with T4 DNA Ligase (JenaBioscience, Germany). Ligated constructs were transformed to chemically competent *E. coli* cells. Competent *E. coli* cells were prepared following the Hanahan (1983) protocol. In brief, 150 ng of DNA was transformed to 200 µl chemically competent *E. coli* and incubated on ice for 30 min. Next, *E. coli* cells were subjected to a heat shock (42 °C) for 2 min, and afterwards 1 ml of SOC-medium was added. After 1 h incubation at 37 °C with vigourous shaking (600 rpm), *E. coli* cells were plated on 1.5% LB-agar and incubated overnight at 37 °C.

2.3.3 Protein expression in E. coli cells

VHH antibody domains were expressed in the periplasm of *E. coli RV308* or *E. coli BL21(DE3)* by high cell density fermentation under non-limited growth conditions (Horn et al. 1996). Initially, *E. coli* cells from a glycerine stock were inoculated to shaking flask M9-medium cultures. In order to remove all traces of complex media and adopt *E. coli* cells to growth in the minimal media, two pre-cultures were cultivated at 26 °C, until OD_{550} ~2.0. Next, pre-cultures were used for inoculation of 400 ml culture medium in the Sixfors fermenter (Infors AG, Switzerland) to the start OD_{550} ~0.2. Protein expression was triggered with 1 mM isopropyl β-D-1-thiogalactopyranoside (IPTG), when the *E. coli* cells reached OD_{550} ~60. After IPTG induction culture was growing for additional 4 h, reaching a final OD_{550} ~100. Owing to the unlimited conditions for growth (constant supply of nutrients), the *E. coli* cell culture yielded 100 g of fresh weight per 400 ml. In case of periplasmic expression, dry weigh constitutes ~20% of fresh weight. Of that, half are proteins, and 2–4% comprise recombinant antibody domains. The total yield of pure antibody domains from the 400 ml *E. coli* culture broth equals approximately 40–80 mg. *E. coli* cell pellet was harvested by centrifugation (20 min, 4 °C, 6,500 g; Beckman centrifuge Avanti J-20 XP, rotor JLA 8.1000)

and stored at –80 °C.

2.3.4 SDS-PAGE and Western blot analyses

To test the expression level of proteins, double sample aliquots were withdrawn during the fermentation process. Two samples were taken from each time point (0 h sample – before IPTG induction, 2 h and 4 h samples – after IPTG induction), six in total. Subsequently, they were tested with SDS-PAGE and Western blot (WB). All samples from the fermentation were centrifuged (2 min, room temperature (RT), 14,000*g*; Centrifuge 5415C, Eppendorf), resuspended in 20 µl of H_2O and stored overnight in –30 °C. Next day, samples were heated for 20 min in 70 °C, mixed with 4×NuPAGE lithium dodecyl sulfate (LDS) Sample Buffer (Invitrogen) and applied on the NuPAGE 4–12% Bis-Tris precast polyacrylamide gel (Invitrogen) with the protein standard (SeeBlue Plus2, Invitrogen). Electrophoresis was carried out in NuPAGE 2-(N-morpholino) ethanesulfonic acid (MES) running buffer (Invitrogen) at 180 V for approximately 35 min. When the run was completed, gel was cut into half. Half of the gel with 3 samples was further processed with WB. Remaining half was stained with Coomassie Brilliant Blue R250, followed by incubation in the destaining solution (Table 2.5).

Table 2.5. Solutions for protein detection after SDS-PAGE

Solution	Composition
Coomassie Blue	0.25% (v/v) Coomassie Brilliant Blue R250, 10% (v/v) acetic acid, 30% (v/v) ethanol
Destaining buffer	10% (v/v) acetic acid, 20% (v/v) ethanol

For the WB analysis gel was electrophoretically transferred via semi-dry blotting to polyvinylidene fluoride (PVDF) membrane, using the WB buffer (Table 2.6). Next, the membrane was blocked with 2% bovine serum albumin (BSA) in tris-buffered saline (TBS) for 1 h, washed three times with the TBS, containing 0.1% tween (TBST). Subsequent 0.5 h incubation with the primary antibody (mouse, anti-$[His]_6$ tag antibody, Qiagen), was followed by three times for 5 min washing with TBST and three times for 5 min washing with TBS. Next, membrane was incubated for 0.5 h with secondary antibody (goat, anti-mouse IgG (Fc), alkaline phosphatase conjugated, Thermo Fisher Scientific) and washed six times as described previously. Colorimetric detection was performed with PNPP (p-nitrophenyl phosphate, disodium salt), substrate (Pierce) for AP.

Table 2.6. Buffers for WB

Buffer	Composition of the buffer
WB buffer	25 mM Tris, 0.2 M glycine, in 20% (v/v) ethanol, pH 7.4
TBST	150 mM NaCl, 50 mM Tris-HCl, 0.1% (v/v) Tween-20, pH 7.4
TBS	150 mM NaCl, 50 mM Tris-HCl, pH 7.4

2.3.5 Purification of the VHH-domains (monovalent and AP-fusion)

40 g of the frozen *E. coli* cell pellet was resuspended in the disruption buffer (Table 2.7) and filtrated. Next, *E. coli* cells were disrupted in a cell homogeniser (Emulsiflex-C550, Avestin). Afterwards, 0.5% Tween was added and pH adjusted to 8.0 with 1 M NaOH. After centrifugation for 90 min at 30,000 *g* in 4 °C (BECKMAN centrifuge Avanti J-20 XP, rotor JA-14) the supernatant was filtered consecutively through 1.2 μm and 0.45 μm filtration membranes.

Protein purification was performed in two chromatography steps on an Äkta Explorer 901 system (GE Healthcare). Purification of the $[His]_6$ tag monovalent antibody domains was performed by an immobilised metal ion affinity chromatography (IMAC), followed by a reversed phase chromatography (RPC). 50 ml NiNTA (26 XK, GE Healthcare, Germany) and 20 ml Source-RPC (HR 16, GE Healthcare, Germany) columns were applied. Before loading the bacteria crude extract, columns were equilibrated with the washing buffers (Table 2.7 and 2.8). For the NiNTA column a step gradient of the elution buffer was applied. This included increasing concentrations of elution buffer: 7%–washing step, 40%–elution and 100%–final washing step. For the Source-RPC column a linear gradient of the elution buffer was applied. Collected fractions were frozen in liquid nitrogen and lyophilised (Christ, Alpha 1–4). Purity level of the proteins was checked with the SDS-PAGE and the protein concentration was measured. Pure fractions containing VHH antibody fragments were stored in –30 °C.

Table 2.7. Buffers for IMAC

Buffer	Composition of the buffer
Disruption buffer	50 mM sodium phosphate, 1 M NaCl, 20 mM imidazol, pH 8
Wash buffer	50 mM sodium phosphate, 300 mM NaCl, 20 mM imidazol, pH 8
Elution buffer	50 mM sodium phosphate, 300 mM NaCl, 250 mM imidazol, pH 8

Purification of the $[His]_6$ antibody domains fused with AP, was carried out with IMAC and ion exchange chromatography (IEC). For the IMAC, a 50 ml NiNTA column was used and a three-step gradient (10%, 40% and 100%) of elution buffer was applied. A QSepharose

Table 2.8. Buffers for RPC

Buffer	Composition of the buffer
Wash buffer	H_2O with 0.1% trifluoroacetic acid (TFA)
Elution buffer	Acetonitril with 0.1% TFA

column (anion exchanger, 16 XK, GE Healthcare, Germany) was used for the IEC; a linear gradient of elution buffer was applied. Buffers for IEC purification of the particular VHH domain differed slightly and their content is listed in Table 2.9. Purity of the proteins was checked with the SDS-PAGE, protein concentration was measured and pure fractions were frozen in liquid nitrogen and stored in –30 °C.

Table 2.9. Buffers for IEC

VHH domain	Wash buffer	Elution buffer
B10AP	20 mM Tris, pH 8.2	20 mM Tris, 2 M NaCl, pH 8.2
KW1AP	20 mM Tris, pH 7.7	20 mM Tris, 1 M NaCl, pH 7.7
KW2AP	20 mM Tris, pH 8	20 mM Tris, 2 M NaCl, pH 8
KW3AP	20 mM Tris, pH 8.3	20 mM Tris, 2 M NaCl, pH 8.3
B10glu_AP	20 mM Tris, pH 7.2	20 mM Tris, 0.5 M NaCl, pH 7.2
B10scr_AP	20 mM Tris, pH 8.2	20 mM Tris, 2 M NaCl, pH 8.2

An additional purification step was performed for the purification of the B10glu_AP. The purest fractions after NiNTA and QSepharose purification were concentrated with size exclusion filters (Amicon Ultra, Ultracel-50 K, Millipore) following the manufacturer instructions.

2.3.6 Determination of protein size, purity, and concentration of the purified proteins

The purified proteins were thermally denatured by heating for five minutes in 95 °C. Next, the size, and the level of purity was tested with SDS-PAGE, as described in section 2.3.4. Determination of the protein concentration in the solution was carried out according to method described by Gill and von Hippel (1989). Before the absorption measurement, the proteins were denatured with 6 M guanidine hydrochloride and 20 mM sodium phosphate (pH 6.5). The molar extinction coefficient was calculated based on the number of tyrosines, tryptophans and cysteines in the protein sequence (Gill and von Hippel 1989).

Alternatively, the concentration of the protein was measured with Bradford assay (Bradford 1976), which requires an acidic solution of Coomassie-dye reagent (Coomassie Brilliant Blue G-250, Bio-Rad). This dye shifts protein absorbance from 465 nm to 595 nm; the reagent

changes the colour from brown to blue upon binding with a protein. BSA was used as a protein standard for the preparation of a calibration curve. Absorption at wavelengths of 280 nm and 595 nm was measured with a UV-Vis spectrophotometer (Bio Photometer, Eppendorf).

2.3.7 Enzyme-linked immunosorbent assay (ELISA)

Streptavidin coated plates (Reacti-Bind Streptavidin High Binding Capacity Coated 96-well plates, Pierce) were used for ELISA. Prior to immobilisation of biotinylated target proteins, plates were washed three times for 5 min with TBST buffer containing 0.2% (v/v) of BSA. Next, 100 µl of biotinylated Aβ40 fibrils were applied per well, and agitated at 150 rpm for 1 h. Subsequently, two five-minute-long washes with TBST were performed. They were followed by blocking the plate with 2% BSA in the TBST buffer. Plate was agitated at 300 rpm for 1 h at RT, or alternatively, left overnight at 4 °C. Next, the plate was washed three times with TBST. 100 µl of either 0.5 µg/ml B10AP, B10glu_AP, or B10scr_AP were added per well. 1 h incubation with agitation at 150 rpm was followed by six washing steps (three times for five minutes with TBST, and three times for five minutes with TBS). To analyse the binding between antibodies and fibrils a colorimetric reaction was performed. The plate was incubated with gentle agitation (150 rpm) for 0.5 h with a substrate for AP, i.e., PNPP. The reaction was stopped by addition of 50 µl 2 M NaOH per well. The absorption was measured at 405 nm, using BMG FLUOstar OPTIMA plate reader. A blank solution (TBS buffer) was used as reference.

2.3.8 Spot blot

Nitrocellulose membranes (0.1 µm; Protran, Whatmann) were used for the spot blot assays. 30 µl of amyloid fibrils or oligomers were spotted in triplicates on two membranes. One membrane was subsequently incubated for 1 h in a 2% Ponceau S solution (Sigma-Aldrich) and washed with H_2O. Ponceau S staining was used to confirm equal protein load, and for Aβ40 oligomers and Aβ40 fibrils was set to 100% (as a full staining reference). The second membrane was blocked with a 2% BSA solution in TBST buffer for 1 h. Next, the membrane was washed two times for five minutes with TBST, followed by 1 h incubation of the membrane with antibody fragments fused with alkaline phosphatase. In case of amyloid fibrils spotted on the membrane B10AP (0.5 µg/ml), B10scr_AP (0.5 µg/ml), and B10glu_AP (0.5 µg/ml) in TBST buffer were used. KW1AP (1 µg/ml) in TBST buffer was used in case of oligomers spotted on the membrane. Next, membrane was washed three times for five minutes with the TBST buffer, and three times for five minutes with the TBS buffer.

Colorimetric reaction was developed with nitro-blue tetrazolium chloride and 5-bromo-4-chloro-3'-indolyphosphate p-toluidine salt (NBT/BCIP, Roche), which constitutes a substrate for AP. Densitometric quantification of the color intensity was performed with TotalLab software.

2.4 Selection of VHH antibody from the camelid phage library

2.4.1 Biotinylation and immobilisation of the target

B10AP was biotinylated prior to be used as an antigen for the phage display with commercial peptide libraries. 7 μM B10AP was incubated for 1 h, at RT with 15 μM of Sulfo-NHS-LC biotin (Pierce) in 10 mM Hepes buffer (pH 7.4). Reaction was quenched by addition of 10 mM Tris-HCl, pH 8.5 (5% v/v). To remove non-reacting biotin reagent, biotinylation reaction mixture was dialysed against 10 mM Hepes buffer, 150 mM NaCl (pH 7.4). Presence of one molecule of biotin per one B10AP molecule was confirmed with mass spectrometry. Another target for the phage display, biotinylated Aβ42 oligomers were prepared by mixing of N-biotinylated synthetic Aβ42 peptide (MoBiTec) with unbiotinylated synthetic Aβ42 peptide (Bachem) in a 1:10 molar ratio. Aβ42 oligomers were prepared according to preparation I and IV, as described in section 2.6.2. Prior to phage selection procedures, biotinylated proteins (B10AP or Aβ42 oligomers) were immobilised on streptavidin-coated magnetic beads (Dynabeads-280M Streptavidin, Invitrogen).

2.4.2 Phage display procedure

The recombinant, fully synthetic antibody phage library used for the VHH selection was generated in HKI by G. Habicht and M. Siegemund (Habicht 2002). Construction of the library was based on *Camelidae* VHH antibody fragments. The diversity of the phage library equalled 6×10^8; the library consisted of 10^{11} clones. VHH antibody fragments were displayed on the surface of the M13 phage as a fusion protein with pIII phage coat protein. HKI antibody library was read out by phage display. Phage display procedure includes several consecutive and repeatable steps.

First, biotinylated Aβ42 oligomers were immobilised on the streptavidin coated magnetic beads in panning buffer (Table 2.10) and agitated (500 rpm) for 1 h. Second, streptavidin beads with the immobilised antigen were blocked by 1 h incubation with 2% BSA, followed by washing with panning buffer and addition of BSA-blocked library phages, displaying VHH domains. Phages were incubated with the target for 1 h at RT, with shaking (500 rpm). Unbound phages were pulled out from the solution during 20 washing steps (ten washes with

Table 2.10. Buffers and solutions for phage display selection

Solution	Composition
Panning buffer	10 mM Hepes, 150 mM NaCl, pH 7.4
Panning buffer with Tween	10 mM Hepes, 150 mM NaCl, 0.05% Tween, pH 7.4
Elution buffer	0.1 M HCl, titration to pH 2.2 by adding glycine
Neutralization buffer	2 M Tris
Precipitation solution	17% PEG 6000, 3.3 M NaCl, 1 mM EDTA

panning buffer containing 0.05% Tween, followed by ten washes with the panning buffer only). Elution of phages bound to the target, was performed by 2 min incubation with the HCl/Glycine (pH 2.2) solution (Table 2.10).

Eluted phages were transferred to the new tube and neutralised with 2 M Tris. Phage solution was subsequently used for transfection of XL1-Blue *E. coli* cells, which were grown to OD_{550} ∼0.6. Transfected cells were incubated, without agitation for 0.5 h in 37 °C and plated on the 2% LB agar plates, containing chloramphenicol as a selection marker. On the following day, cells were scrubbed from the plates. Phages were amplified in an *E. coli* liquid culture, in presence of M13 helper phages. Expression of the phage proteins was induced with the 1 mM of IPTG. To recover the enriched phages from the XL1-Blue *E. coli* cells, phages were precipitated. First, overnight *E. coli* culture was cooled on ice for 30 min, centrifuged (20 min, 7,000 rpm, 4 °C) and the phage containing supernatant transferred to a sterile 50 ml falcon tubes, filled with 25 ml ice-cold precipitation solution (Table 2.10). Phages were precipitated by incubation with precipitation solution for 1 h , at 4 °C, followed by centrifugation (20 min, 7,000 rpm, 4 °C). Precipitated phages along the side of the tube, were resuspended in the 17 ml of the panning buffer and again precipitated by addition of 20 ml cold PEG. 1 h incubation on ice, was followed by centrifugation (20 min, 7,000 rpm, 4 °C) and final resuspension of the concentrated phages (visible precipitate on the side of the tube) in 4 ml panning buffer. Titer of the precipitated phages was determined as followed. Dilution series of the phages (from 10^3 to 10^{14}) were performed and transfected of the *E. coli* cells in the growing phase (OD_{550} ∼0.5–0.7). Transfected *E. coli* cells were incubated for 0.5 h without agitation, at 37 °C and subsequently plated on the 1.5% LB small agar plates, containing chloramphenicol as selection marker. Next, plates were incubated overnight at 37 °C. Phage titer was calculated based on the number of *E. coli* colonies, which appeared on the plates.

Precipitated library phages were used for the next selection round. The whole process of selection, precipitation, and titer determination was performed four times in total. Different

blocking reagents were used interchangeably between rounds (i.e., 2% BSA and 2% skim milk, Merck). After four rounds of selection, single phage clones were isolated. For this purpose, XL-Blue *E. coli* cells, infected with phages, were diluted and plated on several 1.5% LB agar plates. The lowest dilution (10^4–10^5) allowed the isolation of single colonies. 40 random, single colonies were further amplified; the single phage clones were precipitated, as described previously. Single phage clones were subsequently sequenced, or tested for binding to the target with phage ELISA.

2.4.3 Panning with the peptide library

B10AP, biotinylated and immobilised on streptavidin beads (Dynabeads-280M Streptavidin, Invitrogen), was used as an antigen in the selection with the peptide library. Two different peptide libraries were used. First, Ph.D.-7 library (New England Biolabs) consisted of $\sim 2.8 \times 10^9$ M13 phages, displaying a linear heptapeptide on their surface. Second library, Ph.D.-C7C (New England Biolabs), consisted of $\sim 2.8 \times 10^9$ M13 phages, displaying a disulphide-constrained, cyclic heptapeptide. Due to the oxidising conditions during the phage assembly, the disulphide bridge is created; the displayed peptide is presented as a loop on the phage surface. I performed three rounds of selection with both peptide libraries, following the protocol provided by manufacturer (New England Biolabs). After three rounds of panning, the DNA of 43 single clone phages was isolated and sequenced. Two predominant, repeating DNA sequences emerged. They were translated into amino acid sequences and synthesised chemically (EMC-microcollections).

2.4.4 Phage ELISA

Phage ELISA was carried out on streptavidin-coated plates (Reacti-Bind Streptavidin High Binding Capacity Coated 96-well plates, Pierce). The ELISA plate was coated with 100 µl of biotinylated antigen per well (2 µg of Aβ42 oligomers, or 2 µg of B10AP, dissolved in panning buffer), or with the panning buffer only (negative control). Next, plate was incubated for 1 h at RT, with shaking at 150 rpm. Prior to the blocking of the antigen with 2% BSA, the plate was washed twice with the panning buffer, each time for five minutes. Subsequently, the wells were washed three times for five minutes with the panning buffer, and the single clone phages were added (100 µl per well). Following, the plates were incubated for 1 h at RT, with shaking at 150 rpm. Afterward, the plate was washed three times with the panning buffer, and three times with the panning buffer containing 0.05% Tween. Later, each well received 100 µl of HRP anti-M13 Monoclonal Conjugate (conjugate of horseradish peroxidase with

mouse anti-M13 monoclonal antibody, GE Healthcare), diluted 1:5,000. In the next step, the plate was incubated for 1 h; six washing steps followed – three times with the panning buffer containing 0.05% Tween, and three times with the panning buffer. Finally, 100 µl of ABTS substrate solution (Roche) was added to each well. The ELISA signal was developed during the incubation of the plate for 0.5 h. The absorption was measured at 450 nm, using the BMG FLUOstar OPTIMA plate reader. A blank solution served as reference; it was derived from an identical procedure, with exclusion of the antigen (panning buffer only).

2.5 SPR analysis

2.5.1 Biotinylation and immobilisation of amyloid aggregates

Aβ40 peptide was biotinylated in a molar ratio 1:1 (biotin : amyloid peptide) with Sulfo-NHS-LC-Biotin (Pierce). Biotinylation was carried out by 1 h incubation of biotin and Aβ40 peptide in H_2O at RT. The excess of the biotin reagent was removed with RPC chromatography and biotinylation of Aβ40 peptide was verified with mass spectrometry. Prior to immobilisation of the biotinylated Aβ40 peptide on the streptavidin (SA) sensor chip surface (Biacore), disaggregation procedure was performed. 1 mg of Aβ peptide was dissolved in 2 ml 1:1 mixture of 1,1,1,3,3,3-hexafluoro-2-propanol (HFIP) and trifluoroacetic acid (TFA). After 4 h of incubation at RT HFIP and TFA were evaporated under steady stream of nitrogen. The dry peptide was dissolved in 0.15% ammonium hydroxide, vortexed vigorously and exposed to ultrasonic waves for 1 min and lyophilised. Disaggregated peptide was stored in –80 °C.

For preparation of 1:10 (biotin : peptide) biotinylated Aβ40 oligomers, 0.1 mg of biotinylated Aβ40 peptide was mixed with 0.9 mg of unbiotinylated Aβ40 peptide and resuspended in 100% HFIP, incubated for 15 min at RT, diluted 1:10 with H_2O and further incubated for 15 min. Next, larger aggregates were removed by centrifugation (15 min, 13,000 rpm, RT) and 80% of supernatant containing biotinylated Aβ40 oligomers was withdrawn. Biotinylated oligomers were immobilised on SA sensor surface (Biacore), which was activated with NHS/EDC cross-linker (Pierce).

To prepare biotinylated Aβ40 fibrils for the SPR measurements, 1 mg of Aβ40 peptide was dissolved in 50 mM Na_3BO_3 buffer (pH 9) and incubated for 1 week at RT. Biotinylation of the Aβ40 fibrils was performed in 50 mM Na_3BO_3 buffer (pH 9) with Sulfo-NHS-LC-Biotin (Pierce) in a molar ratio 1:100 (biotin : Aβ peptide). Biotinylation reaction mixture was dialysed against 10 mM Hepes buffer (pH 7.4), containing 150 mM NaCl. Biotinylated Aβ40 fibrils were immobilised on a SA chip (Biacore).

2.5.2 SPR measurements

Monovalent antibody domains (24 B10 single site mutants, KW2 and KW3) were injected on a SA chip in a series of concentrations – from 800 nM to 25 nM. Bivalent antibody domains (B10AP, KW1AP, KW2AP and KW3AP) were injected on the SA sensor in a series of concentrations – from 200 nM to 6.25 nM. Each antibody concentration was injected twice. SPR measurements were taken in 10 mM Hepes buffer (pH 7.4), 150 mM NaCl, 3 mM ethylene-diaminetetraacetic acid, 0.005% (v/v) surfactant Tween20 with Biacore 2001. aK_D was calculated based on 1:1 steady state affinity model. SPR measurements of the B10 antibody domains, in presence of P1 or P2 peptide (Table 2.11) as a competitor, were performed on the SA sensor under the same conditions as the analysis of the monovalent VHH.

Table 2.11. Conditions for the competitive SPR analysis

B10 (control)	B10 + P1 peptide	B10 + P2 peptide
800	400 + 4,000	400 + 4,000
400	400 + 2,000	—
200	400 + 1,000	—
100	400 + 500	—
50	400 + 250	—
25	400 + 125	—
–	400 + 62.5	—
–	400 + 31.25	—

Concentrations (nM) of B10, P1 and P2 peptides taken for SPR measurements

Molar stoichiometry of KW1-oligomer complexes was calculated based on the SPR measurements (maximum binding capacity of the oligomer coated sensor surface and the response level of immobilised Aβ40 oligomers) and the mass of the KW1 and Aβ40.

2.6 Preparation of the amyloid aggregates

2.6.1 Amyloid-like fibrils

Aβ40 fibrils. Recombinant Aβ40 peptide (1 mg/ml, expressed in HKI by U. Knüpfer) was dissolved in the 50 mM Hepes buffer (pH 7.4), 50 mM NaCl and incubated for 1 week in 37 °C. Alternatively, 1 mg/ml (230 μM) of synthetic Aβ40 peptide (Bachem) was dissolved in 50 mM Na_3BO_3 buffer (pH 9) and incubated for 1 week at RT.

Aβ42 fibrils. Synthetic Aβ42 peptide (0.5 mg/ml, Bachem) was dissolved in the 50 mM Na_3BO_3 buffer (pH 9) and incubated for 5 days at RT.

Ccβ fibrils. Synthetic Ccβ peptide (1 mg/ml, JPT Peptide Technologies) was dissolved in the 200 mM sodium phosphate buffer (pH 7.2) and incubated for 1 week at 37 °C (Kammerer et al. 2004).

Calcitonin fibrils. To obtain the calcitonin fibrils, 1.5 mg/ml of the calcitonin (Bachem) was incubated in 20 mM sodium acetate buffer (pH 7.5) for 1 week at RT (Reches et al. 2002).

Ure2p(10–39). Synthetic Ure2p(10–39) peptide (0.25 mg/ml, JPT Peptide Technologies) was dissolved in the 10 mM sodium phosphate buffer (pH 7.4). Fibrils formed immediately as a visible precipitate (Chan et al. 2005).

β_2-microglobulin(20–41). Fibrils were obtained by dissolving synthetic β_2-microglobulin (20–41) peptide (JPT Peptide Technologies) at a concentration of 0.25 mg/ml, in the 20% trifluoroethanol (TFE), 10 mM HCl, 1 mM NaCl buffer (pH 7.5), followed by 1 day incubation at 25 °C (Iwata et al. 2006).

2.6.2 Amyloid oligomers

Preparation I of Aβ40 and Aβ42 oligomers: Aβ peptide (1 mg) was dissolved in 450 µl of 100% HFIP, resuspended by vigourous agitation, incubated for 15 min at RT and subsequently diluted 1:10 with H_2O. After further 15 min incubation, larger aggregates were removed by centrifugation (15 min, 14,000 *g*, RT) and 80% of the supernatant containing Aβ oligomers was withdrawn (according to Habicht et al. 2007).

Preparation II of Aβ40 and Aβ42 oligomers: Aβ oligomers (0.25 mg/ml) from preparation I were subjected to stirring (using small bar stirrer) in 1.5 ml eppendorf tube containing four 18-gauge needle holes in the cap. This allowed for the slow evaporation of the HFIP and H_2O, and subsequent exposure of spherical oligomers to air-water interface. After 12 h stirring oligomers solution was transferred to a new tube (adapted from Kayed et al. 2009).

Preparation III of Aβ40 and Aβ42 oligomers: Aβ peptide (0.5 mg) was dissolved in ice-cold 100% HFIP to 1 mM final peptide concentration, incubated for 1 h at RT and for further 10 min on ice. Next, the HFIP was evaporated by overnight incubation at RT with an open lid. Subsequently, all traces of the HFIP were removed by drying down the peptide on a SpeedVac (Savant) for 10 min. Dry peptide was dissolved in 35 µl dimethyl sulfoxide (DMSO), diluted with 1.13 ml ice-cold F12 medium, without phenol red (Invitrogen) and incubated for 24 h at 5 °C. The solution was then centrifuged (14,000 *g*, 10 min, 5 °C) and supernatant containing oligomers was transferred to the new tube (adapted from Klein 2002).

Preparation IV of Aβ42 oligomers: Aβ42 peptide (1 mg) was dissolved in the 167 µl

100% HFIP, vigorously mixed and incubated with shaking (400 rpm) overnight at 37 °C. Next, the solution was sonicated for 5 min and HFIP was evaporated on a SpeedVac (Savant). The dry peptide was resuspended in 5 mM DMSO, followed by two cycles of sonication and vortexing (20 seconds each). After addition of 400 μM phosphate-buffered saline (PBS) (20 mM NaH_2PO_4, 140 mM NaCl, pH 7.4) and 2% (v/v) of SDS, solution was incubated for 6 h at 37 °C, diluted with 3 volumes of H_2O and further incubated for 18 h (37 °C). Centrifugation (3,000 *g*, 20 min, RT) was followed by sample concentration by ultrafiltration (Amicon Ultra, 30 cut-off, Millipore). To remove SDS, the last step was repeated 3 times and after each ultrafiltration, the retentate has been resuspended in 4 times diluted PBS (5 mM NaH_2PO_4, 35 mM NaCl, pH 7.4). The final solution volume (45 μl concentrated sample) was centrifuged (10,000 *g*, 10 min, RT) and supernatant containing preparation IV of Aβ42 oligomers withdrawn. Aliquots were frozen in liquid nitrogen and stored in –80 °C for a couple of months (adapted from Barghorn et al. 2005).

2.7 TEM measurements

The morphology of Aβ aggregates was assessed with TEM. Samples for TEM were negatively stained with 2% (v/v) uranyl acetate, using a droplet technique. 5 μl of an amyloid solution with a concentration of 0.1 mg/ml was placed on a formvar coated copper grid (Plano) and 5 minutes incubated. Next, the grid was washed three times by dropping it in H_2O. Washed grids were submerged into a drop of 2% (v/v) uranyl acetate solution for negative staining. Specimens were analysed with a Zeiss 902 electron microscope equipped with on a Orius SC 1000 CCD camera (Gatan) and operated at an acceleration voltage of 80 kV. 50,000× or 85,000× magnification was used for imaging.

2.8 ATR-FTIR spectroscopy

For ATR-FTIR spectroscopy measurements, Aβ40 oligomers (preparation I and II) were concentrated to 2 mg/ml with Amicon Ultra-4 centrifugation filters with 30 kDa cut-off (Millipore). Aβ42 oligomers (preparation I and II) were concentrated by centrifugation (15 min, 14,000 rpm, RT) to 2 mg/ml. Final preparations of all oligomers were examined with TEM, to confirm whether the sample was free from fibrillar aggregates. Immediately prior to analysis residual HFIP was evaporated under steady stream of N_2 for 30 min. Infrared spectra of oligomers were recorded in water. All spectra were acquired on a Bruker Tensor-27 FTIR instrument equipped with a BIO-ATR-II cell and a photovoltaic LN-MCT detector cooled

with liquid nitrogen. The final spectra are average of the 64 scans after buffer subtraction. Spectra were collected at RT with an aperture of 6 mm and at a spectral resolution of 4 cm^{-1}. The resulting spectra were processed by atmospheric compensation.

2.9 ThT fluorescent measurements

ThT spectra of amyloid fibrils and aggregating Aβ peptide were recorded at RT, with a fluorimeter (RF-5301 PC, Shimadzu), using an excitation wavelength of 482 nm. Measurements were performed in 50 mM Hepes buffer (pH 7.4) with 50 mM NaCl, in a 5-mm path length cuvette (Hellma). Every sample consisted of 20 μM ThT (Sigma) solution and 5 μM of Aβ fibrils, or 5 μM other Aβ aggregates. Aliquots of Aβ aggregates for ThT fluorescent measurements have been withdrawn every hour during the 24 h Aβ incubation assay.

2.10 Disaggregation assay

50 μM of Aβ40 fibrils were incubated with or without 5 μM of KW1AP in 50 mM Hepes (pH 7.4), 50 mM NaCl for 1 week at 37 °C. Next, samples were centrifuged (14,000 rpm, 30 min, RT) and fractionated for supernatant and pellet. The pellet fractions was resuspended in the original buffer volume. An aliquot of the sample before centrifugation, supernatant and pellet fraction were analysed with SDS-PAGE and TEM.

2.11 Aβ peptide incubation assay

0.5 mg/ml of recombinant Aβ40 peptide was incubated in 50 mM Hepes (pH 7.4), 50 mM NaCl for 24 h at 37 °C, without shaking. Every hour three equal-volume-aliquots of the Aβ40 sample were withdrawn, tested for binding to KW1AP with spot blot, analysed with TEM, and ThT fluorescence.

2.12 Site directed mutagenesis of KW2 and KW3

The TAG 'amber' stop codons from the DNA sequences of KW2 and KW3 were replaced into CAA triplet, coding for glutamine. Replacement of the stop codon was performed with a two-step PCR by using the QuickChange II XL Site Directed Mutagenese Kit (QiaGen), following the manufacturer instructions. Briefly, two different primer sets (Table 2.4) were used to introduce the point mutation into the DNA sequence of KW2 and KW3. In the first PCR cycle the point mutations were introduced and two DNA fragments for each

VHH domain generated. The second DNA cycle was performed to assemble the two DNA fragments (Figure 2.1). Proper introduction of the point mutation was confirmed by DNA sequencing. DNA of KW2 and KW3 domains without stop codons were subsequently cloned into *p41_6His* and *ptetpA6H* vectors and used for transformation of competent *E. coli RV308* cells.

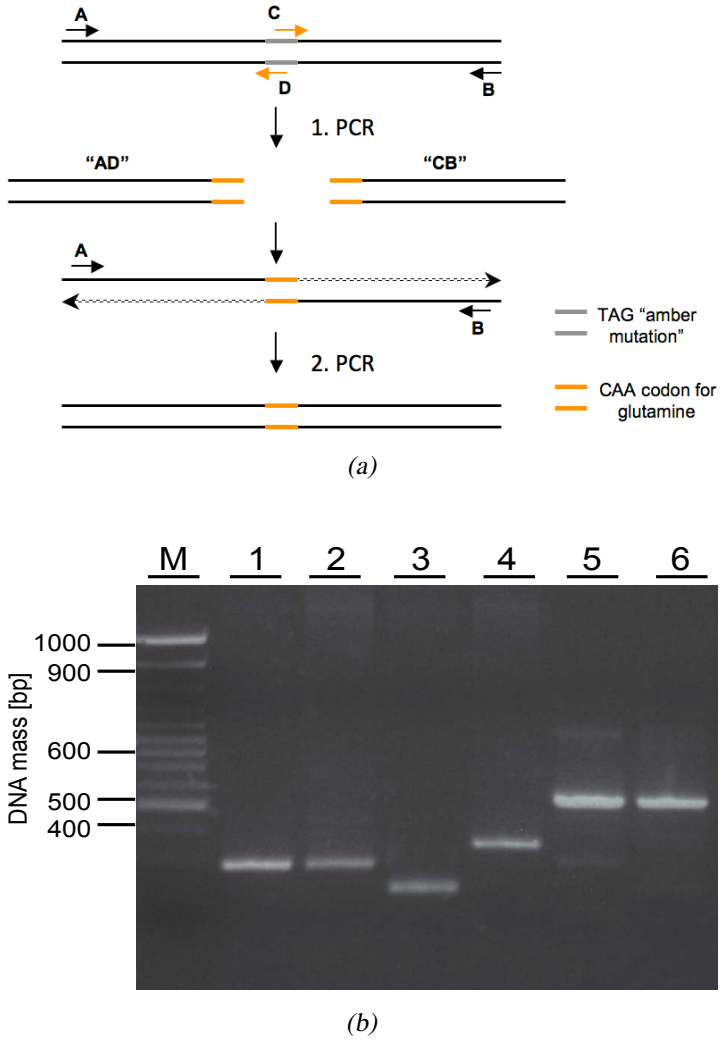

Figure 2.1. Replacement of the 'amber' codon in KW2 and KW3 DNA sequences. Two different primer sets were used in two rounds of PCR. A and B external primers (black arrows) cover whole VHH fragments and C and D internal primers (orange arrows) insert the CAA codon in place of amber codon. The primers A-D were used for the first PCR cycle. It resulted in generation of two DNA fragments void of amber codon. Second PCR was performed only with external primers (A,B) to assemble two shorter DNA fragments, which resulted in DNA coding for VHH without stop codons *(a)*. PCR fragments are visualised on a DNA agarose gel. (1) and (2): AD and CB fragments of KW2 sequence; (3) and (4) AD and CB fragments of KW3 sequence; (5) and (6) assembled DNA sequences of KW2 and KW3 respectively, containing CAA glutamine codons *(b)*.

2.13 Generation of B10 variants

Two variants of the B10 antibody fragments – B10glu and B10scr, were generated from the synthetic DNA fragments (GeneArt). The synthetic DNA fragments coding for B10glu and B10scr were cloned into *ptetpA6H* expression vectors, transformed to competent *E. coli BL21(DE3)* cells and expressed as a fusion protein with alkaline phosphatase. Large scale expression of B10glu_AP and B10scr_AP was performed in the periplasm of *E. coli BL21(DE3)* cells, in 400 ml vessels in TB medium. Purification of B10scr_AP and B10glu_AP was carried out as described in section 2.3.5.

Chapter 3

Results

3.1 Selection of an antibody fragment against Aβ42 oligomers

Oligomers are thought to constitute the most toxic Aβ species in the brain (Walsh and Selkoe 2004). KW1, an antibody fragment selected previously, is conformationally specific to Aβ40 oligomers, but does not recognise Aβ42 oligomers (Morgado et al. 2012). I attempted to select an antibody fragment directed against Aβ42 oligomers. Selection of such an antibody would enable the comparisons of the two oligomeric binders, and provide the information about the surface structure of prefibrillar Aβ aggregates.

3.1.1 Preparation and structural features of Aβ42 oligomers

I used the phage display technique to select an antibody against Aβ42 oligomers. For the purpose of the phage display selection, I prepared and characterised two variants of oligomeric Aβ42 aggregates. These two variants of Aβ42 oligomers are referred to as preparation I and preparation IV. Both oligomeric entities were presented as antigens in the VHH antibody selection process. The two antigens were used to increase the diversity presented structures, thus increasing the probability of a successful selection of an antibody fragment specific to at least one of the Aβ42 conformers.

Two different protocols were implemented to generate these oligomers. Preparation I of Aβ42 oligomers was obtained by dissolving Aβ42 peptide in HFIP. This organic solvent was shown to break down the β-sheet structure, disrupt hydrophobic forces in amyloid preparations, and in result prevent the aggregation of Aβ peptide into fibrils (Barghorn et al. 2005, Stine Jr et al. 2003). After 15 minutes of incubation, the solution was diluted 1:10 with H_2O, and incubated for further 15 minutes. Subsequently, the sample was centrifuged; the supernatant containing the oligomers was withdrawn (Kayed et al. 2003). Prepared entities were structurally analysed with TEM. An aliquot of the sample was spotted on carbon-copper

grids, and negatively stained with uranyl acetate. TEM images revealed small spherical species 5–15 nm diameter; fibrils could not be detected in this sample by negative staining (Figure 3.1a).

Preparation IV of Aβ42 oligomers was obtained by dissolving 1 mg of Aβ42 peptide in 1 ml of 100% HFIP. Subsequent evaporation of HFIP was followed by resuspention of the peptide in DMSO, sonication, and dilution with PBS to 400 μM. Next, the sample was incubated for 6 h in presence of 0.2% SDS, diluted with H_2O, and incubated for additional 18 h. Subsequently, the sample was centrifuged and concentrated by ultrafiltration; the supernatant containing the concentrated Aβ42 species (ca. 5 mg/ml) in PBS was withdrawn (Barghorn et al. 2005). Resultant Aβ42 oligomers were determined with TEM as non-fibrillar particles with diameters of 7–20 nm (Figure 3.1a).

To test their stability, the prepared oligomers were incubated at different temperatures for a certain time. Aβ42 oligomers (preparation I) were incubated in 4 °C in presence of 10% HFIP for several weeks. Their stability was tested with TEM (Figure 3.1b). Two-weeks-old samples were full of the spherical aggregates and free from fibrils, but after that time, some fibrillar aggregates started to appear. Aβ42 oligomers (preparation IV) were stable and free from fibrils for 3 days after incubation in PBS at 4 °C (Figure 3.1b). Preparation IV of Aβ42 oligomers was aliquoted, frozen in liquid nitrogen and stored at –80 °C for several weeks. Prior to further analyses, preparation IV was thawed and diluted in PBS.

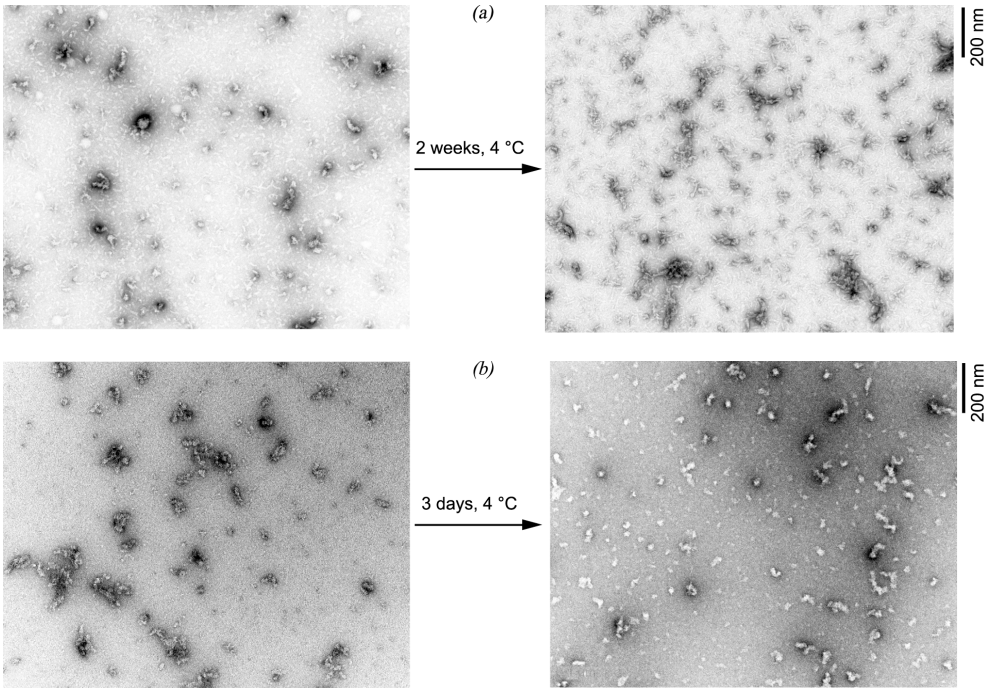

Figure 3.1. TEM images of Aβ42 oligomers visualised by negative staining. *(a)* Preparation I of Aβ42 oligomers: fresh and incubated in 10% HFIP at 4 °C for 2 weeks; *(b)* Preparation IV of Aβ42 oligomers: fresh and incubated in PBS buffer at 4 °C for 3 days.

3.1.2 Selection of the VHH domain against Aβ42 oligomers

For the selection of the binders targeting Aβ42 oligomeric states, a recombinant VHH phage library generated at the HKI was used. In order to facilitate binding to streptavidin-coated paramagnetic beads, both preparations of Aβ42 oligomers had to be biotinylated prior to the selection procedure. Biotinylation of oligomers was achieved by mixing N-biotinylated synthetic Aβ42 peptide with unbiotinylated Aβ42 peptide in a 1:10 molar ratio. Subsequently, the biotinylated Aβ42 oligomers (preparation I and IV) were prepared according to the procedures described in section 2.6.2.

Two different selection strategies were tested in order to generate a highly specific binder (Table 3.1). Both selections were carried out in presence of a competitor. A competitive selection involves usage of two antigens, of which one is immobilised and serves as a target, while the second is dissolved in the solution. Cross-reacting with the competitor, the binders are eliminated together with unbound phages during the panning procedure. Panning is defined as the incubation of the library with the target, followed by washing away of the unbound phages, and elution of the bound phages. Alternatively, competitive conditions are obtained by the immobilisation of the mock antigen, followed by a preselection panning round. Preselection is the incubation of the library with the mock target; it enables the disposal of the cross-reacting binders. Unbound phages are withdrawn, and are subsequently used in the actual selection. Selection under competitive conditions provides some unique advantages (e.g., elimination of cross-reactivity, high selectivity of the binders), which would not be possible to obtain with vaccination.

To remove unspecific binders, each selection strategy included two blocking reagents, i.e., skim milk and BSA. Those blocking reagents were used alternately throughout the panning

Table 3.1. Comparison of the first and the second selection strategy

Selection strategy	Target for preselection	Competitor in the solution	Target [μg]	Number of colonies	Phage titer
First	Aβ40 oligomers (30 μg)	Absent	Aβ42 oligomers (preparation IV) $^{I}20$; $^{II}10$; $^{III}5$; $^{IV}1$	$^{I}1.0 \times 10^{6}$ $^{II}1.2 \times 10^{4}$ $^{III}1.0 \times 10^{5}$ $^{IV}2.5 \times 10^{5}$	$^{I}2 \times 10^{11}$ $^{II}4 \times 10^{11}$ $^{III}6 \times 10^{10}$ ^{IV}single colony
Second	Aβ42 fibrils (30 μg)	Aβ42 peptide I cycle: 150 μg III cycle: 250 μg	Aβ42 oligomers (preparation I) $^{I}25$; $^{II}20$; $^{III}15$, $^{IV}10$	$^{I}1.0 \times 10^{6}$ $^{II}1.0 \times 10^{4}$ $^{III}6.5 \times 10^{5}$ $^{IV}1.0 \times 10^{5}$	$^{I}1 \times 10^{11}$ $^{II}1 \times 10^{10}$ $^{III}1 \times 10^{11}$ ^{IV}single colony

Superscript Roman numerals indicate the order of the panning cycles

cycles. The excess of blocking reagents in the solution excluded the unspecific binders: phages displaying VHH unspecific to the target bound either to skim milk or to BSA, and were subsequently washed away.

A preselection round was performed as an initial step of both selection strategies. The purpose of preselection was to exclude the cross-reacting binders from the library, because they bind to different Aβ conformers instead of the intended target. For the preselection, Aβ40 oligomers in the first selection strategy, and Aβ42 fibrils in the second selection strategy were used. The first selection consisted of four panning cycles, and was carried out in presence of a competitor in the solution. For this purpose, a tenfold surplus of freshly dissolved Aβ42 peptide (acting as the competitor) was added to the solution. Biotinylated Aβ42 oligomers from preparation IV were used as the antigen, and attached to the solid surface (streptavidin-coated paramagnetic beads). The washing steps enabled the removal of all binders that cross-reacted with the competitor (Figure 3.2). The second selection strategy also consisted of four panning cycles, but it was performed in absence of a competitor in the solution. Biotinylated Aβ42 oligomers (preparation I), immobilised on streptavidin-coated paramagnetic beads served as the antigen. Both selections were carried out in parallel. A comparison of the two selection strategies is given in Table 3.1.

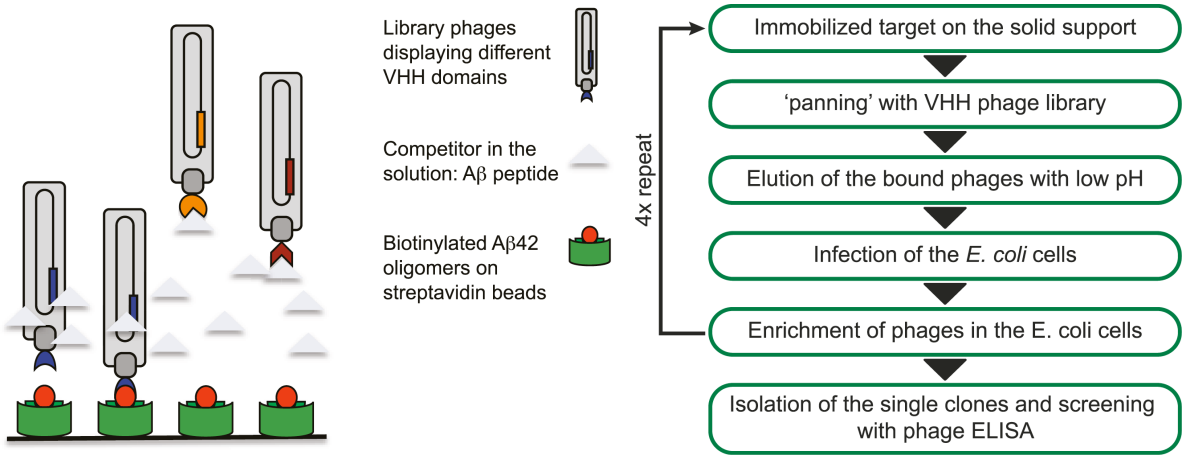

Figure 3.2. Selection in a competitive environment using the phage display procedure. Phages displaying specific antibody domain bind to the immobilised target. Unspecific phages and cross-reacting with Aβ42 peptide, are eluted in consecutive 20 washing steps *(a)*. Schematic of the phage display selection *(b)*.

3.1.3 Evaluation of the specificity of selected VHH domains

To test whether the applied procedures were successful, ten single phage clones per selection strategy were isolated. Next, phage clones were amplified in *E. coli* cells, and

tested for binding to Aβ42 oligomers with phage ELISA. The principle of phage ELISA differs slightly from a conventional ELISA. Instead of using purified antibodies, phage ELISA uses whole M13 phages carrying VHH domains. Colorimetric detection is facilitated by a secondary anti-M13 antibody, which is conjugated with HRP. Biotinylated Aβ42 oligomers, immobilised on the streptavidin-coated ELISA plates with 96 wells, were used as a target for the phage ELISA. Control wells were filled with Hepes buffer.

The results of the phage ELISA are presented in Figure 3.3. I found that the signal produced by the binding to Aβ42 oligomers was generally strong, and comparable between all of the tested clones AND the negative control (M13 helper phages). Optical density (OD) signal of the phage ELISA ranged between 0.6 and 1.2 for the binding of the isolated clones with Aβ42 oligomers. M13 helper phages also produced a strong binding signal for Aβ42 oligomers (OD=1). No significant ELISA signal was detected for the reaction between isolated clones and the Hepes buffer; OD for these wells was below 0.2.

Such high panning efficiency, with all of the isolated single phage clones binding to the target, is unlikely. Should the selection be successful, I expected to obtain a binding signal only for a few selected binders. In addition, the helper phages should not have produced a binding signal to Aβ42 oligomers, since they do not display VHH domains on their surface. Additional tests were performed to verify whether the selection was successful. Forty single

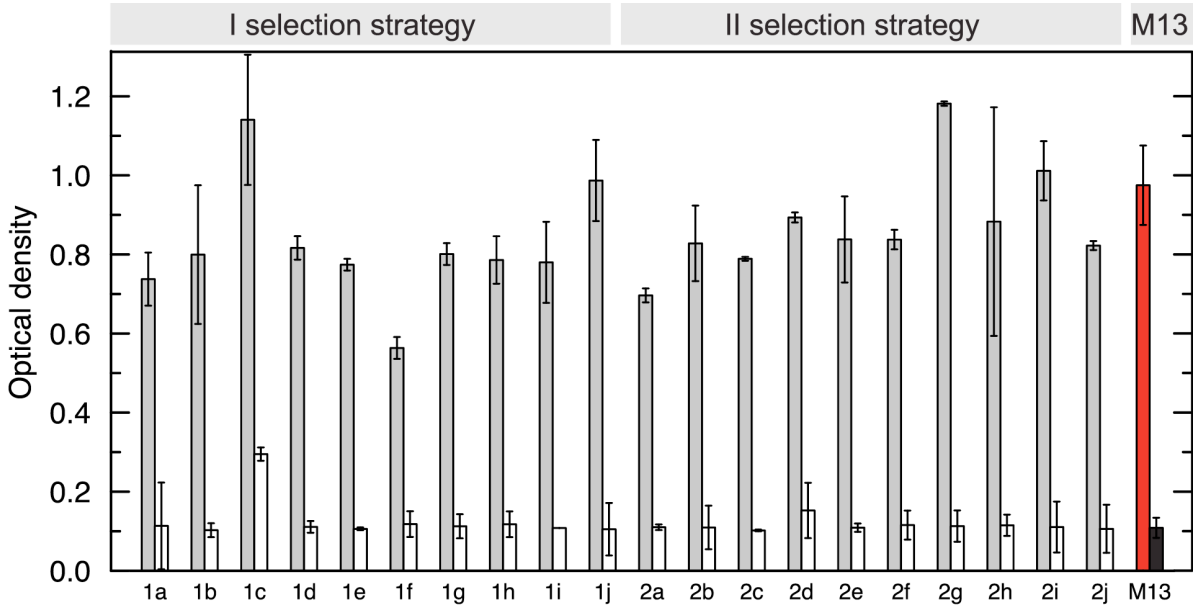

Figure 3.3. Results of the phage ELISA from two selection strategies. Grey bars: signal generated by binding of single phages to biotinylated Aβ42 oligomers. White bars: signal generated by binding of single phages to Hepes buffer (control). The binding of M13 helper phages to Aβ42 oligomers (red bar) and Hepes buffer (black bar) served as a negative control. 1a–1j: single phages isolated from the first selection strategy; 2a–2j: single phages isolated from the second selection strategy. Error bars: SD (n = 2–3).

clones which had passed the fourth round of panning (including the twenty tested with phage ELISA, and additional twenty clones picked at random) were amplified and sequenced. Analysis of their DNA sequences revealed that all of the forty selected binders were unique. In theory, selection of forty successful oligomer binders is possible, but it would result in an enrichment of their DNA sequences. M13 helper phages, used as a negative control for phage ELISA, also strongly reacted with Aβ42 oligomers. This fact suggests an unspecific interaction.

Additional phage ELISA was performed to test whether the interaction between the oligomers and M13 phages is concentration-dependent. Biotinylated Aβ42 oligomers were used as the immobilised ligand, while M13 helper phages were used as the binding partner. The aim of this experiment was to exclude unwanted cross-reactivity between M13 helper phages and Aβ42 oligomers. In the case that the interaction between Aβ42 oligomers and helper phages was dependent on oligomers' concentration, I would establish the minimum concentration at which the reaction with phages does not occur. This concentration of oligomers would be then used for the next selection procedure.

Different concentrations of biotinylated Aβ42 oligomers (preparation I and preparation IV), ranging from 2 to 0.02 μg/well, were used for the phage ELISA. Hepes buffer was used as a negative control, as it does not react with M13 phages. Interaction between Aβ42 oligomers and M13 phages was detected with the anti-M13 antibody conjugated with HRP.

Aβ42 oligomers at concentrations equal to, or exceeding 1 μg/well reacted strongly with helper phages (OD > 0.7). No interaction could be detected at concentrations equal to, or lower than 0.2 μg/well for preparation I, and at concentrations equal to, or lower than 0.1 μg/well for preparation IV. These results suggest that the interaction between oligomers and M13 helper phages is concentration-dependent (Figure 3.4). The problem of unspecific interaction between M13 phages and Aβ42 oligomers could thus be overcome by decreasing the concentration of the antigen.

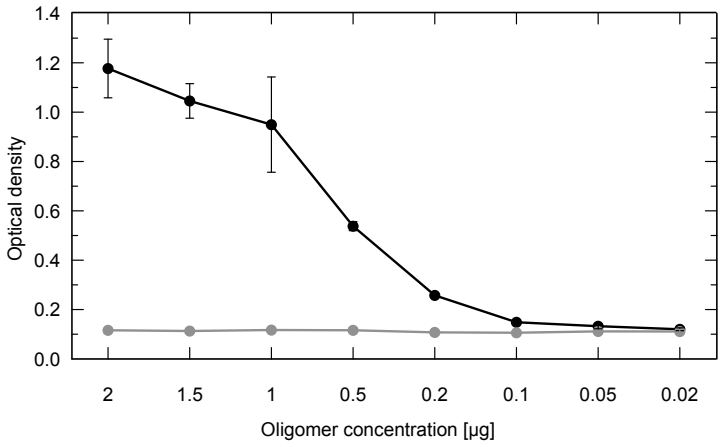

(a)

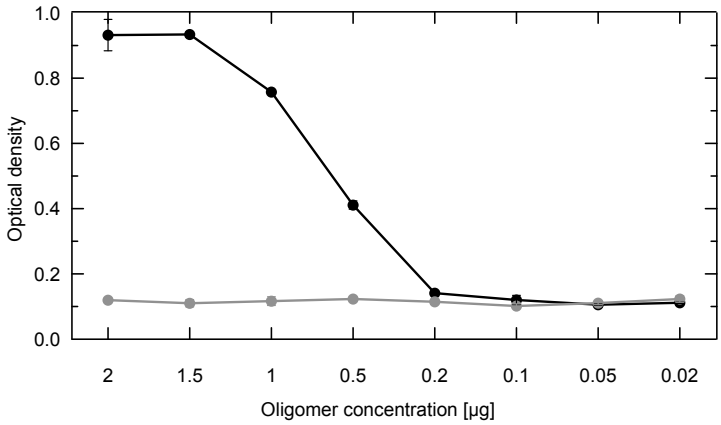

(b)

Figure 3.4. Binding of wild type M13 helper phages to Aβ42 oligomers. Black dots: concentration-dependent binding of M13 helper phages to preparations I *(a)* and IV *(b)* of Aβ42 oligomers. Grey dots: interaction of M13 helper phages with Hepes buffer. Error bars: standard deviation (SD; n = 2–3).

3.1.4 Optimisation of the selection strategy

Since both selection strategies failed to generate binders specific for Aβ42 oligomers, I performed an additional selection under modified conditions. Based on the previous ELISA results, I used between 0.5 and 0.15 µg of preparation I, and between 0.2 and 0.05 µg of preparation IV. The selections of binders specific for both preparations were carried out in parallel. The comparison of the two selection procedures is given in Table 3.2. After three panning cycles, I picked twenty clones from each selection. The clones were sequenced and tested for binding to Aβ42 oligomers with phage ELISA.

The phage display selection directed against preparation I failed to isolate a specific antibody domain. Even though DNA sequence was identical in eight of the twenty isolated clones, phage ELISA revealed that none of the twenty clones specifically interacted with Aβ42 oligomers (data not shown). A specific binder also did not emerge from the phage display selection directed against preparation IV: the sequences of all of the twenty clones were different. A strong phage ELISA signal (data not shown) between M13 helper phages

Table 3.2. The differences in conditions of selection strategies against preparations I and IV of Aβ42 oligomers.

Preparation	Amount of target	Competitor	Phage DNA sequences*	Outcome of antibody selection
I	0.5–0.15 µg	Aβ42 fibrils during preselection (20 µg)	8 identical	one VHH domain; no affinity to Aβ42 oligomers
IV	0.2–0.05 µg	Aβ42 peptide in the solution (100 µg)	all different	no VHH domain selected

* out of twenty in total.

and Aβ42 oligomers indicate the unspecific interaction.

Since both selection strategies failed to determine an antibody fragment specific for Aβ42, I proceeded to the characterisation of the existing Aβ binders.

3.2 Molecular characteristics and assessment of specificity of fibril-specific antibody fragments

3.2.1 Large-scale expression and purification of B10 and B10AP

The B10 VHH domain, directed against Aβ40 fibrils, had previously been generated with the phage display selection technique (Habicht et al. 2007). Recombinant availability of B10 facilitated the generation of the genetic fusion protein with AP; the product of the fusion was termed B10AP (Figure 3.5).

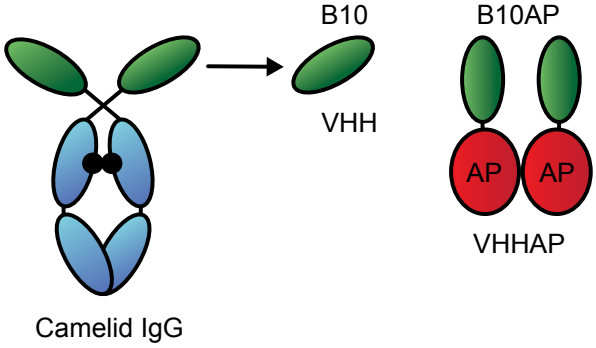

Figure 3.5. Dimerisation of the VHH domain. Schematic illustration of whole camelid IgG, VHH domain and the bivalent VHH-AP after genetic fusion with alkaline phosphatase.

B10 and B10AP were periplasmically expressed in *E. coli* cells. Large-scale expression was performed under strictly controlled conditions in 400 ml vessels, in a process called high cell density fermentation (Figure 3.6a). The expression yielded 100 g of *E. coli* cells (fresh weight). WB analyses were carried out to test the expression level of the recombinant antibody domains after each fermentation. The resultant 16 kDa and 63 kDa bands on a PVDF membrane indicated that both B10, and B10AP were successfully expressed (Figure 3.6b).

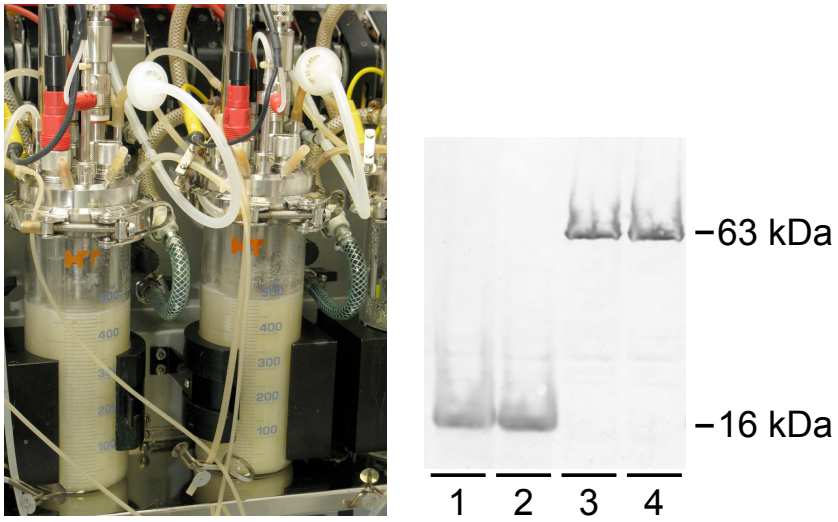

(a) *(b)*

Figure 3.6. Large-scale expression of B10 and B10AP. B10 fermentation in 400 ml vessels *(a)*. Expression of the B10 and B10AP was triggered by addition of 1 mM IPTG and visualised with WB *(b)*. 63 kDa bands correspond to B10AP (line 1 and 2). B10 is represented as a 16 kDa bands (line 3 and 4); lines 1 and 3 show expression level two hours after IPTG induction; lines 2 and 4 show the expression four hours after addition of the IPTG. The fermentation was carried out in collaboration with Uwe Knüpfer (HKI, Jena).

NiNTA and RPC chromatographic columns were used to purify B10; B10AP was purified with NiNTA and QSepharose columns (see section 2.3.5 for the detailed conditions). The two-step purification produced pure B10 domains; their purity was confirmed with SDS-PAGE under denaturing conditions. The 16 kDa and 63 kDa bands on the Coomassie-stained gel corresponded to the monovalent B10 and the bivalent B10AP, respectively (Figure 3.7).

3.2.2 Screening of the B10 epitope with a peptide phage library

Several biochemical (e.g. ELISA, spot blot) and biophysical (e.g. SPR) techniques have been applied to determine the conformational specificity of B10 to Aβ40 fibrils (Habicht et al. 2007). However, the B10 epitope and the detailed binding mechanism remained unclear. I aimed to acquire more precise information about the B10 epitope with the use of two commercial peptide phage libraries. Both libraries consisted of 10^9 unique seven amino-acid sequences displayed on the surface of the M13 phages. The first of those libraries was a 'cyclic' library, where each peptide was constrained by a cysteine disulphide bridge, and displayed in a loop form (Figure 3.8a); in the second, 'linear' library, each peptide was displayed in a linear form (Figure 3.8b).

B10AP served as bait for the peptide ligand selection. Immobilisation of the antigen is required for phage display. It was achieved in the following way: B10AP was N-terminally

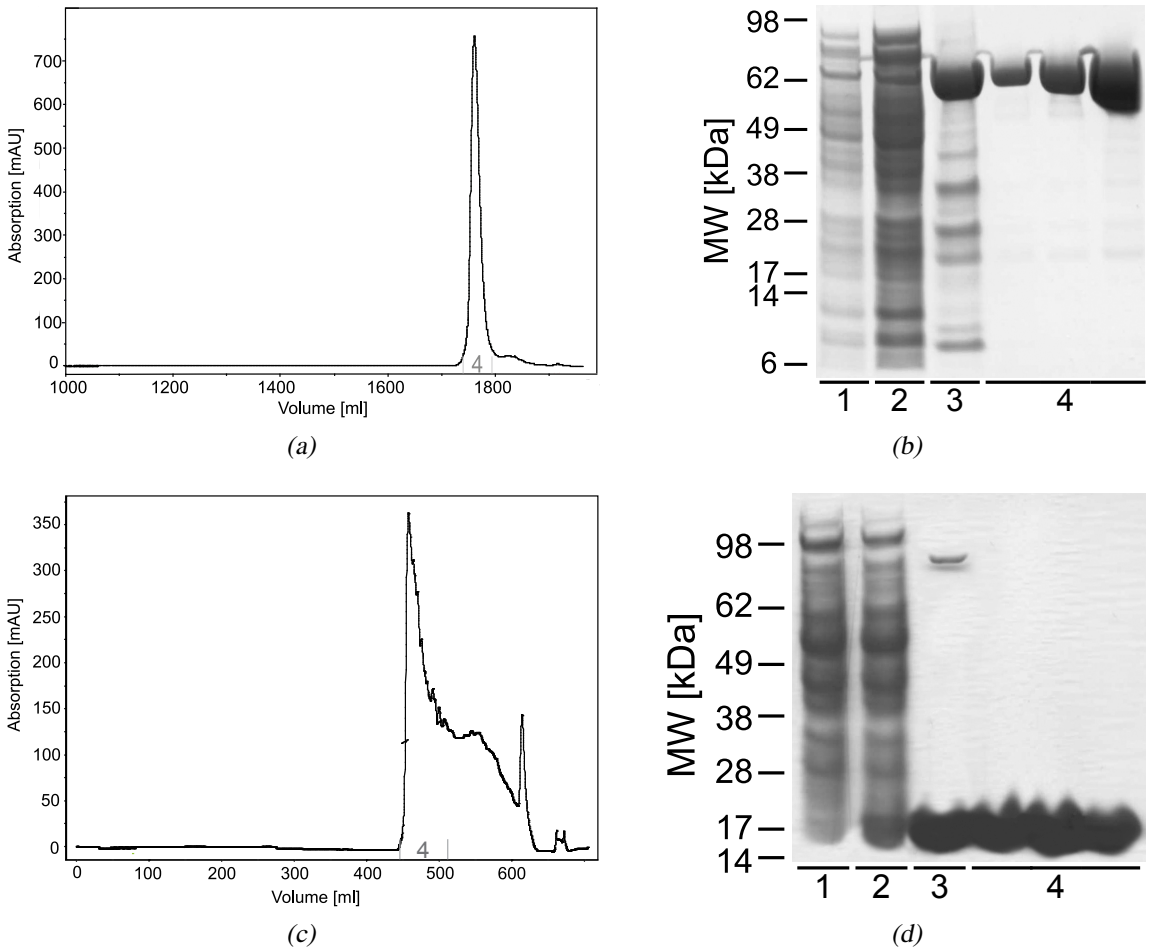

Figure 3.7. Purification of B10AP and B10. Chromatograms obtained after final purification steps of B10AP *(a)*and B10 *(c)*. The coomassie-stained gels after two-step purification of B10AP *(b)*and B10 *(d)*. Lines on the gels: 1: lysate; 2: flow through after NiNTA; 3: eluate after NiNTA; 4: eluate after IEC ∼63 kDa B10AP protein *(b)*, and eluate after RPC ∼16 kDa B10 protein *(d)*. MW: molecular weight.

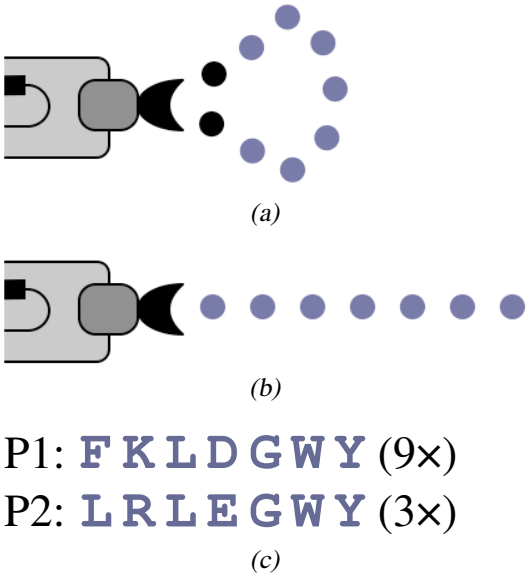

Figure 3.8. Selection with peptide libraries. Schematic illustration of the cyclic peptide library: seven amino acid peptide (slate circles) is constrained by two cysteines at the end (black circles) and displayed on M13 surface as a loop *(a)*, and linear library: seven amino acid peptide (slate circles) displayed in a linear way on the M13 phage tip *(b)*. Two peptide sequences (P1 and P2) selected from the cyclic library after three rounds of panning *(c)*.

biotinylated prior to the selection procedure (as described in section 2.4.1), and immobilised on streptavidin-coated paramagnetic beads. Three rounds of panning were performed with each of the two libraries. To test whether the selection was successful, the DNA of forty individual M13 phage binders (twenty from each library) was isolated and sequenced.

The DNA sequences of all of the clones from the linear library were unique. In contrast, panning with the cyclic library selected two predominant binding motifs, i.e., two sequences appeared more than once among the twenty sequenced clones. These two DNA sequences were translated into their respective amino acid sequences; they are referred to here as P1 and P2 (Figure 3.8c). Among the twenty clones from the cyclic library, P1 occurred nine times, while P2 appeared three times. P1 and P2 peptides were synthesised chemically, and checked for binding to B10 with SPR.

To test whether selected peptides can inhibit the binding of B10 to amyloid fibrils, competitive conditions were chosen for the SPR study. Prior to the injection of B10 onto the fibril-coated SPR chip, a 400 nM sample of B10 was mixed with various concentrations of P1; these concentrations ranged between 31.25 and 4000 nM. Subsequently, the interaction of the mixture with Aβ40 fibrils was tested. The strength of the B10-fibril interaction was independent of the concentration of P1; similar SPR signals were produced by a sample of B10 mixed with P1, and by an untreated sample of B10. Clear differences in the SPR signal were observed for the variants with various B10 concentrations (Figure 3.9a), but the SPR signal was not changed by the addition of P1 (Figure 3.9b). In the case of the P2 peptide, only one concentration was tested; 4 μM were combined with a 400 nM sample of B10, and examined for binding to Aβ40 fibrils. Similarly to P1, no effect was found on the B10-fibril interaction (Figure 3.9c). SPR analysis did not confirm that the binding of the selected peptides to B10 was specific. This indicates that the seven amino-acid ligands were insufficient to inhibit the binding of B10 to Aβ40 fibrils, and to define the structural epitope of B10.

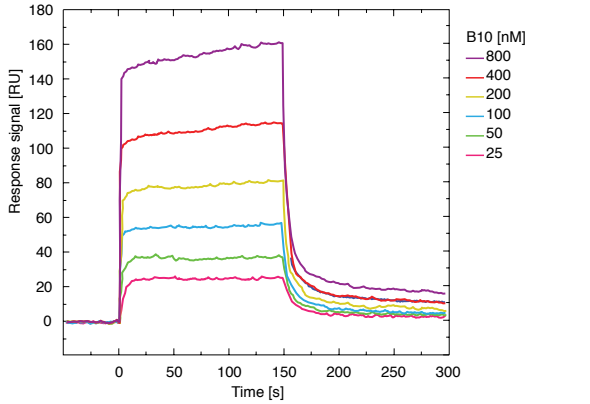

(a)

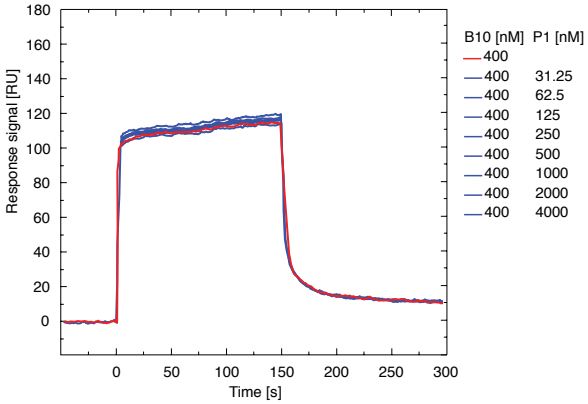

(b)

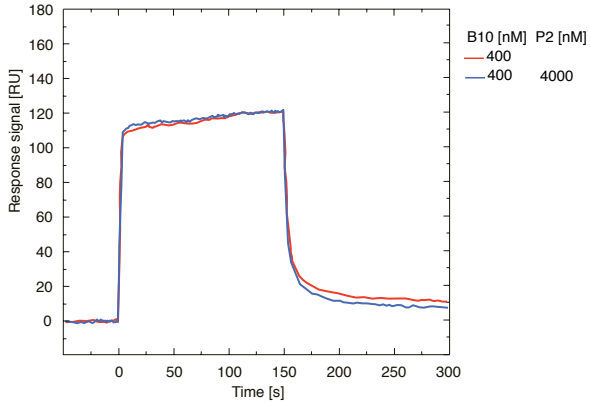

(c)

Figure 3.9. Effect of P1 and P2 peptides on the binding of B10 to Aβ40 fibrils. SPR response curves of the B10 binding to Aβ40 fibrils *(a)*. SPR responses from the interaction of the B10-P1 mixture with fibrils *(b)*. SPR responses from the interaction of the B10-P2 mixture with fibrils *(c)*. SPR studies were performed in collaboration with Peter Hortschansky (HKI, Jena).

3.2.3 Characterisation of the B10 binding specificity

In order to test the binding properties of B10, several different amyloid or amyloid-like fibrils (Table 3.3) were prepared, and characterised structurally. All of the tested fibrils possess a generic amyloid backbone structure, as verified with ThT fluorescence, X-ray diffraction, or ATR-FTIR spectroscopy. However, they vary with regard to length of the polypeptide chains (full-size proteins and peptide fragments), general morphology (curvilinear, worm-like fibrils, or straight fibrils), chirality of the polypeptide backbone (peptide consisting of D-amino acids or L-amino acids), handedness of the fibril supertwist (left handed or right handed), and presence of parallel or antiparallel β-sheet structure. Furthermore, some of the analysed fibrils are associated with diseases (e.g., hSAA or transthyretin), while others are not (e.g., glucagon or apomyoglobin fibrils). The fibrils are depicted in Figure 3.10, and their characteristics are summarised in Table 3.3.

To assess the specificity of B10AP to previously analysed fibrils, a spot blot analysis was performed. For the spot blot assay, amyloid and amyloid-like fibrils were immobilised on a nitrocellulose membrane, and tested for binding to B10AP (Figure 3.11). The alkaline phosphatase moiety of B10 facilitated a colorimetric detection of B10 binding to fibrils,

Table 3.3. Characteristics of amyloid or amyloid-like fibrils

Polypeptide chain component	Characteristic features	No. of negatively charged residues	Conditions of preparation
Aβ40	Long, straight	7 out of 40	1 mg/ml; 50 mM sodium borate pH 9.0 RT; 7 d
Ccβ	Short, straight	6 out of 17	1 mg/ml; 200 mM sodium phosphate pH 7.2; 37 °C; 7 d
Aβ(16–22)	Long, straight	1 out of 7	0.5 mg/ml; H_2O; pH 7.4 10 mM sodium azide; RT; 10 d
Insulin	Long, straight	4 out of 51	1 mg/ml; H_2O pH 2.0; 60 °C; 2 d
Glucagon	Long, straight	3 out of 29	1 mg/ml; 50 mM sodium phosphate pH 3.0; 4 °C; 2 d
Apomyoglobin	Short, curvilinear	21 out of 153	1 mg/ml; 50 mM sodium borate pH 9.0; 65 °C; 7 d
G-Helix	Long, straight	1 out of 18	1 mg/ml; 50 mM sodium borate pH 9.0; 60 °C; 7 d
L-hSAA(1–12)	Long, straight	2 out of 12	10 mg/ml; 10% acetic acid pH 2.0; RT; 1 d
D-hSAA(1–12)	Long, straight	2 out of 12	10 mg/ml; 10% acetic acid pH 2.0; RT; 1 d
hSAA(2–21)	Short, straight	3 out of 20	10 mg/ml; 50 mM sodium phosphate pH 1.0; RT; 4 d
hSAA	Short, curvilinear	16 out of 104	10 mg/ml; 50 mM sodium phosphate pH 1.0; RT; 4 d
mSAA	Short, curvilinear	16 out of 103	5 mg/ml; 50 mM sodium phosphate pH 3.0; 37 °C; 2 d
Human calcitonin	Short, straight	1 out of 32	1.5 mg/ml; 20 mM sodium acetate pH 7.5; RT; 7 d
HET-s(218–289) pH 3	Long, straight	9 out of 71	1.5 mg/ml; 40 mM boric acid; pH 3.0 10 mM citric acid; 6 mM NaCl; 37 °C; 7 d
HET-s(218–289) pH 7.5	Long, straight	9 out of 71	1.5 mg/ml; 150 mM acetic acid pH 7.5 (adjusted with 3 M Tris) RT; immediate formation of fibrils
PABN1-(+7)Ala	Long, straight	28 out of 152	1 mg/ml; 5 mM potassium phosphate pH 7.4; 150 mM NaCl 1% sodium azide; 37 °C; 30 d
Ure2p(10–39)	Short, straight	2 out of 30	0.25 mg/ml; 10 mM sodium phosphate pH 7.4; RT; immediate fibril formation
β2-microglobulin (20–41)	Long, straight	3 out of 22	0.25 mg/ml; 20% TFE; 10 mM HCl 1 mM NaCl; pH 7.5; 25 °C; 1 d

eliminating the need to use a secondary antibody. Equal loading of the fibrillar proteins on nitrocellulose membrane was confirmed with Ponceau S staining.

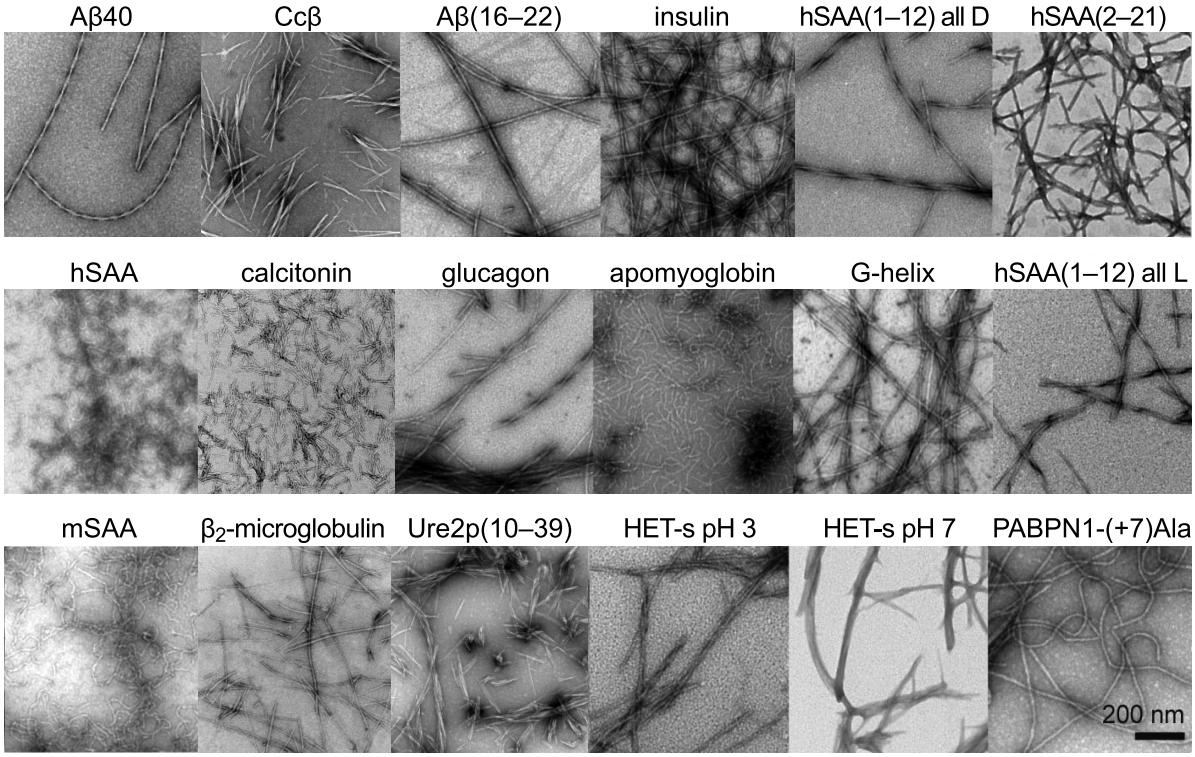

Figure 3.10. Negatively stained TEM images of *in vitro* amyloid or amyloid-like fibrils tested for binding to B10AP. TEM images obtained in collaboration with Christian Haupt (MPRU, Halle)

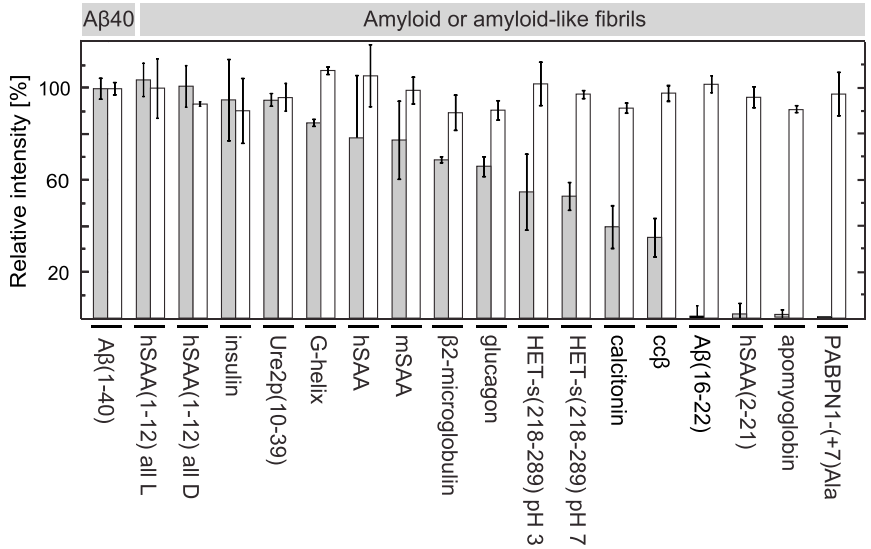

Figure 3.11. Assessment of the B10AP specificity to amyloid fibrils. Grey bars: B10AP staining; white bars: Ponceau S staining. B10AP and Ponceau S staining of Aβ40 fibrils was used as reference for full staining. Spot blot assay was performed in collaboration with Christian Haupt (MPRU, Halle).

Most of the analysed fibrils (i.e., insulin, Ure2p (10-39), G-helix, or hSAA) showed a strong interaction with B10AP, and were thus categorised as B10-positive. Such a common recognition mechanism cannot be easily explained on the morphological level, since B10 recognises long, straight fibrils (e.g., Aβ40 or glucagon fibrils), as well as short, curvilinear fibrils (e.g., mSAA or hSAA fibrils). Interestingly, B10 equally binds fibrils derived from

different polypeptide chains, as well as fibrils with opposite chirality – such as D-hSAA(1-12) and L-hSAA(1-12). However, some of the tested fibrils did not show a significant interaction with B10AP (they were categorised here as B10-negative), even though their morphological or structural features are not distinctively different to B10-positive fibrils. B10-negative fibrils also include fibrils derived from the same polypeptide chain, but from its different fragments (e.g., Aβ(16–22) or hSAA(2–21)). Furthermore, B10 binding is neither stereospecific, nor dependent solely on the presence of the parallel β-sheet structure. These observations indicate that the presence of the amyloid-backbone structure of the fibrils does not suffice to explain the B10-fibril interaction.

3.2.4 Relevance of positively charged CDRs of B10 for Aβ fibril recognition

Previous analysis of the B10 binding specificity revealed that B10 possesses a poly-amyloid-specific binding. The 23-residues-long CDRs of B10 contain nine positively charged amino acids, while negatively charged residues are absent (Figure 3.12). This suggests that ionic interactions may be involved in how B10 recognises fibrils. To examine the effect of the positively charged residues, 23 single-site B10 mutants were generated by replacing each amino acid in the CDRs with alanine (performed in collaboration with C. Haupt, MPRU, Halle). The binding of the B10 mutants to amyloid fibrils was tested with SPR: 1:100 N-terminally biotinylated Aβ40 fibrils and 1:1 biotinylated Aβ40 disaggregated peptides were immobilised on a streptavidin-coated SPR sensor chip. Various concentrations of the B10 mutants were applied, and the affinity for fibrils was measured. A steady state affinity model was fitted to the raw SPR data.

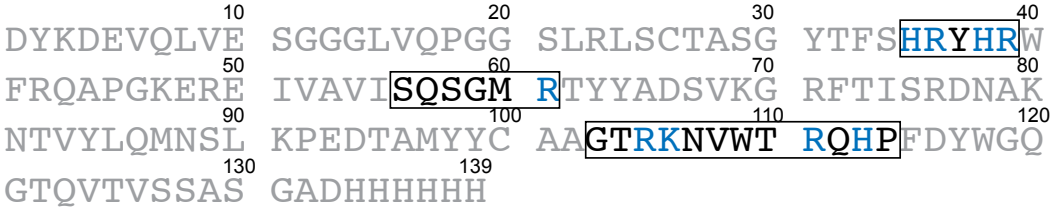

Figure 3.12. Amino acid sequence of B10. Blue: positively charged CDR residues; black: uncharged CDR residues; grey: framework residues.

We found that the aK_D of the different mutants varied significantly, with the lowest value observed for the T104A mutant (386 ± 46 nM), and the highest for the R39A mutant (2,950 ± 742 nM). These values were compared with previously determined aK_D for monovalent B10 (475 ± 54 nM). In general, it became clear that the mutations of all positively charged residues decreased the affinity of B10 to amyloid fibrils (Figure 3.13). No significant effect

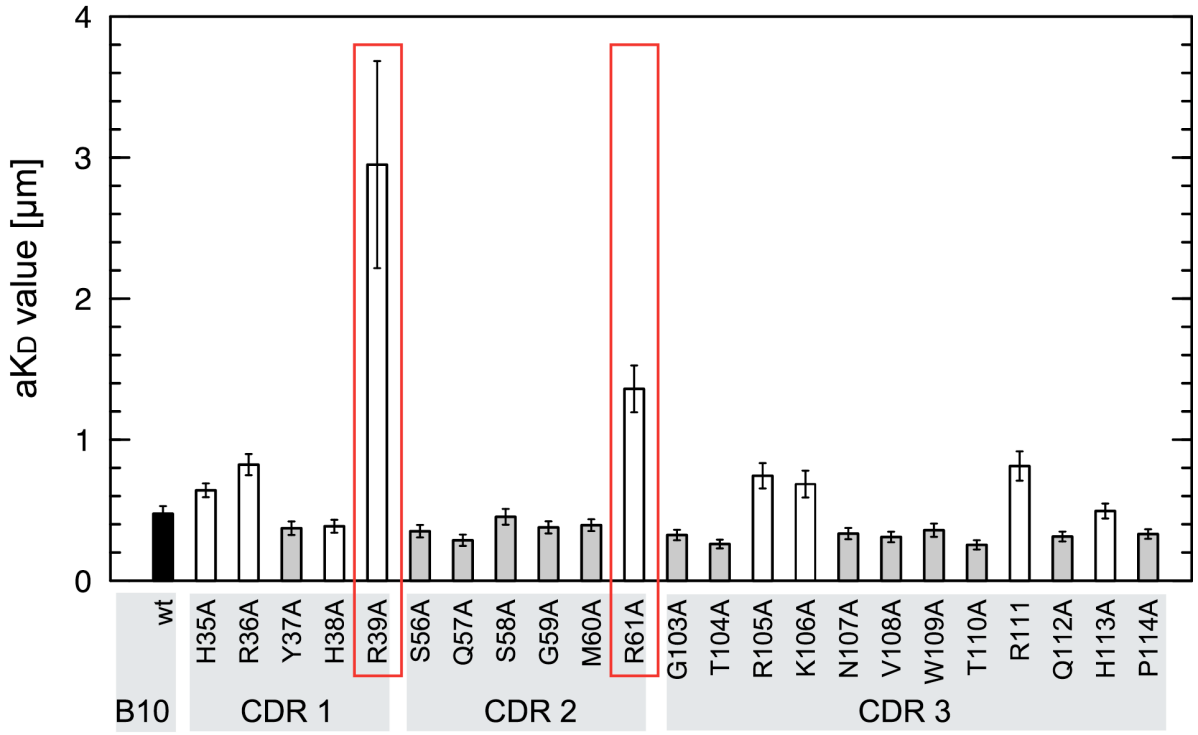

Figure 3.13. Evaluation of the B10 mutants affinity to Aβ40 fibrils. Apparent K_D for every single alanine B10 mutant was measured with SPR. White bars: basic residues; grey bars: uncharged residues; black bar: wild type B10 (control). Two mutants with the highest influence on the B10 affinity to fibrils are circumscribed in red. aK_D: apparent dissociation constant; wt: wild type. SPR studies were performed in collaboration with Peter Hortschansky (HKI, Jena).

was observed for those mutants in which an uncharged residue was replaced with alanine. The most pronounced effect was observed for two mutants: R39A (Figure 3.14a) and R61A (Figure 3.14b). Subsequently, we generated a R39/61A double mutant, and tested its binding to Aβ40 fibrils (Figure 3.14c). Its affinity for fibrils was so weak that determination of the aK_D value was not possible (Figure 3.14d). Analysis of the B10 crystal structure shows that R39 is situated within a β-strand, inside the B10 structure. Furthermore, R39 forms polar contacts with several residues within the CDR3 and thus partially stabilises it. These observations may explain the striking influence of R39A mutant on the B10 affinity to Aβ40 fibrils. Residue R61 is located on the surface of the B10 structure, and is the only basic residue within the CDR2 (Figure 3.15). The positively charged residues, present within the CDRs of B10, have a strong influence on the affinity of B10 to fibrils; this influence indicates that ionic interactions are involved in B10-fibril recognition.

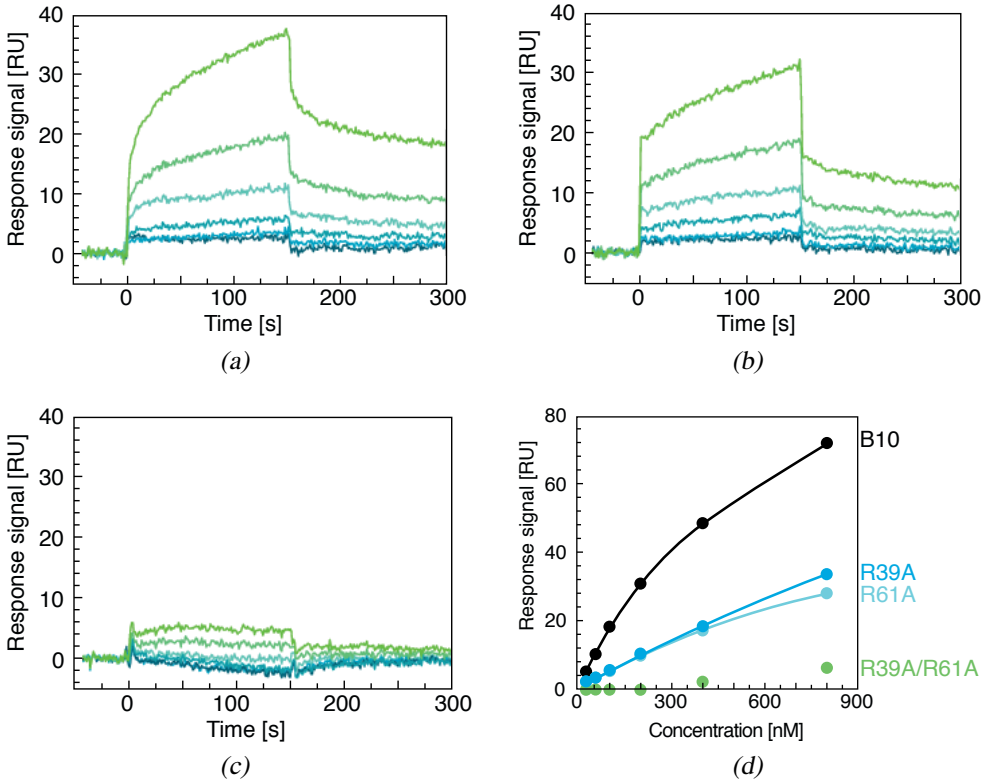

Figure 3.14. Interaction of the B10 mutants with Aβ40 fibrils. SPR response curves of the R39A *(a)*, R61A *(b)*and R39A/R61A *(c)*B10 mutants interaction with Aβ40 fibrils. Kinetic fits of the wild type B10 and its mutants R39A and R61A, provided at the steady state binding. No fit is provided for R39A/R61A mutant due to the very low response signal. Data were fitted with a steady state affinity model *(d)*.

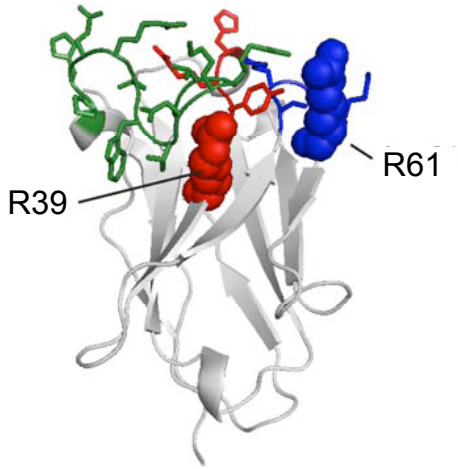

Figure 3.15. Crystal structure of B10. The positions of CDR residues R39 and R61 are shown in the B10 crystal structure. Red: CDR1; blue: CDR2; green: CDR3. In collaboration with Isabel Morgado (MPRU, Halle)

3.2.5 Analysis of the structural recognition of two B10 variants with scrambled CDRs

3.2.5.1 Generation of the two B10 variants

Two additional B10 variants were constructed to further demonstrate the relevance of the positively charged amino acids within the CDRs for fibril binding. The B10 mutants were

generated from synthetic genes, which were obtained from a commercial source.

The sequential analysis of the CDRs of B10 showed the importance of positively charged residues for the interaction with Aβ fibrils. This observation suggests the existence of an acidic potential on the surface of Aβ fibrils. However, it has previously been demonstrated that amyloid fibrils interacted with heparin, or other highly sulphated glycosoaminoglycanes. This, in turn, suggested that the surface of the fibril has basic properties (Kisilevsky 2000). Therefore, B10glu – the first variant – was designed so that all of the positively charged residues in the CDRs were replaced with glutamic acid. B10glu was generated to test the influence of the negatively charged residues in CDRs, in absence of positively charged residues, on the interaction with Aβ fibrils. The second variant – B10scr – was constructed to test the relevance of the positions of the particular amino acids. This variant contained the same amino acids within the CDRs, but their order was randomly rearranged (Figure 3.16).

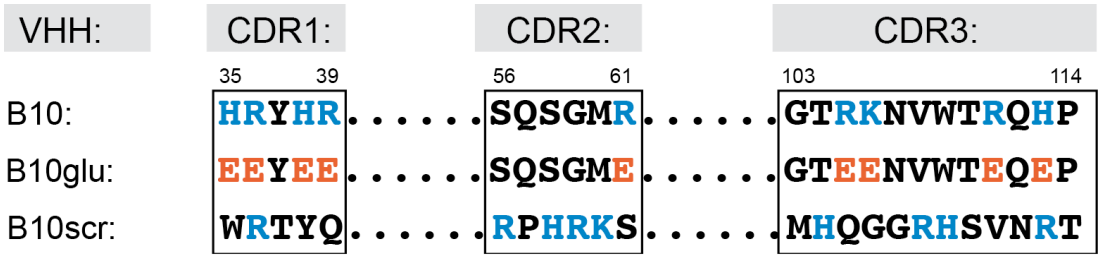

Figure 3.16. CDRs of B10 and two variants of B10. Blue: basic residues; red: acidic residues.

The obtained synthetic genes were cloned into an expression vector *ptetpA6H* for the fusion with AP. Large scale expression of B10scr_AP and B10glu_AP was carried out by means of periplasmic secretion in an *E. coli* strain *RV308*. Purification of the B10scr_AP and B10glu_AP variants was performed according to the basic protocol for B10AP; some modifications were applied wherever necessary (see section 2.3.5). The final results of the purification of both B10 variants are shown in Figure 3.17.

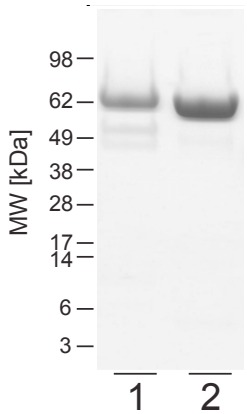

Figure 3.17. Results of the B10 variants purification. B10 variants (63 kDa) on the Coomassie-stained SDS-PAGE after ion exchange purification. Lane 1: B10glu_AP; lane 2: B10scr_AP.

3.2.5.2 *Analysis of the interaction of B10 variants with Aβ fibrils*

Spot blot and ELISA assays were carried out to analyse the binding properties of the B10 variants. For the spot blot assay, Aβ40 fibrils were spotted on a nitrocellulose membrane. Ponceau S staining was performed to confirm equal protein load on the membrane; Aβ40 fibrils were taken as the reference for maximum staining (Figure 3.18). Subsequently, the membrane was incubated with B10scr_AP, B10glu_AP, and B10AP. B10AP staining of Aβ40 fibrils was defined as the reference for maximum staining. The analysis showed that staining intensity of Aβ40 fibrils with B10scr_AP is as strong as with B10AP. In contrast to B10scr_AP, B10glu_AP variant showed significantly reduced staining intensity of fibrils – only 20% of that obtained with B10AP.

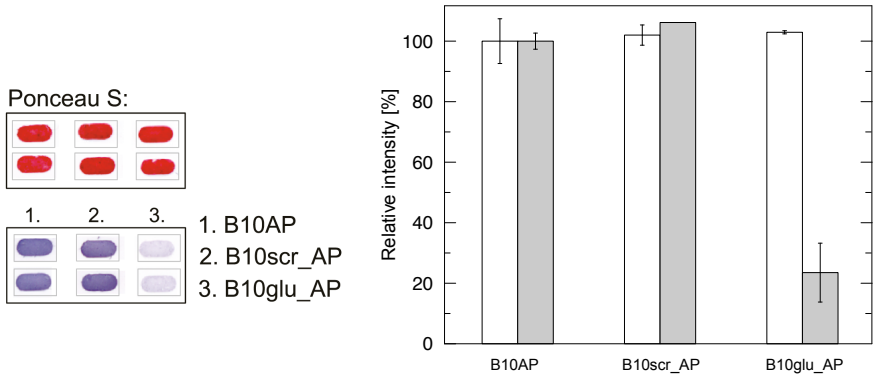

(a) *(b)*

Figure 3.18. Spot blot assessment of the B10 variants interaction with Aβ40 fibrils. Staining of Ponceau S or B10AP and its variants to Aβ40 fibrils as indicated (duplicates shown) *(a).* Quantified Ponceau S and B10 variants staining intensities. White bars: staining of Aβ40 fibrils with Ponceau S. Grey bars: staining level of B10AP, B10scr_AP and B10glu_AP to Aβ40 fibrils *(b).*

The removal of the basic residues prevented B10 binding to the fibrils. This result confirmed the importance of the positively charged residues within CDRs for the B10-fibril recognition. However, it came as some surprise that the different arrangement of the amino acids within the CDRs of the B10scr_AP did not affect its affinity to fibrils. This demonstrates that the B10scr_AP mutant, despite of a different conformational arrangement, is a functional antibody which binds to amyloid fibrils.

To confirm the interaction between the B10scr_AP and Aβ40 fibrils, and the lack of the interaction for B10glu_AP, an ELISA study was performed. Four different amounts of biotinylated Aβ40 fibrils were immobilised on a streptavidin-coated ELISA plate, and incubated with B10AP, B10scr_AP and B10glu_AP. The ELISA signal was developed by colorimetric detection of the AP moieties (Figure 3.19). The most intense B10AP and B10scr_AP signals were produced with the highest amounts of Aβ40 fibrils. The strength

of the ELISA signal was slightly weaker at lower amounts of fibrils. Almost no interaction between fibrils and B10glu_AP was detected, regardless of their concentration. Therefore, the ELISA results fully confirmed the spot blot analysis.

Both analyses indicated that not the actual arrangement of the basic residues within the CDRs, but their presence alone is key to the interaction with the fibrils. The presence of several basic residues, and formation of a highly basic surface potential, are necessary for the B10-fibril binding to occur.

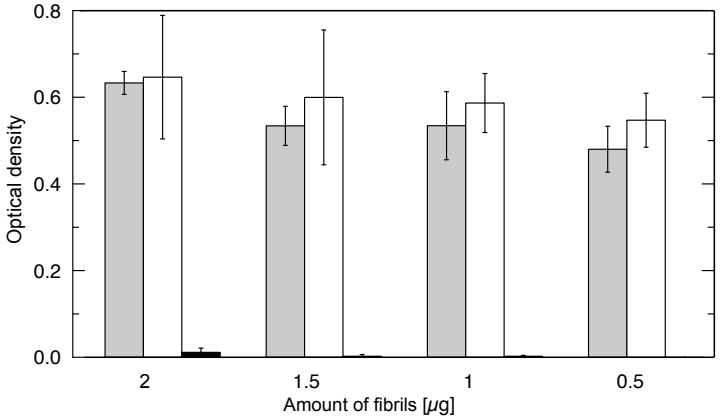

Figure 3.19. Examination of binding of the B10 variants to Aβ40 fibrils with ELISA. Binding of B10AP (grey bars), B10scr_AP (white bars) and B10glu_AP (black bars) to Aβ40 fibrils. Labels at the bottom indicate the amounts of the fibrils per well.

3.2.6 Investigation of KW2 and KW3 VHH domains

3.2.6.1 Generation of functional KW2 and KW3 VHH domains

Apart from B10, two other Aβ40 fibril specific binders were generated *in house* from the HKI library. They were termed KW2 and KW3 VHH domains. I compared the KW2 and KW3 with B10 to further understand the mechanism of binding of VHHs with fibrils.

It was necessary for the further analysis to express the two antibody fragments at high yields. To reach this goal, the TAG 'amber' nonsense codon was removed from the initial KW2 and KW3 coding sequences (which were obtained by phage display), and replaced with a codon for glutamine. Subsequently, KW2 and KW3 genes were cloned into expression plasmids, and expressed in the *E. coli RV308* strain as monovalent or bivalent (fused with AP) molecules. KW2, KW3 and their AP derivatives were purified as described earlier for B10.

3.2.6.2 Measurements of the affinity of KW2 and KW3 to Aβ40 fibrils

The conformational sensitivity of KW2 and KW3 to Aβ40 fibrils was established with spot blot and ELISA assays (K. Wielgmann, unpublished data). To ascertain the aK_D value of KW2 and KW3 for binding to Aβ40, SPR measurements were taken. In addition to KW2 and KW3, KW1 and B10 domains were used as a controls for SPR study; B10 served as a positive

control, while KW1 served as a negative control. The sensor chip used for the SPR analysis was coupled with Aβ40 fibrils and disaggregated Aβ40 peptide.

The aK_D values were calculated based on the SPR response signals (Figure 3.20). aK_D values calculated for the interaction between Aβ40 fibrils and monovalent VHHs were 190 ±29 nM and 186 ±28 nM for KW2 and KW3, respectively. The AP-fusions produced smaller aK_D values due to the bivalent functionality. aK_D values were 30 ±1.6 nM for KW2AP and 11 ±1.0 nM for KW3AP. These values corresponded well to the B10AP affinity for Aβ40 fibrils calculated earlier (Habicht et al. 2007). As expected, KW1 and KW1AP did not show any interaction with Aβ40 fibrils. The studied VHH domains did not produce a significant response in the flow cell with the immobilised disaggregated Aβ40 peptides. These data show that KW2 and KW3 are comparable with B10 with regard to the affinity to fibrils .

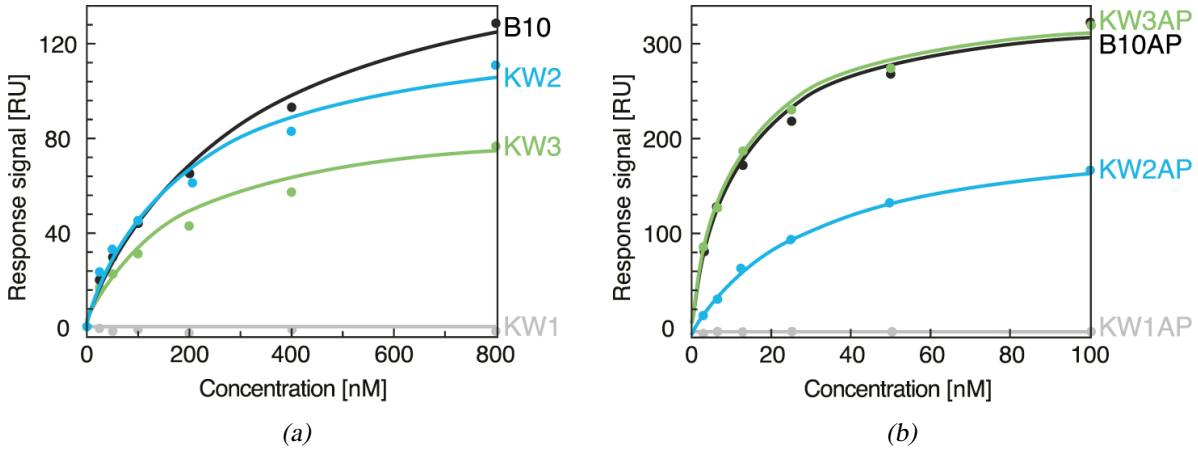

Figure 3.20. Affinity of VHH domains for Aβ40 fibrils. Different concentrations (ranging from 800 to 25 nM) of B10, KW1, KW2, KW3 *(a)*and their AP derivates - concentrations ranging from 100 to 3.125 nM *(b)*were applied on Aβ40 fibril-coated sensor chip and their binding at steady state was measured. Steady state fits (coloured lines) were obtained from the SPR responses from each VHH concentration. SPR measurements were performed in collaboration with Peter Hortschansky (HKI, Jena).

3.2.6.3 Sequence analysis of KW2 and KW3 domains

Previous analyses of B10 revealed that positively charged amino acids in CDRs are responsible for the binding to Aβ40 fibrils. To search for potential commonalities among the fibril binders, I examined the CDRs of KW2 and KW3. I found striking similarities to B10 in terms of the enrichment of the positively charged residues in the CDRs (Figure 3.21). Seven of twenty residues in the CDRs of KW2 are positively charged; four of those are arginines. In KW3, eight of twenty amino acids in CDRs are positively charged, with six arginines, one lysine, and one histidine. Negatively charged amino acids are absent in both KW2 and KW3, similarly to our previous observations of B10. In contrast to B10, however,

the CDR3 regions of KW2 and KW3 contain only nine residues, while CDR3 of B10 is longer, containing twelve residues. Moreover, the CDRs of the three examined VHHs differ in terms of the positions of the positively charged residues, as well as their occurrence in the individual CDRs (Figure 3.21). The CDR1 of B10 and KW2 contains four basic residues, whereas the CDR1 of KW3 contains a single one. Furthermore, the CDR2 of KW2 and B10 contains only one basic residue, while three basic residues occur in the CDR2 of KW3. Finally, the CDR3 of KW2 contains two basic residues, which is two fewer than the CDR3 of both B10 and KW3. Interestingly, the two most prominent positions in B10 in terms of fibril binding – R39 and R61 – are occupied by the same residues in KW2, but differ in case of KW3 by one substitution: position 39 is occupied by tryptophan instead of arginine. Despite the differences in the position of the basic residues, however, B10, KW2, and KW3 show an equally strong affinity to Aβ40 fibrils. These results emphasize the role of the basic residues in fibril binding, and indicate that the position of the basic residues within the CDR is of minor importance, unless sufficient quantity of basic residues is present.

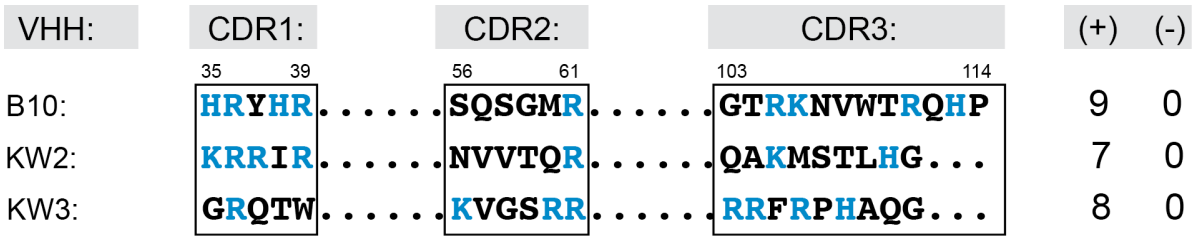

Figure 3.21. CDRs of fibril specific VHH domains. Antigen binding regions of B10, KW2 and KW3 are rich in positively charged (+) residues (marked in blue), whereas negatively charged (–) are absent.

3.3 Molecular characteristics and assessment of specificity of KW1, an oligomer-specific antibody fragment

3.3.1 Analysis of the conformational sensitivity of KW1 antibody fragment

KW1 and KW1AP, antibodies directed against Aβ40 oligomers, were also generated *in house* from the HKI library. To express KW1, it was cloned into the *p41_6His* expression vector, resulting in a monovalent VHH expression – as a single antibody domain. To generate KW1AP, KW1 was cloned into the *ptetpA6H* vector (for the bivalent expression). The cloning process was followed by recombinant expression of both VHHs in the periplasmic space of *E. coli* cells. KW1 and KW1AP were purified with two-step column chromatography, similarly to the purification of B10 (section 3.2.1). KW1 and KW1AP bind to Aβ40 oligomers, but neither to Aβ fibrils, nor to disaggregated Aβ peptide, as established with ELISA and spot bot assays (Morgado et al. 2012). The ability of KW1 to recognise a certain

structural arrangement, but not merely a polypeptide chain, qualifies it as a conformationally sensitive antibody.

To obtain the Aβ40 oligomers for the analyses of the conformational specificity of KW1, I dissolved the Aβ40 peptide in 100% HFIP, followed by dilution with H_2O (ratio 1:10), and centrifugation (see section 2.5.1 for the detailed protocol). HFIP is known to prevent aggregation of oligomers into amyloid fibrils; it also stabilises the transient oligomeric species. Prior to the investigation of the conformational specificity of KW1 to oligomers, I tested the stability of Aβ40 oligomers by incubation in a 10% HFIP solution at 4 °C for 4 weeks. Aliquots of Aβ40 oligomers were taken directly after preparation, and after the incubation. The aliquots of oligomers were negatively stained with 2% uranyl acetate and analysed with TEM. Obtained images confirmed the absence of fibrillar aggregates in the oligomeric preparations in both samples – directly after the preparation, and after the four-week-incubation period (Figure 3.22). The morphology of Aβ40 oligomers did not change significantly. This demonstrates that HFIP acts as a sort of a conformational trap, capable of stabilising the oligomers for several weeks.

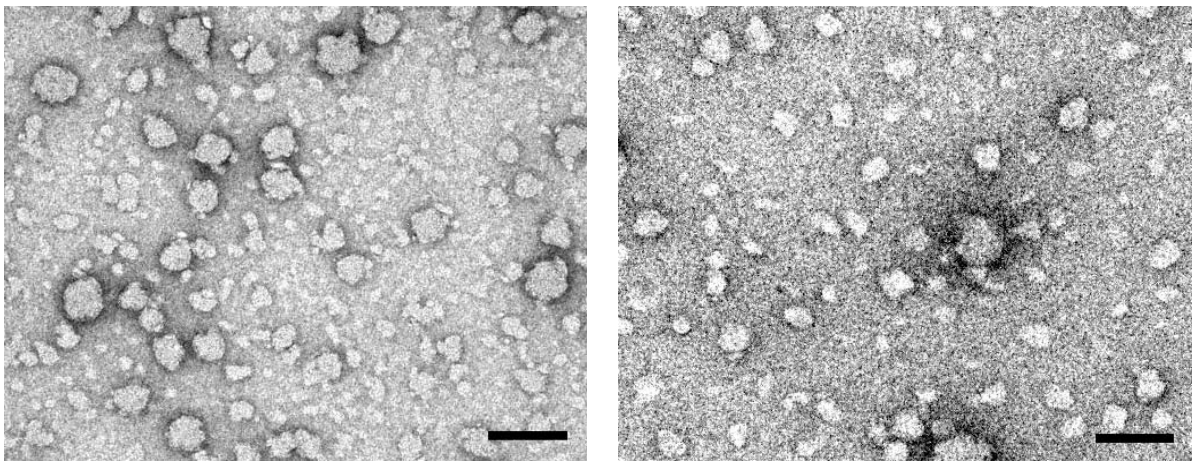

(a) *(b)*

Figure 3.22. Negatively stained Aβ40 oligomers. TEM images of Aβ40 oligomers in 10% HFIP directly after preparation *(a)*, and after four weeks of incubation period at 4 °C *(b)*. Scale bars: 100 nm.

I performed SPR measurements to further confirm the observation that KW1 binds to Aβ40 oligomers. To immobilise the target – a prerequisite for the SPR measurements – the biotinylated Aβ40 oligomers were attached to a streptavidin-coated SPR sensor chip (Figure 3.23a). To account for the transient nature of the oligomeric species, the oligomers were stabilised on the sensor chip by means of EDC-NHS cross-linking. In addition to the Aβ40 oligomers, the sensor chip was coupled with Aβ40 fibrils and disaggregated Aβ40

peptides on the other flow cell; it served as a control. Six different concentrations of KW1AP (200, 100, 50, 25, 12.5, and 6.25 nM) were applied to the sensor chip. Based on the SPR response signals, the aK_D was determined (Figure 3.23b). It equalled 43.5 ±4.9 nM for KW1AP binding to Aβ40 oligomers. Molar stoichiometry of binding, measured with SPR, equalled 1:13 (KW1:Aβ).

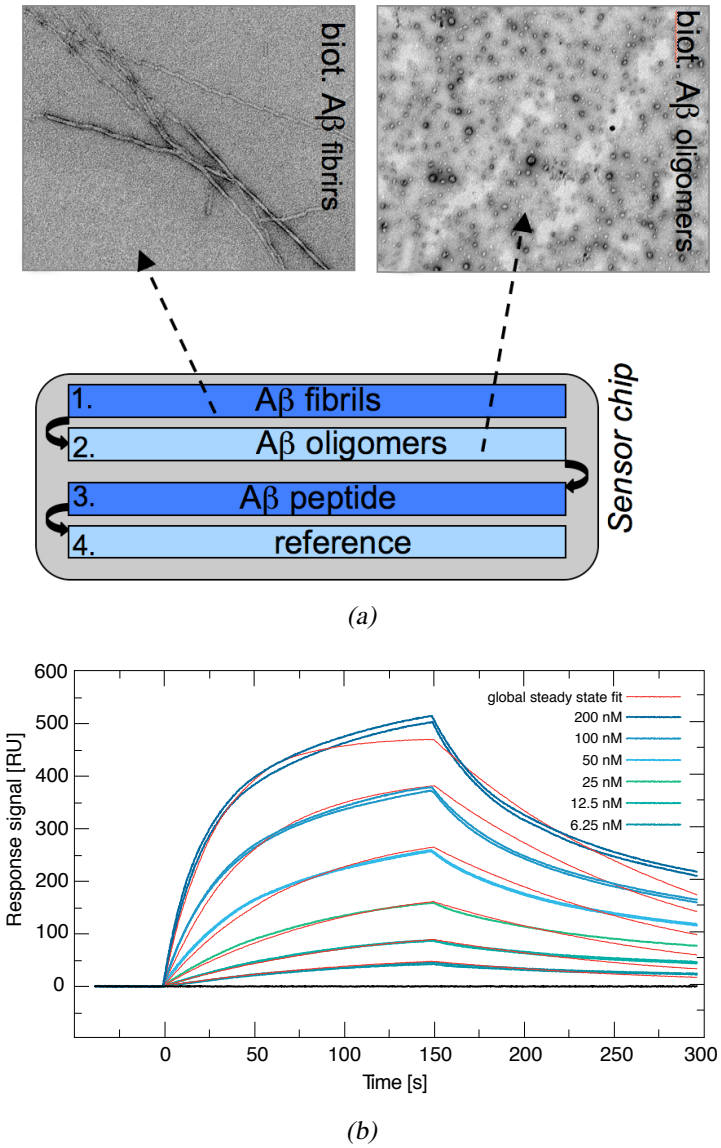

Figure 3.23. KW1AP affinity to Aβ40 oligomers. Biotinylated Aβ40 fibrils, oligomers, and disaggregated peptide were immobilised on a streptavidin-coated SPR sensor chip. Fourth flow cell served as a reference. Presence of appropriate amyloid structures was confirmed with TEM *(a)*. SPR response curves of the KW1AP binding to Aβ40 oligomers (pale blue lines). Colour indicates increasing concentration of KW1AP (from 6.25 to 200 nM). Two measurements were performed for each concentration. Red lines represent global steady state fit *(b)*. Apparent dissociation constant was measured based on the steady state affinity model. SPR measurements were performed in collaboration with Peter Hortschansky (HKI, Jena).

3.3.2 The effect of KW1AP on disaggregation of Aβ40 fibrils

KW1AP binds to oligomers, which are known to be precursors of amyloid fibrils. It has been demonstrated for other antibodies that their binding may disaggregate amyloid conformers (Solomon et al. 1997). To test whether KW1AP can dissociate the preformed Aβ40 fibrils, I carried out the following procedure: KW1AP was incubated with Aβ40 fibrils (molar ratio 1:10) in 50 mM Hepes buffer (pH 7.4) at 37 °C. As a control, Aβ40 fibrils were

kept under identical incubation conditions, except for the presence of KW1AP. After one week, the samples were centrifuged and analysed with SDS-PAGE and TEM (Figure 3.24). SDS-PAGE revealed that insoluble aggregates (pellet fraction, 4 kDa band) were present in both samples: incubated in presence of KW1AP, or in its absence. Furthermore, mature fibrils were found in both samples before centrifugation, as well as in the pellet fraction after centrifugation (as established with TEM). Soluble forms of Aβ were observed neither on the SDS-PAGE (in the supernatant), nor on the TEM images. The obtained results indicate that KW1AP does not disintegrate preformed fibrils. As indicated by the 63 kDa band on the SDS gel, KW1AP was primarily observed in the total sample before centrifugation, and in the supernatant fraction. Presence of the 63 kDa band (KW1AP) in the pellet fraction might be caused by the partial precipitation of the KW1AP, which may have resulted from the incubation at 37 °C for one week, rather than from its interaction with fibrils. These data indicate that KW1AP does not destabilise preformed Aβ40 fibrils.

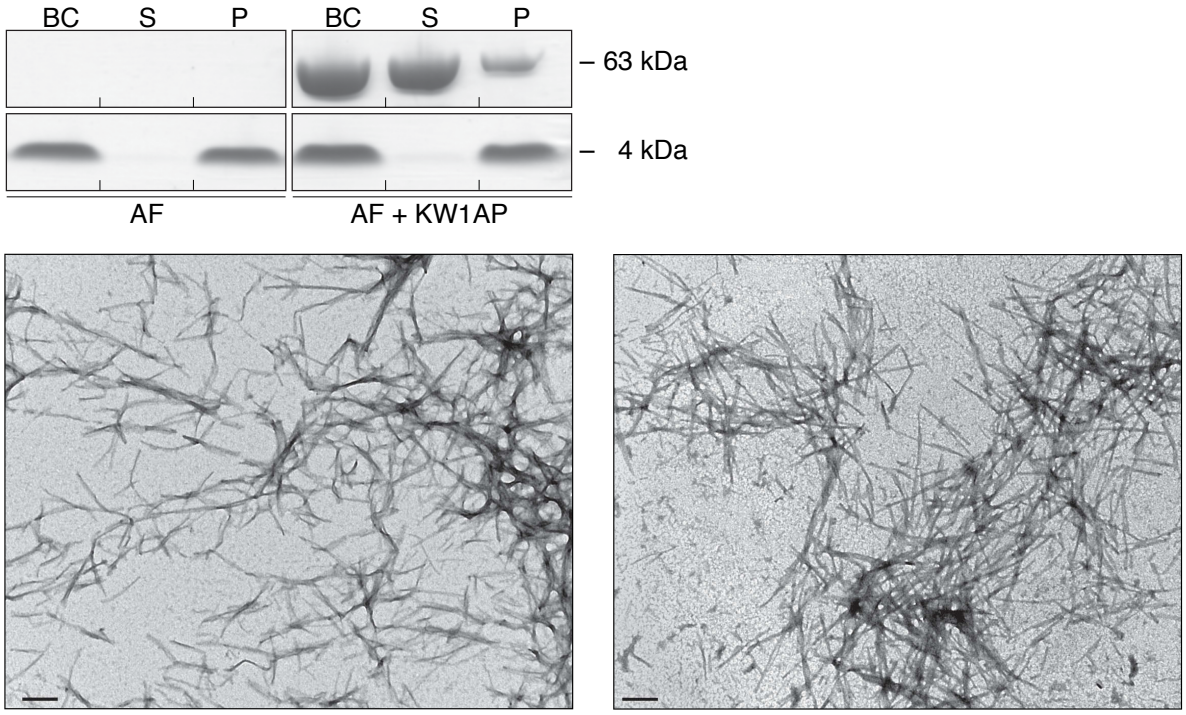

Figure 3.24. Evaluation of the potential of KW1AP to disaggregate Aβ. Aβ (4 kDa bands) and KW1AP (63 kDa bands) on the Coomassie-stained gel after one-week incubation of Aβ fibrils (AF) in presence or absence of KW1AP. Samples from the fraction before centrifugation (BC), from the supernatant (S), and from the pellet (P) are presented on the gel (top panel). Negatively stained TEM images show the presence of AF after incubation with KW1AP from the BC (bottom left) and P (bottom right) samples. Scale bar: 200 nm.

3.3.3 Investigation of the KW1AP oligomeric epitope formation

I carried out a 24 h kinetic assay to investigate KW1AP epitope formation during the β-amyloid aggregation. Initially, I verified the dynamics of Aβ40 fibril formation with ThT. It is known that the binding of ThT to Aβ40 aggregates leads to a significant increase in the ThT fluorescence (Hortschansky et al. 2005). For the purpose of this analysis, 0.5 mg/ml of Aβ40 peptide was incubated in 50 mM Hepes buffer (pH 7.4) at 37 °C for 24 h. An aliquot of the incubated Aβ sample was withdrawn every hour throughout the whole time course of the experiment. The aliquot was taken for the ThT fluorescence measurement, preparation of the TEM grids, and for the verification of the KW1AP binding with spot blot. ThT fluorescence measurements revealed a characteristic Aβ aggregation kinetic curve, split into two phases (Hortschansky et al. 2005): nucleation-dependent lag (4.5 h) and growth phase (4.5–9 h) were well resolved, and the plateau was reached after 9–10 h (Figure 3.25). Analysis of the Aβ aggregates with TEM confirmed the ThT observation. First Aβ aggregates appeared on TEM images after 4 h of incubation, which corresponds to the increase of ThT fluorescence. Mature fibrils appeared after 9 h, and were present in every TEM sample until the end of incubation period (Figure 3.26). The appearance of the fibrils on the TEM images corresponded with the plateau of the elevated ThT signal.

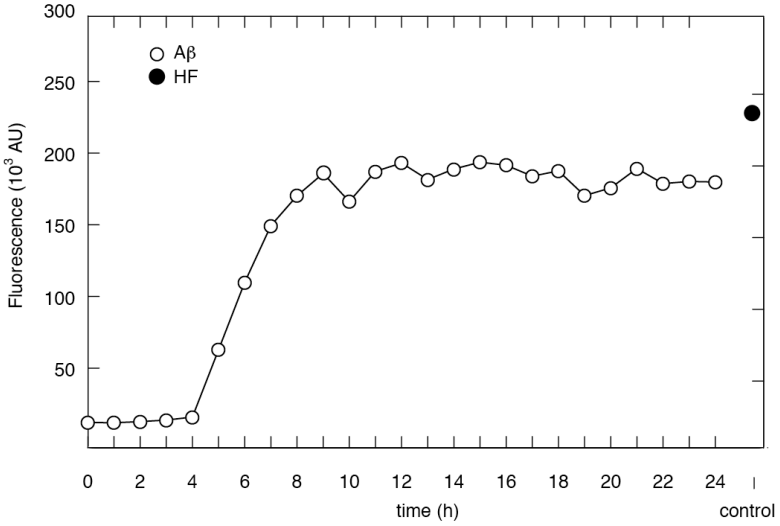

Figure 3.25. Measurements of ThT fluorescence. Aggregation of the Aβ40 peptide was monitored with ThT fluorescence (open circles). ThT fluorescence signal, recorded from mature Aβ40 fibrils prepared one week earlier was used as a positive control (solid circles). HF: mature Aβ fibrils in Hepes buffer (pH 7.4).

KW1AP moiety was used for the spot blot assessment of KW1 binding to aggregating Aβ, to eliminate the need to use a secondary antibody. In the spot blot assay, increasing staining signal from KW1AP was observed after 6 h and onwards. It peaked at 8 h (85%), and fluctuated until the end of the experiment at 24 h; the signal of Ponceau S staining was stable throughout the whole incubation period, thus confirming the equal load of Aβ proteins on the spot blot membrane (Figure 3.27).

These data indicate that the epitope which is recognised by KW1AP occurs during the Aβ

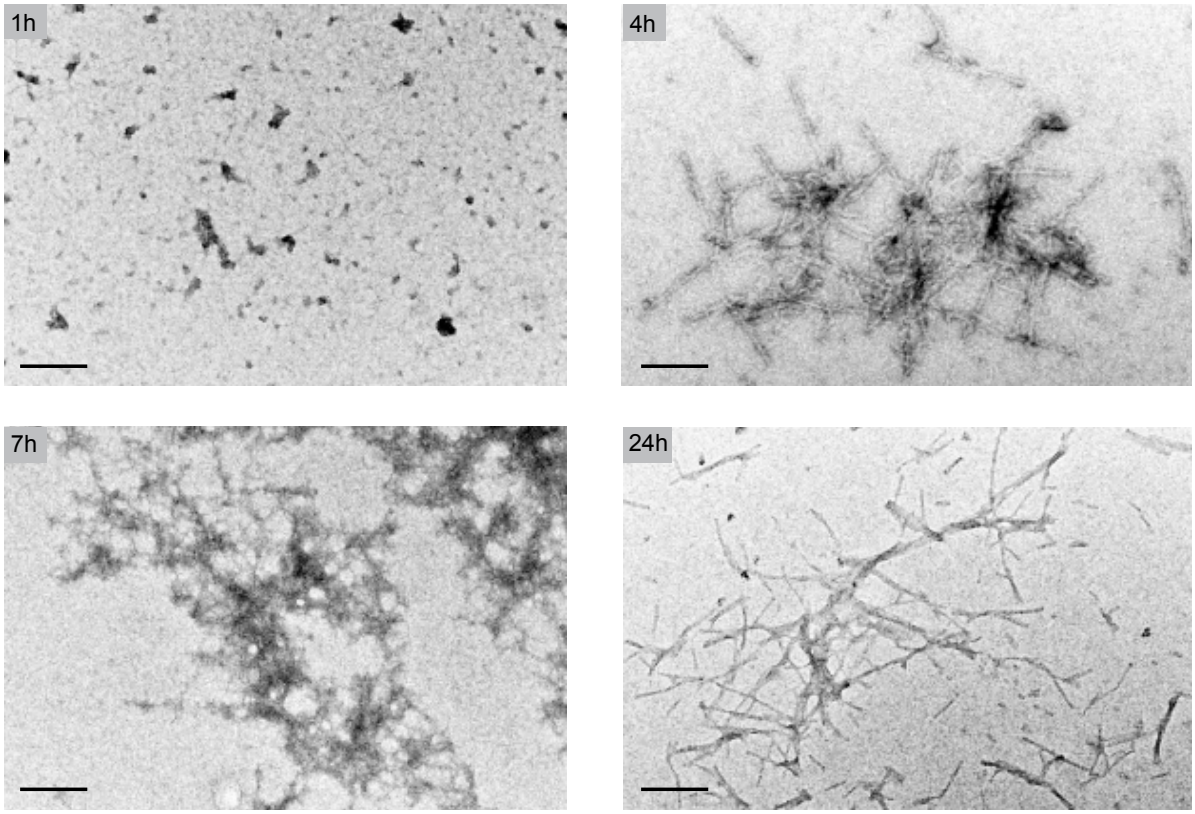

Figure 3.26. Aβ40 aggregates during the 24h incubation assay. TEM images taken at various stages of Aβ40 peptide incubation in 50 mM Hepes buffer (pH 7.4). Scale bars: 200 nm.

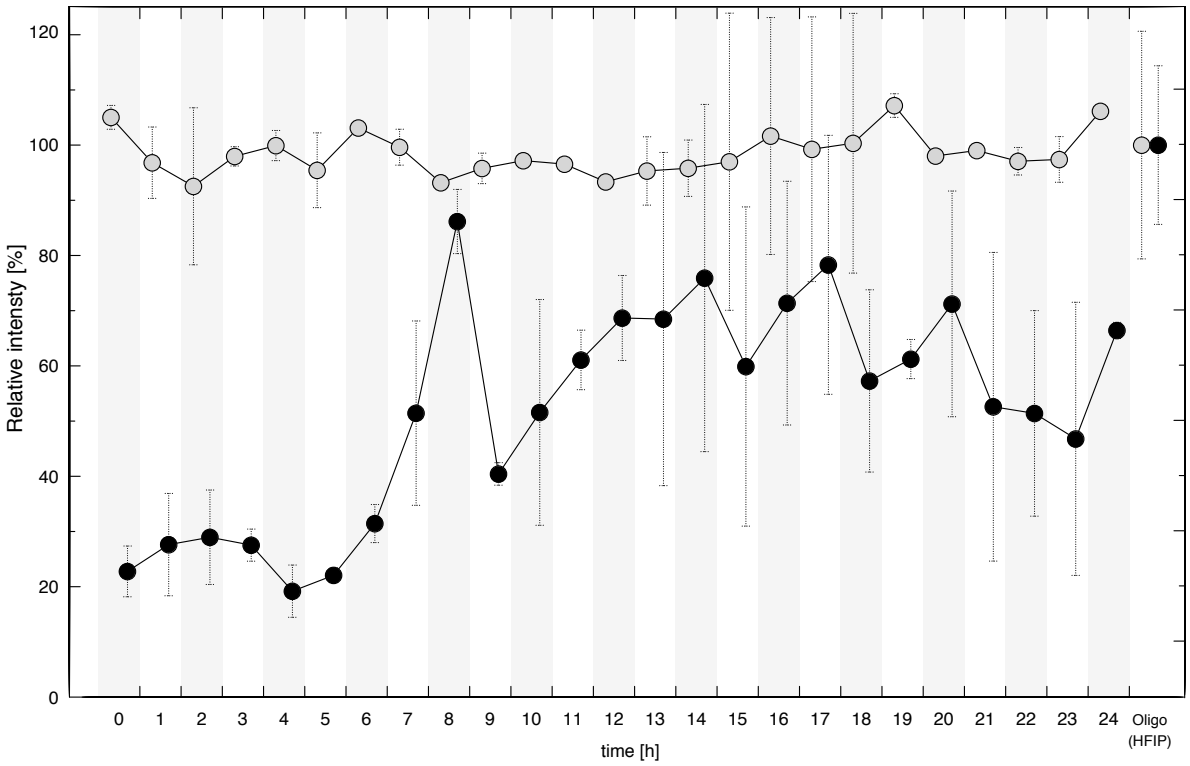

Figure 3.27. KW1AP staining of aggregating Aβ. Black dots: Aβ staining with KW1AP; grey dots: Aβ staining with Ponceau S. Staining of 10% HFIP oligomers with Ponceau S and KW1AP served as a full staining reference (separated grey and black dot, respectively). Error bars: SD (n = 2–3).

aggregation pathway (KW1AP signal between 40 and 90%, from 6 to 24 h), and is formed before mature fibrils are present. In regard to the metastable character of oligomers and their heterogeneous structure, the fluctuating pattern of the KW1AP signal may suggest their transient presence.

The fact that definite binding (∼100%) signal from KW1AP was not reached may indicate that the epitope of KW1AP did not manifest itself fully. The lack of oligomeric structures on TEM images may not necessarily assert that oligomers are absent during the process of Aβ aggregation; instead, they might have not been captured due to the one-hour-long sampling intervals.

3.3.4 Structural analysis of various Aβ-derived oligomeric aggregates

To test specificity range of KW1AP, I performed structural studies of chosen oligomeric species. These oligomers were prepared according to seven different protocols. The oligomeric species were derived from Aβ40 and Aβ42 peptides, but different conditions of preparation were applied (Table 3.4; see also section 2.6.2). Subsequently, I characterised them morphologically with TEM, and structurally with ATR-FTIR. Table 3.4 also contains a compilation of characteristic features of studied oligomeric species derived from Aβ40 (preparation. I, II and III) and Aβ42 (preparation I, II, III and IV).

The TEM analysis revealed that, except for preparation II of Aβ42 which generated curvilinear morphologies, all Aβ oligomer preparations produced spherical conformers (Figure 3.28). Preparation I and II of Aβ40 as well as preparation II of Aβ42 yielded relatively homogeneous oligomer populations. The remaining preparations provided a mixture of morphologically diverse species.

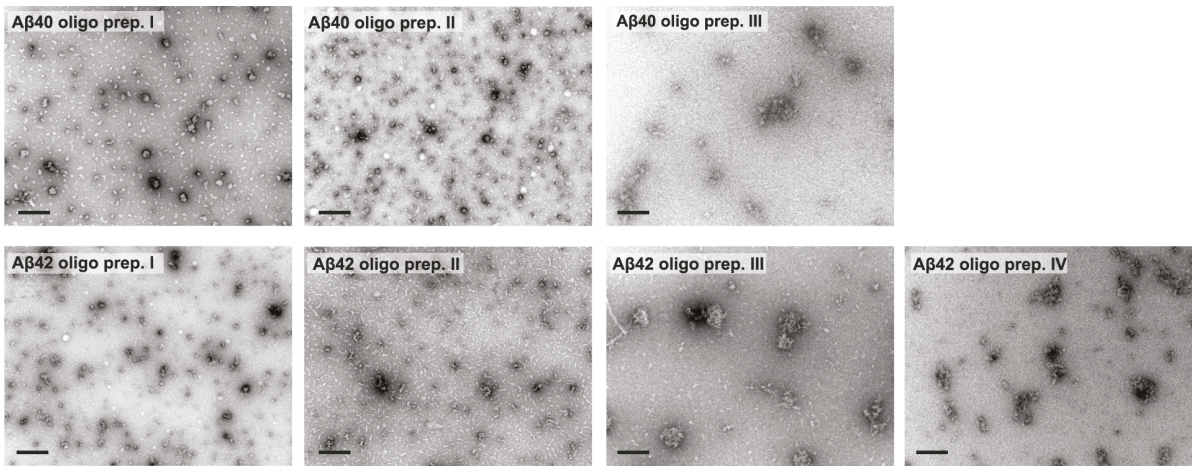

Figure 3.28. Structure of Aβ oligomers. TEM images of various oligomeric structures: preparation I, II and III of Aβ40 oligomers (top row) and preparation I, II, III and IV of Aβ42 oligomers (bottom row). Scale bars: 200 nm.

Table 3.4. Characteristics of selected oligomeric Aβ aggregates used in my research

Oligomers	Preparation	Structural features	Interaction with KW1AP	Preparation conditions after
Aβ40	I	7–50 nm; spherical appearance; anti-parallel β-sheet (Habicht et al. 2007)	strong	Habicht et al. (2007)
	II	7–10 nm; spherical appearance; parallel β-sheet	strong	Kayed et al. (2009)
	III	5–20 nm; spherical appearance; anti-parallel β-sheet (Sarroukh et al. 2010)	none	Sarroukh et al. (2010)
Aβ42	I	5–15 nm; spherical appearance; anti-parallel β-sheet	weak	Kayed et al. (2003)
	II	8–25 nm; curvilinear appearance; anti-parallel β-sheet	very weak	Kayed et al. (2009)
	III	7–25 nm; globular appearance; anti-parallel β-sheet (Cerf et al. 2009)	none	Klein (2002)
	IV	7–20 nm; globular appearence; anti-parallel β-sheet (Eckert et al. 2008)	none	Barghorn et al. (2005)

Details of oligomer preparations are given in section 2.6.2

To gain insight into the secondary structure of oligomers analysed previously with TEM, I performed structural study using ATR-FTIR. The ATR-FTIR is often use to distinguish between a parallel and an antiparallel β-sheet structure based on the analysis of the amide I region (1600-1700 cm^{-1}; (Miyazawa and Blout 1961)). Presence of two components within the amide I region, a major (with a reflectance maximum at $\sim$1630 cm^{-1}), and a minor (with a reflectance maximum at $\sim$1695 cm^{-1}), indicates an antiparallel β-sheet structure; presence of only the major component indicates a parallel β-sheet structure.

I recorded the FTIR spectra of Aβ40 oligomers (preparation I and II), and Aβ42 oligomers (preparation I and II). The oligomers were prepared according to the procedure described in section 2.8. The maxima of the amide I region of all examined oligomers were in the range of 1630 cm^{-1}, marking a significant content of β-sheet structure (Figure 3.29). Additionally, a minor component was observed in the spectra of preparation I of Aβ40 oligomers, and preparations I and II of Aβ42 oligomers, thus signifying an antiparallel β-sheet structure in those species. The minor component was absent in case of preparation II of Aβ40 oligomers, indicating a parallel β-sheet structure. As far as the remaining Aβ aggregates are concerned, earlier FTIR studies revealed that preparation III of Aβ40 oligomers and preparation III and

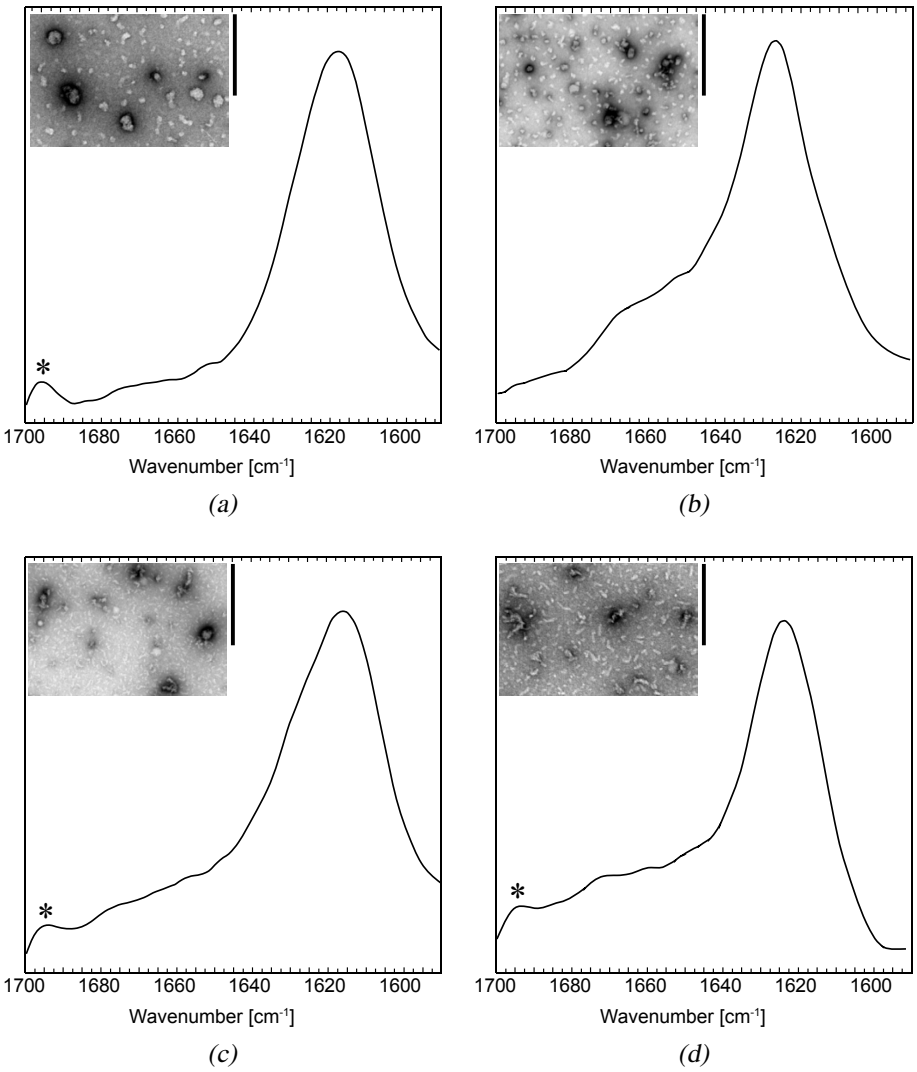

Figure 3.29. ATR-FTIR spectra from the amide I region of Aβ oligomers. Spectra were recorded in H_2O for four different preparations of oligomers: preparation I of Aβ40 oligomers *(a)*, preparation II of Aβ40 oligomers *(b)*, preparation I of Aβ42 oligomers *(c)*, preparation II of Aβ42 oligomers *(d)*. ∗ indicates the peak at ∼1695 cm^{-1}. Insets show TEM images of respective oligomeric preparations. Scale bar: 200 nm.

IV of Aβ42 oligomers possess an antiparallel β-sheet structure (Sarroukh et al. 2010, Cerf et al. 2009, Eckert et al. 2008).

3.3.5 Specificity assessment of KW1AP

To assess the specificity range of KW1AP antibody to the oligomeric species, I carried out a spot blot analysis. For this purpose, seven previously structurally characterised Aβ-derived oligomeric preparations (preparations I-III of Aβ40 and preparations I-IV of Aβ42) and six non-Aβ-derived oligomers (SAA(2-21), full length SAA, glucagon, lysozyme, Sup35(7-13), and apomyoglobin) were immobilised on nitrocellulose membrane and tested for binding to

KW1AP. Staining with Ponceau S was performed to confirm equal protein load. The staining of preparation I of Aβ40 oligomers with KW1AP and Ponceau S was used as full staining reference.

Spot blot showed only a weak or no interaction of KW1AP with most examined species (Figure 3.30a). The only significant interaction of KW1AP was observed with preparation II of Aβ40 oligomers. Preparation III of Aβ40 did not show significant staining with KW1AP. KW1AP also did not recognise Aβ42-derived oligomers, except from preparation I, which showed some interaction with KW1AP (Figure 3.30a). Finally, there was no significant interaction between KW1AP and non-Aβ-derived oligomers (Figure 3.30b).

These data let me conclude that KW1AP binds only to a certain type of oligomers, and that this binding is independent from the oligomer's polypeptide origin.

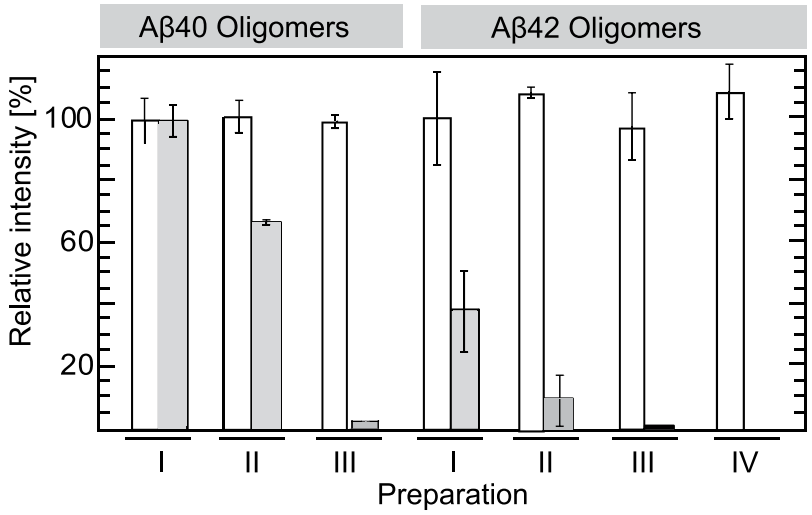

(a)

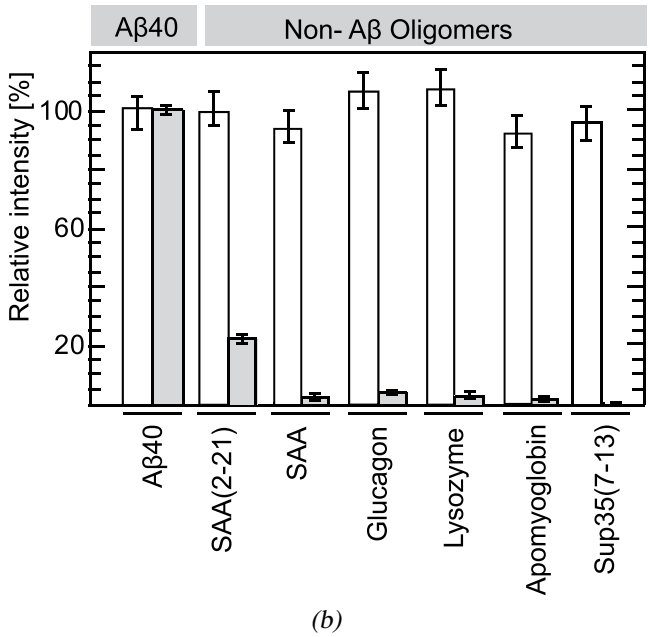

(b)

Figure 3.30. Binding of KW1AP to various oligomers. Several preparations of Aβ *(a)*and non-Aβ *(b)*derived oligomeric species were tested for binding to KW1AP (grey bars). Equal load of the oligomeric species on the membrane was confirmed with Ponceau S staining (white bars). Error bars: SD (n = 2–3). The specificity assessment of the KW1AP was carried out in collaboration with Stefanie Brandt (MPRU, Halle).

Chapter 4

Discussion

In this dissertation, I analysed the structural diversity of Aβ by means of antibody recognition. To improve our understanding of the delicate nature of Aβ aggregates, I employed a whole spectrum of biophysical and biochemical methods. First, I described the selection process of the antibody fragments directed against Aβ42 oligomers. However a specific binder did not emerge during the selection process; therefore I proceeded with a characterisation of previously generated antibody fragments specific to Aβ fibrils (B10, KW2 and KW3) and Aβ40 oligomers (KW1). This characterisation yielded valuable information about the mode of action of the studied antibody fragments, and provided insight into the structure and biochemistry of different Aβ assemblies.

4.1 Selections of the VHH domain against Aβ42 oligomeric species

In an attempt to select a VHH binder specific to Aβ42 oligomers, I applied a camelid phage library from the HKI. I prepared the targeted Aβ42 oligomeric species according to a range of diverse protocols. I also implemented different selection conditions. Nonetheless, a specific binder did not emerge during the selection process. In this chapter, I will discuss the possible causes of this failure, which include the technical (phage display) and methodological limitations (conditions of selection, transient nature of oligomers, and their tendency to aggregate).

The first phage display selection against Aβ42 oligomers, though performed in the presence of two competitors, was unsuccessful. All of the selected binders produced a high signal to Aβ42 oligomer preparations (Figure 3.3), which might point to the successful selection of an anti-Aβ42 oligomers antibody. However, the strong interaction between the M13 helper phages (used as a negative control) and the oligomers, as well as the differences in DNA sequences of the binders, clearly indicated that their interactions with oligomers

were unspecific. Repeated selection under more stringent conditions, with much lower concentrations of the antigen (Figure 3.4), also did not produce the expected output. The high signal produced by selected binders to Aβ42 oligomers might be partially explained by the unspecific binding of coat proteins of the M13 phage. Those proteins are abundantly exposed on the phage surface and may bind with the antigen (Arap 2005). This applies in particular to phage coat protein VIII (pVIII), which is represented on the surface of the M13 phage by 2700 copies (Haigh and Webster 1998). pVIII consists of free segments whose middle part is strongly hydrophobic (Marvin 1998, Haigh and Webster 1998). This type of interaction may be responsible for the unspecific binding to Aβ42 oligomers, which expose hydrophobic patches on their surface (Chen and Glabe 2006). Such interpretation is further supported by the fact that Aβ42 oligomers show an affinity to phospholipid membranes (Williams and Serpell 2011); therefore, the mechanism of M13 phage-oligomer interaction may be analogous.

The relatively low diversity of the HKI camelid phage library is another potential cause of the unsuccessful selection. The library consists of 6×10^8 functional clones (Habicht 2002). The size of the phage-based library is limited by the transformation efficiency of *E. coli* cells. Much higher diversity can be reached in a ribosome-based library, which is only limited by the number of ribosomes used for the reaction, and independent from the transformation efficiency (Hanes and Plückthun 1997). Furthermore, the applied phage display procedures did not include somatic hypermutation. Somatic hypermutation is a powerful mechanism, which occurs naturally during *in vivo* maturation of antibodies (Wagner and Neuberger 1996). This mechanism greatly increases the antibody repertoire, therefore has been replicated in the ribosome display (He and Khan 2005). The ribosome display technique enables the insertion of random mutations into the DNA sequence of antibodies during the PCR steps alternating with the panning rounds (Hanes and Plückthun 1997). Perhaps another, alternative display technique (e.g. ribosome display) could be used instead of phage display in further selections of specific binders against Aβ42 oligomers.

Due to their transient nature, Aβ42 oligomers are a very challenging target. This could be the ultimate cause for the failed selection of a specific binder. In comparison to Aβ40 species, Aβ42 oligomers have an increased tendency to aggregate. The C-terminal end of Aβ42 peptide is very hydrophobic, and the peptides are more likely to interact with each other through hydrophobic interactions. Therefore, the hydrophobicity of the peptide contributes to the metastable character of Aβ42 oligomers. This feature may cause changes in the exhibited structure of Aβ42 oligomers during phage display selection; it may also result in the presentation of diverse epitopes to the VHH antibodies. Presentation of different epitopes

during selection rounds possibly hindered the selection of a specific VHH antibody fragment.

Several antibodies against Aβ42 oligomers, generated during the process of animal immunisation, have recently been described (Gong et al. 2003), but they recognise both oligomers and fibrils (Lacor et al. 2004, Lambert et al. 2007). Furthermore, most of those antibodies constitute polyclonal sera (e.g., A11), which uniformly bind to many Aβ and non-Aβ derived prefibrillar aggregates (Kayed et al. 2003). This is not surprising: in a heterogeneous population of oligomers, there exists a relatively high probability for polyclonal sera to bind to different epitopes. In contrast, VHH domains are monoclonal. They can bind to only one epitope; selecting a specific binder from among them is thus more challenging.

Despite the failed selection attempt, I argue that *in vitro* selection of binders against chosen Aβ42 oligomeric species is a potentially successful approach. Some specific requirements should be met: reaction conditions should be chosen carefully; the optimisation of panning conditions should not be limited to the concentration of the antigen, but should also include the type of the competitor and furthermore, cross-reactivity should be minimised. To account for the tendency of oligomers to aggregate, as well as their sensitivity to solution conditions, factors like salt concentration, the choice of buffers, and the system of elution should also be revised.

4.2 Common binding mechanism of fibril-specific VHH domains

The aim of this dissertation was to clarify the molecular mechanisms of the interaction between B10, KW2, and KW3 antibody fragments and amyloid fibrils. Elucidation of these mechanisms would enable better understanding of the structure of fibrillar Aβ aggregates. In this section, I will address these issues with particular emphasis on molecular recognition pattern of the B10 antibody domain.

4.2.1 Linear ligands are insufficient to define the B10 epitope

Although the specificity of B10 for fibrillar Aβ40 aggregates was well determined (Habicht et al. 2007), the B10 epitope remained to be established. My attempts to characterise the B10 epitope with seven amino acid peptides derived from phage libraries were unsuccessful (see section 3.1.2). In spite of the fact that two peptides were enriched after three rounds of panning, none of them acted as a Aβ40 fibril competitor – as verified with the SPR study (Figure 3.9). These results imply that the seven-residue peptide is incapable of defining the conformational nature of B10 epitope. Similar endeavours to determine epitopes of conformation-sensitive NU1, NU2 and NU4 anti-Aβ antibodies are described in

the literature (Lambert et al. 2007). It was shown that short, Aβ-derived peptide fragments did not suppress the binding of NU antibodies to Aβ conformers. However, pre-incubation of NU antibodies with longer, 28 amino acid peptide fragments strongly inhibited the binding to Aβ conformers (Lambert et al. 2007). My results indicate that seven amino acid peptides in linear or cyclic form (Figure 3.8) are insufficient to determine the B10 epitope; this provides indirect evidence for the higher complexity of the conformational epitope of B10.

4.2.2 Molecular basis of the conformation-specific binding of B10 to amyloid fibrils

A deeper understanding of the conformational specificity of B10 to amyloid fibrils was provided by the investigation of the B10 complementary binding regions. SPR analysis of 24 B10 alanine single mutants revealed that B10 recognition of Aβ40 fibrils is mediated by electrostatic interactions (Figure 3.13). Replacement of positively charged groups by alanine in B10 significantly diminished the affinity of B10 to fibrils (Figure 3.13). Furthermore, the double B10 mutant (R39/61A) did not interact with Aβ40 fibrils; therefore, I conclude that cationic residues in CDRs of B10 are involved in fibril recognition. This conclusion was further reinforced by the finding of Haupt et al. (2011b), who tested the effect of chemical modifications of charged groups on Aβ40 fibrils (Figure 4.1a). Aβ40 fibrils with carboxyl groups modified by glycinamide did not show any interaction with B10AP (Figure 4.1b; Haupt et al. 2011b). Due to the fact that Aβ40 fibrils containing -NH_2 groups masked by NHS-biotin were still recognised by B10AP, it was concluded that fibril -COOH groups constitute structural components responsible for binding to B10. In addition, the lack of interaction between B10AP and carboxyl-modified fibrils was further demonstrated for G-helix and insulin fibrils (Figure 4.1b; Haupt et al. 2011b). Accumulated data emphasise the importance of negatively charged groups on fibrils for B10 antibody binding. This fact is consistent with previous reports asserting that the binding of serum amyloid P component (Thompson et al. 2002) and the apolipoprotein E (Gunzburg et al. 2007) depends on the negatively charged groups on fibrils; albeit this type of interaction with fibrils is not common, especially in the context of antibody recognition. The basic surface properties of amyloid fibrils are well documented, since they were shown to react with anionic polymers like heparin or glycosoaminoglycanes (Kisilevsky 2000). The B10 recognition mechanism also significantly differs from Aβ-sequence-specific antibodies. Their interactions with fibrils are based on the recognition of the combined cationic and anionic surfaces on fibrils (Gardberg et al. 2007, Basi et al. 2010).

The crystal structure of B10 was determined at 1.8 Å resolution. It revealed a unique property of B10, namely a substantially flat complementary binding region (Haupt et al.

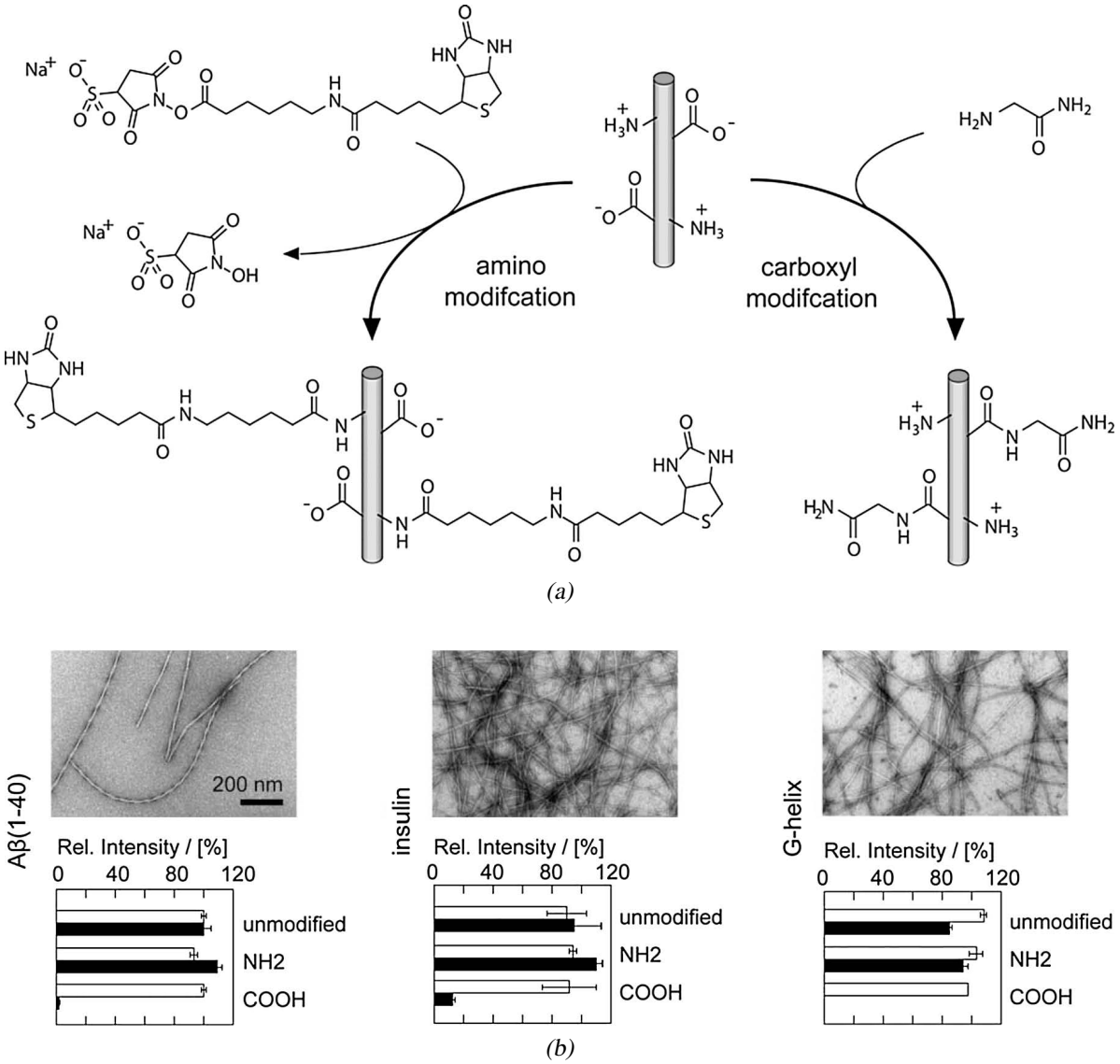

Figure 4.1. Modifications of fibrils influence the mechanism of recognition with B10. Amyloid fibrils were chemically modified with either NHS-biotin (to mask the amino groups), or with glycinamide (to cover carboxyl groups on their surface) *(a).* Negatively stained TEM micrographs of Aβ40, insulin and G-helix fibrils. B10AP (black bars) and Ponceau S (white bars) staining intensities of modified fibrils. Unmodified fibrils were used as a reference for full staining *(b).* Images after Haupt et al. (2011b).

2011b). The structure of the B10 CDRs is distinct from previously published sequence specific antibodies directed against β-amyloid. Sequence-specific antibodies contain deep binding pockets, formed by grooves of CDR1, CDR2 and CDR3. They encompass the N-terminal part of the β-amyloid sequence (Gardberg et al. 2007, Basi et al. 2010). In the case of B10, its flat recognition site perfectly matches the structurally even surface of amyloid fibrils (Figure 4.2; Haupt et al. 2011b). The complementarity of the B10 surface arises from the very regular surface pattern of amyloid fibrils. This pattern comprises ∼4.7 Å main chain repeats between β-strands (Marshall and Serpell 2009), and 5–12 Å side chain separation

along the fibril axis (Fändrich 2007). The CDRs of B10 cover the region of approximately seven β-strands from the common core structure of amyloid fibrils (Haupt et al. 2011b). This is in accordance with the 1:10 molecular stoichiometry of B10 binding to fibrillar Aβ40, determined earlier using SPR (Habicht et al. 2007).

The accumulated data show that the B10 binding mechanism is unique. Mechanism of fibril recognition by B10 involves both, electrostatic interactions and binding of the regular surface pattern of Aβ40 fibrils.

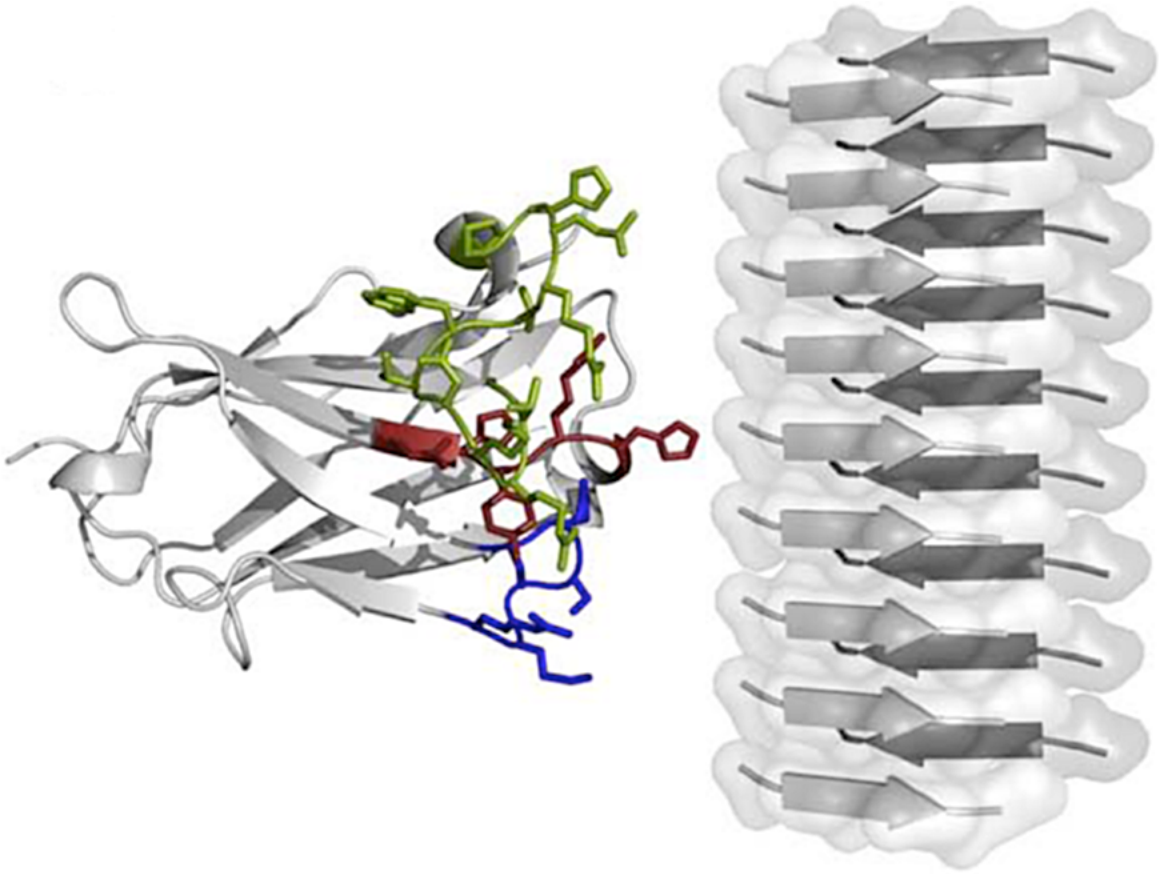

Figure 4.2. Surface complementarity of B10 and amyloid fibrils. The flat binding surface of B10 complements the regular, structurally even surface of Aβ40 fibrils. Images after Haupt et al. (2011b).

4.2.3 B10 recognises a regular surface pattern of amyloid fibrils

The B10 antibody domain has previously been shown to recognise both the fibril and the protofibril state of Aβ40; however, an interaction with oligomers or disaggregated peptides was not observed (Habicht et al. 2007). Detailed assessment of the binding specificity of B10 revealed that B10 recognises a whole spectrum of amyloid or amyloid-like fibrils. The analysed fibrils differed significantly with regard to chirality of the backbone, handedness of the fibril supertwist, presence of parallel or antiparallel β-sheet structure, length and origin

of the amino acid sequence, or morphological appearance. Nevertheless, they all displayed amyloid characteristics. Except for a small group of fibrils, which did not reproducibly react with B10, the majority of the examined fibrils did. However, none of the aforementioned fibrils' characteristics can explain the interaction of the fibrils with B10AP. The non-reactive, 'B10-negative' fibrils display no obvious morphological or structural features which could clearly prevent from binding of B10. Furthermore, some fibrils (i.e., Aβ(16–22) or hSAA(2–21)) were derived from peptides fragments, which full polypeptide sequence formed 'B10-positive' fibrils.

In vivo examination of amyloid tissue sections provided further evidence for the selective B10 recognition of amyloid fibrils. It revealed that B10 binding is correlated only with certain pathological amyloid conditions, i.e., Alzheimer's disease and human cardiac ATTR amyloidosis (Haupt et al. 2011a). However, B10 was not able to distinguish between fibril morphologies from the same protein (Haupt et al. 2011a). All *in vitro* fibrils examined with B10 contained negatively charged amino acids. The lack of B10 interaction with fibrils containing acidic residues demonstrates that the presence of negatively charged groups on the fibrils alone cannot explain the B10-fibril interaction. Detailed examination of the PABPN1–(+7)Ala fibrils, which did not react with B10AP, provided a partial understanding of the B10 binding mechanism. The cross-β structure of PABPN1–(+7)Ala is formed by poly-alanine extensions, and thus contains few charged residues in the core (Sackewitz et al. 2008); hence, charged residues are not exposed on the surface of the cross-β structure. B10 was also demonstrated to bind to anionic polymers, which are devoid of a protein-specific polypeptide backbone, like DNA or heparin (Haupt et al. 2011a). However, no significant interaction was observed between B10 and β-sheet-rich globular proteins, or intrinsically disordered peptides (Haupt et al. 2011a). The fact that B10 does not react with β-sheet-rich proteins (i.e., Pel-15 pectate lyase or p22 tailspike protein) imposes structural constraints on the B10 recognition mechanism. Furthermore, the globular proteins are rich in surface-exposed acidic residues; nevertheless, binding with B10 does not occur. The arrangement of amino acids in globular proteins, as shown for the transthyretin or P-15 pectate lyase (Figure 4.3a; Haupt et al. 2011a), causes irregular surface texture with mixed positively- and negatively-charged groups. In contrast, 'B10-positive' Aβ42 fibrils or HET-s(218–289) fibrils (Wasmer et al. 2008) display a regular pattern of charges on their surface (Figure 4.3b; Haupt et al. 2011a). In light of this evidence, I conclude that exhibition of negative charges and their arrangement in a regular pattern on the fibril surface are plausible causes of the B10 recognition.

Finally, the B10-fibril interaction mechanism strongly resembles that of a class of pattern recognition receptors typical for innate immunity (i.e., RAGE: receptors for advanced glyca-

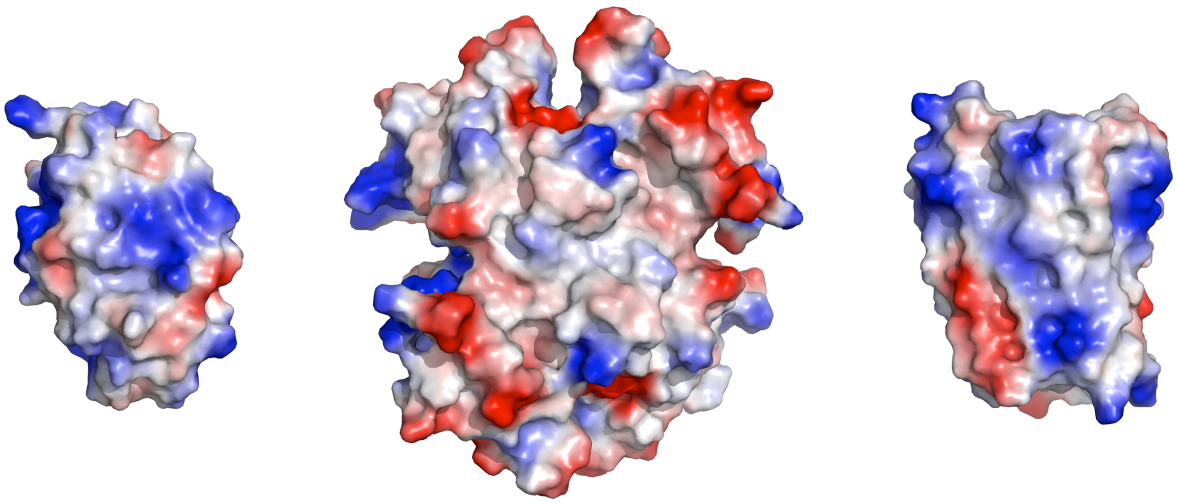

(a) Lysozyme *(b)* Transthyretin *(c)* Pel-15

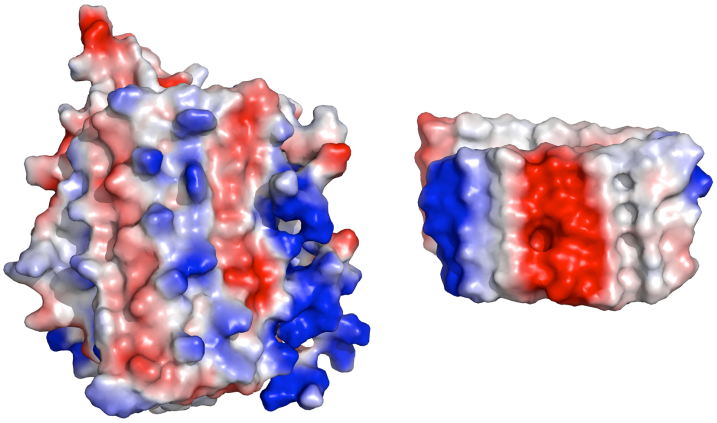

(d) HET-s(218–289) *(e)* Aβ(1–42)

Figure 4.3. Comparison of electrostatic surface potential of globular and fibrillar proteins. Globular proteins: lysozyme *(a)*, transthyretin *(b)*, and Pel-15 *(c)*, are rich in unequally distributed, negatively charged residues. In contrast, negatively charged residues on the surface of HETs(218–289) *(d)* and Aβ42 *(e)* fibrils are distributed regularly. Colour indicates the surface charge potential (red: negative; blue: positive; white: neutral). Images after Haupt et al. (2011b).

tion end products). This similarity arises from the fact that the RAGE multiligand specificity is characterised with strongly basic surface electrostatic potential (Haupt et al. 2011a). This electrostatic potential imposes a mechanism of recognition via positively charged residues (Xie et al. 2008). Additionally, a positively charged electrostatic surface of the RAGE-VC1 fragment (containing the ligand binding site; Dattilo et al. 2007), has many similarities with the B10 binding site (Figure 4.4). The binding region of the RAGE-VC1 fragment does not display apparent irregularities. Such irregularities are also not observed in the CDRs of B10 (Haupt et al. 2011a). This suggests that the binding region is flexible, making it prone to rearrangement upon binding to a fibril. The RAGE-VC1 fragment was also proved to bind to mature Aβ40 fibrils, but not to disaggregated peptides (Haupt et al. 2011a) – analogous to B10 (Habicht et al. 2007). Furthermore, RAGE-VC1 recognises most of the 'B10-positive' fibrils, while the interaction with 'B10-negative' fibrils was not observed, with the exception

of Aβ(16-22) fibrils (Haupt et al. 2011a). Remarkably, similar recognition mechanisms of RAGE-VC1 fragment and the B10 domain emerged from radically different pathways; the first evolved naturally, while the second was engineered biotechnologically with the use of genetic methods (Haupt et al. 2011a).

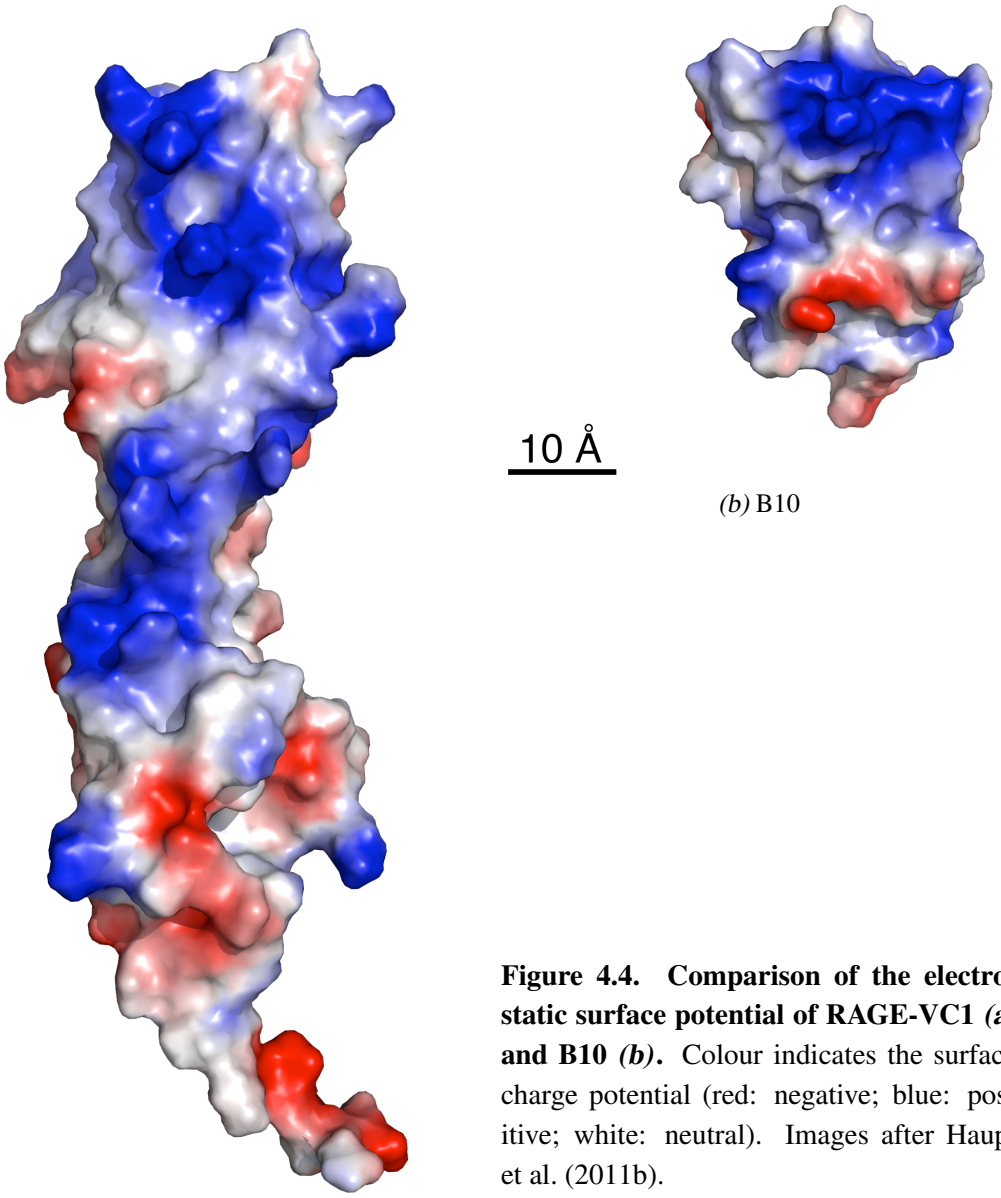

(a) RAGE-VC1

(b) B10

Figure 4.4. Comparison of the electrostatic surface potential of RAGE-VC1 *(a)* and B10 *(b)*. Colour indicates the surface charge potential (red: negative; blue: positive; white: neutral). Images after Haupt et al. (2011b).

4.2.4 Random rearrangement of B10 CDRs does not affect the interaction with fibrils

The analysis of binding properties of the two B10 variants: B10scr and B10glu, indicates that random rearrangement of the residues in the CDRs does not influence the B10 interaction with fibrils. The crystal structure of B10 does not display a regular pattern in the binding site, but suggests considerable plasticity of this region. The flexibility of the binding site makes it

prone to rearrangement upon binding to an antigen (Haupt et al. 2011b). This feature of B10 may, at least partially, explain the strong affinity of the B10scr variant to Aβ40 fibrils; B10scr contains the same residues in CDRs as B10, but those residues are randomly rearranged. In contrast, the B10glu variant, in which positively charged residues were replaced with glutamic acid, did not interact with Aβ40 fibrils. This fact supports the previous finding that cationic groups in the CDRs of B10 are essential for fibril recognition (Haupt et al. 2011b).

The observation that B10scr is capable of complexing Aβ40 fibrils, in spite of the random reordering of amino acids in CDRs, gained additional support after the assessment of KW2 and KW3 binding properties. I demonstrated that those two VHH domains show strong binding affinity to Aβ40 fibrils (Figure 3.20). Furthermore, they recognise neither freshly dissolved Aβ peptide, nor oligomeric Aβ species, which is similar to B10. The affinity to fibrils, and a simultaneous lack of interaction with oligomeric or disaggregated Aβ peptide, qualifies KW2 and KW3 as conformation-specific antibodies. In addition, KW2AP and KW3AP, have shown a very high specificity to a range of 'B10-positive' amyloid or amyloid-like fibrils (Figure 4.5). The interaction of KW2AP was decreased with only two types of

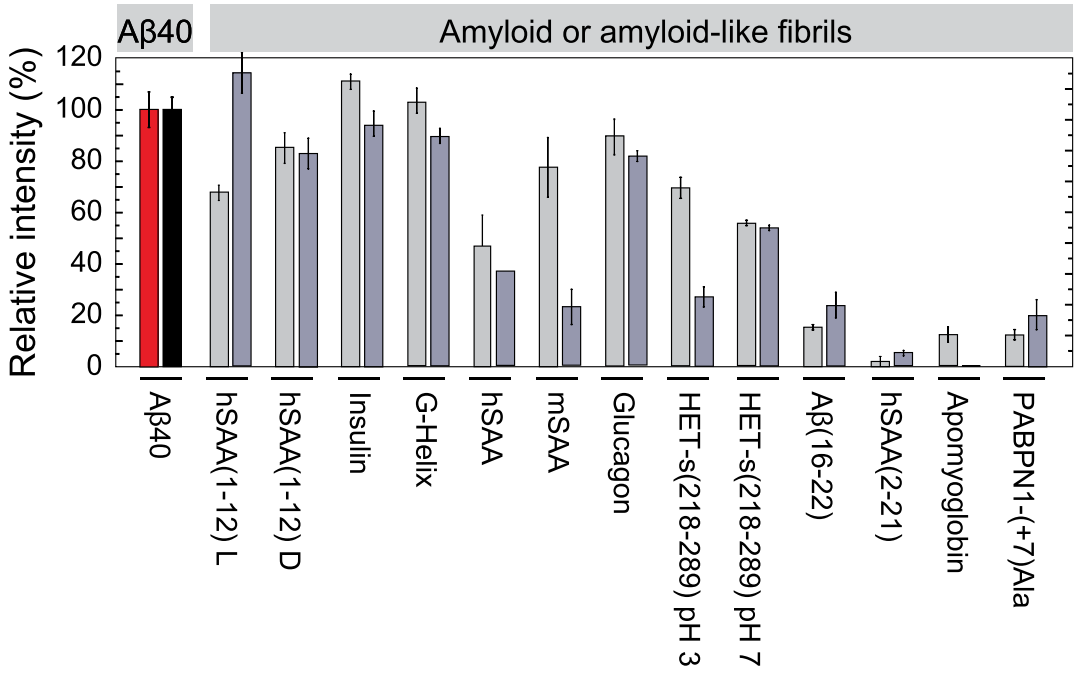

Figure 4.5. Comparison of binding properties of KW2AP and KW3AP. KW2AP (grey bars) and KW3AP (slate bars) staining level of different amyloid or amyloid-like fibrils. KW2AP and KW3AP staining of Aβ40 fibrils was used as reference for full staining (red bar). Equal load of proteins on the membrane was confirmed with Ponceau S staining; Ponceau S staining of Aβ40 fibrils was used as reference for full staining (black bar); Ponceau S staining of the remaining fibrils was within 10% range of the reference (data not shown). Experiment was carried out by Karin Wieligmann (HKI, Jena).

fibril (i.e., hSAA(1-12) all L, and full-length hSAA); KW3AP staining was reduced for the full-length hSAA and mSAA fibrils. Remarkably, the fibrils that did not interact with B10AP

('B10-negative' fibrils) were also not recognised by KW2AP and KW3AP. The data presented here indicate that the fibril recognition mechanism of B10, KW2, and KW3 is similar.

Striking binding similarity of KW2, KW3, and B10 can putatively be explained by the presence of positively charged residues in the CDRs of those antibodies (Figure 3.21). Since the crystal structures of KW2 and KW3 are not yet available, an ultimate explanation of their binding mode cannot be provided. Nonetheless, the presence of multiple positively charged amino acids, and the absence of negatively charged ones, appears to play a key role in the binding mechanism.

The framework residues sometimes also participate in antigen binding (Kabat et al. 1992). On one hand, this may be a tempting explanation for the common mechanism of binding of VHHs with fibrils; however, it was not confirmed by the crystal structure of B10. On the other hand, this possibility cannot be completely excluded, since the binding region of B10 might undergo rearrangements upon coupling with fibrils.

Given the similarity of B10, KW2, and KW3 binding sites, as well as the resemblance of the recognition pattern of amyloid fibrils, I conclude that the unique VHH framework (Habicht 2002), in combination with a strong cationic binding site, may constitute the functional core for binding of amyloid fibrils by these domains.

4.2.5 Understanding the recognition mechanism of amyloid fibrils

The fact that B10, KW2 and KW3 bind the same fibrils underlines the role of positively charged residues in fibril recognition. The design of VHH, with its unique framework, enables the construction of antibodies with flexible binding sites and multi-ligand specificity. Moreover, the mechanism of B10 binding proposed here is an indirect source of information about surface and structure of fibrils. The highly ordered β-sheet core, common to all fibrils, is insufficient to explain their discrete interaction with ligands; therefore studying the structure of fibrils requires a custom approach that would provide detailed information about their surface. According to structural models, the mid-region and C-terminal end of Aβ are buried in the hydrophobic core of β-sheet (Soreghan et al. 1994), making them inaccessible for antibodies. N-terminal specific antibodies, described by Gardberg et al. (2007), bind to fibrils by taking advantage of the unstructured N-fragment of the Aβ polypeptide. However, their sequence specificity does not facilitate selective Aβ species recognition. Hence, N-terminal specific antibodies cannot discern between Aβ conformers. B10 might be able to distinguish several amyloid pathologies, which are otherwise difficult, or altogether impossible, to diagnose with other amyloid ligands.

Several mechanisms of antibody clearance of Aβ have been proposed. These include the

peripheral sink hypothesis (DeMattos et al. 2001), direct resolution of Aβ (Solomon et al. 1997), and microglia-mediated Aβ clearance mechanisms (Istrin et al. 2006). It remains to be seen which of these categories contain the recognition mechanism of B10. Antibody-mediated clearance of amyloid aggregates might depend on multiple mechanisms. For instance, the ability of B10 to stabilise protofibrils renders them more susceptible to direct resolution, or to proteolytic degradation via microglia activation (Habicht et al. 2007). The understanding of the mechanisms governing the binding of antibodies to amyloid aggregates is crucial for designing effective therapeutic solutions or diagnostic reagents. Based on the data accumulated here, several conclusions can be drawn regarding the fibril-specific *modus operandi* of VHH antibody domains:

- B10 binding is mediated by electrostatic interactions, and requires surface-exposed negatively charged groups on Aβ40 fibrils
- The shape of the B10 binding site restricts the recognition of fibrils containing flat surfaces
- B10 binding to fibrils mirrors the pattern recognition mechanism of RAGE
- The relative arrangement of positively charged amino acids within the CDRs of B10 does not affect the recognition of fibrils
- The mechanism of fibril recognition by KW2 and KW3 antibody fragments is probably the same as in B10

To the best of my knowledge, the data presented here for the first time elucidate the detailed mechanism of recognition of different Aβ40 fibril-specific antibody domains. This mechanism involves both electrostatic forces and surface complementarity.

4.3 Conformational recognition of the Aβ oligomers by KW1

In course of my research project, I assessed biophisically the KW1 antibody domain, generated by phage display selection. The properties of KW1 include specificity to selected Aβ40 conformers. Owing to these properties, KW1 is able to recognise certain oligomer structures. In the following sections, I will discuss these properties in greater detail and compare KW1 with other amyloid binders.

4.3.1 Implications of conformational specificity of KW1 VHH to Aβ oligomers

As established with SPR and ELISA, KW1 shows selective specificity for certain types of Aβ conformers (Morgado et al. 2012). KW1 is able to discriminate specific Aβ40 oligomers from fibrils and disaggregated peptides. Hence, KW1 qualifies as a conformation-specific

antibody fragment. It differs from previously described B10 antibody fragment - specific only for fibrillar Aβ states, as well as from sequence-specific binders, e.g. the mouse monoclonal 6E10 antibody. The sequence-specific antibodies recognise several different Aβ conformations derived from the same polypeptide chain (Vasilevko et al. 2007).

It has recently been demonstrated that incubation of the Aβ peptide in the presence of KW1AP does not prevent formation of ThT-positive structures (Morgado et al. 2012). Yet, the resulting aggregates did not have a typical fibrillar morphology. This suggests that the binding of KW1 does not stabilise the oligomeric state. Instead, it may cause a certain conformational transition of Aβ, which would prevent the assembly of Aβ into mature fibrils. B10AP displays similar inhibitory activities of fibril formation; it also blocks Aβ assembly, but at a later step than KW1AP; B10AP binds to protofibrils and promotes their accumulation (Habicht et al. 2007).

LTP measurements revealed that KW1AP-positive oligomers are synaptotoxic and lead to neuronal impairment in living brain tissue (Morgado et al. 2012). Importantly, KW1AP was shown to completely reverse oligomer-induced neuronal dysfunctions. Other monoclonal antibodies, raised against the N-terminal part of Aβ, show the ability to disassemble Aβ fibrils (Solomon et al. 1996). KW1AP displays a different mode of action. The result of the incubation of KW1AP with pre-formed amyloid fibrils, and the absence of Aβ40 in the supernatant, indicated that KW1AP was unable to disaggregate fibrils. The presence of KW1AP mainly in the supernatant proved that the KW1AP epitope was not presented on mature Aβ40 fibrils (Figure 3.24). This finding indicates that KW1 does not react with already existing amyloid deposits, and points to its potential use as a selective marker specific for toxic soluble intermediates.

The epitope study performed during the 24 h incubation of the Aβ peptide provided a better understanding of the nature of KW1 recognition. The aggregation kinetics of Aβ, monitored with ThT, had two distinctive phases: a well-resolved lag phase with formation of nuclei, followed by a growth phase with elongation of Aβ fibrils (Figure 3.25). This aggregation mode is well-established, and consistent with previous reports (Harper and Lansbury 1997, Chiti et al. 2003). The KW1AP staining pattern suggests that the epitope of KW1AP occurs early in the Aβ aggregation and is present over the whole incubation time (Figure 3.27). This notion, however, is not supported by the TEM images prepared during the Aβ aggregation: the oligomer-like spherical structures were not observed (Figure 3.26). On the other hand, the oligomers were difficult to capture under semi-physiological conditions. The transient character of oligomers was a possible reason for the lack of spherical species on the TEM micrographs. An alternative explanation could be that spherical oligomeric species,

which are a natural target for KW1AP, were formed and stabilised in HFIP. In the HFIP solution, the oligomers took on a particular morphology (Figure 3.22). Hence, oligomers with such morphology need not necessarily appear on the Aβ aggregation pathway.

The results of the 24 h incubation merely demonstrated that KW1AP recognises a certain epitope, which occurs during the Aβ aggregation pathway, as indicated by the 70% staining of KW1AP. The fact that KW1AP also binds spherical, HFIP-stabilised oligomers, confirms that I managed to stabilise an oligomeric conformation, which transiently appears during Aβ aggregation into fibrils.

4.3.2 KW1 specificity in relation to the structure of oligomers

As part of my research project I attempted to assess the specificity of KW1, and to understand the mechanisms governing the recognition of oligomers by KW1. I examined several factors potentially influencing this interaction.

I tested binding of KW1AP to several soluble variants of Aβ conformers. Oligomers derived from the Aβ42 peptide, as well as oligomers originating from non-Aβ sequences, were not recognised by KW1AP (Figure 3.30). Much to our surprise, not all of the Aβ40-derived oligomers reacted with KW1AP. KW1AP was specific only to preparations I and II; reaction with preparation III of Aβ40 oligomers was not observed. Accumulated data indicate that the studied Aβ40 conformers display different structural epitopes (Figure 3.30a). These results suggest that Aβ oligomers, even those derived from the same polypeptide chain, are structurally polymorphic. Owing to its heterogeneity and transient character, the structure of Aβ oligomers is still not fully elucidated. Initially, oligomers were reported to contain a considerable amount of fibril-like, parallel β-sheet structure (Chimon et al. 2007). However Habicht et al. (2007), using FTIR and far-UV circular dichroism, found that the β-sheet structure of Aβ40 oligomers is primarily antiparallel. This was further supported by Ahmed et al. (2010), who showed that oligomers are rich in β-sheet, but it is organised in a different manner to the parallel, in-register, cross-β structure of Aβ fibril. Antiparallel organisation of the β-strands in Aβ oligomers was also confirmed in several other studies (Eckert et al. 2008, Cerf et al. 2009). The Glabe group proposed a recognition mechanism based on the interaction of an antibody with the antiparallel structure of Aβ oligomers (Kayed et al. 2003, 2010). Kayed et al. (2003) also suggested that oligomers recognised by the A11 antibody share a common structure and a common mechanism of toxicity. Given the antiparallel structure of many studied Aβ oligomers, the recognition mechanism proposed by the Glabe group may hold true. Structural investigations of other, non-Aβ derived oligomers, i.e., ones obtained from β_2-microglobulin or PrP(82–146) peptide, revealed that they also possess the antiparallel

β-sheet structure (Fabian et al. 2008, Natalello et al. 2008).

To determine whether the presence of antiparallel structure on oligomers explains its interaction with KW1 antibody fragment, I investigated the secondary structure of several oligomeric preparations with ATR-FTIR. From the obtained infrared spectra, I conclude that the presence of an antiparallel β-sheet structure on oligomers does not alone determine the interaction with KW1AP. FTIR measurements revealed an antiparallel structure of Aβ40 oligomers, namely preparation I (present study) and preparation III (Sarroukh et al. 2010); preparation II was shown to possess a parallel β-sheet structure. Interestingly, KW1AP interacted only with preparation I and II, but not with preparation III of Aβ40 oligomers. Furthermore, I found that there exist more oligomers which do not interact with KW1AP, despite their proposed antiparallel structure; these include preparation I and II of Aβ42 (antiparallel structure established in this study), preparation III of Aβ42 (Cerf et al. 2009) and preparation IV of Aβ42 (Eckert et al. 2008). These results point out that in Aβ oligomers, the content of the antiparallel β-sheet structure alone is insufficient to define the KW1 epitope. The elucidation of the mode of KW1 recognition of Aβ oligomers requires further studies.

The narrow binding spectrum of KW1 is peculiar among oligomeric binders. For instance, polyclonal antibody A11 binds to a whole spectrum of oligomers derived from different preparations, including ADDLs, HMW oligomers, annular protofibrils, as well as non-Aβ oligomers like calcitonin or α-synuclein (Kayed et al. 2003, 2010). Selective specificity of KW1 is also distinct from previously described B10 antibody fragment, which binds to a broad range of amyloid fibrils (Haupt et al. 2011a). However, the data presented here for KW1 are in agreement with the finding of Lafaye et al. (2009): V31-1, an oligomer-specific VHH, is conformationally specific only to LMW Aβ oligomers; it does not react with oligomers of other amyloidogenic polypeptides (Lafaye et al. 2009).

The finding of De Genst et al. (2006) could be a plausible explanation for the unique epitope recognition by VHH domains. De Genst et al. (2006) showed that VHH fragments often possess a convex paratope; they thus exhibit an unusual ability to recognise a unique epitope, often hidden in cleft protein surfaces; such antigen pockets are inaccessible for conventional antibodies. However, the analysis of the crystal structure of KW1 revealed that its binding site cannot be involved in such binding mechanism (Morgado et al. 2012). The CDRs of KW1 are devoid of a deep binding cavity, although they are surely more concave than the flat surface of B10 CDRs. The CDRs of KW1 capture a molecule of benzamidine, an aromatic substance, from the crystallisation buffer (Morgado et al. 2012). Oligomeric residues comprising phenyl rings seemed likely to be part of the epitope of KW1, but incubation of KW1 with 10^5 molar excess of benzamidine did not influence the affinity of

KW1 to oligomers (Morgado et al. 2012). However, the KW1-positive oligomers demonstrate hydrophobic surface properties; they strongly interact with the fluorescent dye ANS (Haupt et al. 2012).

The crystal structure of KW1 (Figure 1.13) suggests that the binding mechanism is different to that previously described in B10 (Haupt et al. 2011b). The lack of a strong electrostatic surface potential of KW1, and the prevalence of hydrophobic residues in the binding region, may indicate that recognition of oligomers by KW1 is governed by hydrophobic interactions rather than by electrostatic interactions (as it is in B10; Haupt et al. 2011b).

Distinct recognition mechanisms of KW1 and B10 are reflected in different structural properties of their ligands. Aβ oligomers lack the structural regularities typical for Aβ fibrils. The oligomers display micelle-like, hydrophobic structures (Fändrich 2012). Furthermore, the transient nature of oligomers might result in dynamic changes in their structure. The character of the KW1-oligomer interaction appears to be more complex than B10 recognition of the regular surface pattern of fibrils, based on electrostatic interactions; however, this will require further studies.

4.4 Final remarks

The conformation-specific antibody fragments directed against Aβ oligomers and fibrils constitute a powerful tool for basic research of Aβ. They discriminate between different conformational states of Aβ and might be used as selective markers for certain amyloid species. In depth analysis of the B10 antibody fragment led to the elucidation of the recognition mechanism of Aβ fibrils. The proposed B10-fibril interaction mechanism depends on the basic CDR residues of B10 and confirms the presence of the strong acidic surface potential on many amyloid fibrils. The fact that B10 recognises many (but not all) amyloid fibrils may make it a selective diagnostic marker for many amyloid pathological conditions.

KW1, like other oligomer-directed antibodies, may aid in the quantification of amyloid aggregates, as well as help us understand how those aggregates form; KW1 may also facilitate the standardisation of protocols for preparation of prefibrillar aggregates. An improved understanding of the KW1 binding mechanism could indirectly provide insights into the structure of Aβ aggregates. Resolving the structure of Aβ oligomers should facilitate the design of target-directed therapeutic strategies. In the future, it may lead to the elimination of toxic Aβ entities from the brains of AD patients. Elucidation of the binding mechanism of KW1 will enable a better understanding of the structural complexity of prefibrillar Aβ conformers. The KW1 antibody fragment, given its selective binding properties, might serve

as a precise diagnostic tool; it possesses the ability to discriminate certain Aβ conformational states. Such a sensitive molecular device is necessary to separate the toxic Aβ aggregates from harmless or inert ones.

The initial human clinical trial with the use of anti-Aβ antibodies was halted due to severe side effects – 6% of the patients developed meningoencephalitis (Schenk 2002). VHH antibodies might overcome such problems, since single chain variable fragments cause neither meningoencephalitis, nor cerebral haemorrhages (Marín-Argany et al. 2011). Hence, VHH antibodies are a promising alternative to classical immunotherapy. In addition, the small size of the VHH enables better tissue penetration, and may facilitate the crossing of the blood-brain barrier (Muruganandam et al. 2002, Jones et al. 2010). VHH domains selected from synthetic libraries might prove to be cheaper and faster, but also more effective alternatives to antibodies generated with animal immunisation.

The monoclonal character of the B10, KW1, KW2 and KW3 enables large-scale production in *E. coli* cells and a fast purification system. Genetic availability of VHHs capacitates construction of new molecular payloads (enzymes, toxins or radionucleotides) with enhanced binding properties and desired functionality (Holliger and Hudson 2005).

Specific recognition of Aβ by small molecules underlies currently tested therapeutic strategies against AD (Lee et al. 2009, Frisardi et al. 2010, Lemkul and Bevan 2010, Ladiwala et al. 2011). In this context antibodies play a very important role. The unique features of VHH domains make them an excellent tool for basic research to study delicate Aβ structure and mechanism of aggregation. Due to their conformational specificity and unique properties, VHH antibody fragments designed to target only selected amyloid aggregates have great potential as robust diagnostic reagents, or as non-immunogenic therapeutics (Holliger and Hudson 2005).

Acknowledgements

I would like to express my gratitude to the supervisor of my PhD project, Dr. Marcus Fändrich from Max-Planck Research Unit (MPRU) in Halle, for his invaluable scientific support. I am thankful to my scientific advisor, Dr. Uwe Horn from Hans Knöll Institute (HKI) in Jena, for his everyday scientific guidance, and to Dr. Peter Hortschansky from HKI in Jena, for our fruitful collaboration, and for helping me with the surface plasmon resonance analyses. I want to thank Prof. Stephan Diekmann from Fritz-Lipmann-Institute in Jena for the supervision of my PhD project.

I would like to thank my colleagues from the working group at MPRU in Halle for their cooperation. I am particularly thankful to Isabel Morgado and Christian Haupt for their support, both scientific and personal. I thank my colleagues and coworkers form HKI in Jena, for their daily cooperation and help, especially Gisela Sudermann and Uwe Knüpfer, for their assistance with the fermentations, and for the handling of the *E. coli* cells. I am also grateful to Tania Jenkins and Eric Allan for the editorial comments on parts of my PhD dissertation.

Finally, I want to thank my family and friends, who supported me all throughout. Special thanks to my boyfriend Mateusz Jochym for his indispensable support and encouragement on all stages of my PhD project.

Summary

Aggregation of the Aβ peptide is believed to be the cause of neurodegeneration of the brain. However, the process of Aβ aggregation, as well as the structure of the intermediate and final Aβ conformers, is not fully understood. Fibrils are the final product of Aβ aggregation. They possess a very regular cross-β structure. In contrast, Aβ intermediates i.e., oligomers and protofibrils, take on spherical or curvilinear structures, respectively. Several studies have indicated that Aβ oligomers possess a considerable β-sheet structure, organised in an anti-parallel manner. Still, more detailed information about their structure is scarce.

It is not entirely clear to what extent particular Aβ conformers contribute to AD. Hence, practically all known Aβ species are targeted therapeutically. The development of diagnostic and therapeutical approaches to AD has caused an increasing interest in immunotherapy. So far, several antibodies targeting Aβ conformers have been described, but the mechanism of their action is still poorly understood.

In my dissertation, I describe several small VHH antibody domains, selected with the use of a camelid antibody library. Those VHH antibody domains are conformationally-specific to different Aβ conformers. B10, KW2, and KW3 antibody domains are specific to Aβ40 fibrils, while KW1 is specific to Aβ40 oligomers. Using various biophysical (e.g., electron microscopy, surface plasmon resonance) and biochemical methods (e.g., enzyme-linked immunosorbent assay, immunoblot), I assessed the molecular mechanism of the binding, and the conformational specificity of particular VHH antibodies to their respective targets.

The recognition of Aβ40 by B10, KW2, and KW3 proceeds in a conformation-specific manner; these antibodies bind fibrils, but they interact neither with Aβ oligomers, nor with the disaggregated Aβ peptide. In addition to Aβ40 fibrils, B10 binds to a range of amyloid-like fibrils. Still, some fibrils (e.g., PABPN1-(+7), Aβ(16–22) fibrils) are not recognised by B10. B10 also fails to bind to β-sheet rich globular proteins (e.g. lysozyme, transthyretin), or to bind intrinsically disordered peptides (e.g., glucagon, poly-L-lysine).

In-depth analysis of the B10 recognition mechanism of Aβ fibrils showed that it involves electrostatic interactions, as well as complementarity of flat surfaces on the antibody and the fibril. Hence, B10 binds to fibrils possessing the following properties: a regular cross-β sheet

structure (responsible for the flat fibril surface), and a regular distribution of anionic surface charges.

KW1 domain binds to Aβ40 oligomers, but neither to Aβ40 fibrils, nor to Aβ disaggregated peptide. Furthermore, KW1 interacts only with a certain type of Aβ40 oligomers, depending on the conditions of the preparation. In contrast, oligomers derived either from Aβ42, or from non-Aβ peptides are not recognised. None of the analysed features of oligomers (i.e., polypeptide origin, morphological appearance, presence of parallel or antiparallel β-sheet structure) predisposes oligomers to act as a KW1 ligand. The recognition of Aβ40 oligomers might be based on hydrophobic interactions, as suggested by the analysis of the crystal structure of KW1.

Antibody domains described in this dissertation constitute an excellent tool for structural research on amyloid aggregates. The mechanism of VHH antibody recognition proposed here is based on ionic (B10-fibrils) and hydrophobic (KW1-oligomers) interactions, and this indirectly provides information about the surface structure of particular Aβ aggregates. Furthermore, the binders described here are capable of distinguishing between different conformational states of Aβ, and may therefore prove useful in an assessment of the pathological relevance of Aβ. Being selective to various Aβ conformers, recombinantly available VHH domains bear a substantial potential as therapeutic or diagnostic agents.

Zusammenfassung

Die Aggregation des Aβ-Peptides wird als Ursache von neurodegenerativen Vorgängen im Gehirn angesehen. Allerdings ist der Prozess der Aβ-Aggregation, sowie die Struktur der dabei auftretenden Aggregate bislang nur unzureichend verstanden. Als Endprodukte der Aggregation bilden sich faserförmige Aggregate, die als Amyloidfibrillen bezeichnet werden. Diese zeichnen sich durch eine gekreuzte β-Faltblattstruktur aus. Dagegen weisen die Vorläuferstrukturen von Amyloidfibrillen, wie Oligomere und Protofibrillen, eine kugelförmige oder unregelmässig gekrümmte Struktur auf. Einige strukturelle Untersuchungen deuten darauf hin, dass Aβ-Oligomere einen erheblichen Anteil an antiparalleler β-Faltblattstruktur aufweisen. Allerdings existieren so gut wie keine detaillierteren Strukturinformationen zu diesen Aggregaten.

Bislang ist nicht vollständig geklärt, welche Rolle bestimmte Aβ-Aggregate für die Alzheimer-Krankheit spielen. Daher sind praktisch alle bekannten Aβ-Aggregate Ziel von therapeutischen Ansätzen. Insbesondere für die Entwicklung von diagnostischen und therapeutischen Strategien für die Alzheimer-Krankeit spielen Antikörper eine zunehmend wichtige Rolle. Eine Vielzahl von Antikörpern gegen verschiedene Aβ-Aggregate wurden in der Vergangenheit veröffentlicht, allerdings sind deren molekulare Mechanismen bislang kaum verstanden.

In meiner Dissertation charakterisiere ich verschiedene VHH-Antikörperdomänen, welche aus einer kameliden Antikörperbibliothek selektiert wurden. Diese VHH-Domänen zeichnen sich durch eine konformationelle Spezifität für verschiedene Aβ-Aggregate aus. Während die Antikörperdomänen B10, KW2 und KW3 spezifisch an Aβ-Fibrillen binden, interagiert KW1 spezifisch mit Aβ-Oligomeren. Unter Verwendung verschiedener biophysikalischer (z. B. Elektronenmikroskopie, Oberflächen-Plasmon-Resonanz-Spektroskopie) und biochemischer Methoden (z. B. enzymgekoppelter Immunadsorptionstest, Immunblot) habe ich den molekularen Mechanismus der Bindung und die konformationelle Spezifität der einzelnen VHH-Antikörper untersucht.

Die Erkennung von Aβ40 durch B10, KW2 und KW3 beruht auf einem konformationsspezifischen Mechanismus. Das heisst diese Antikörper erkennen spezifisch Aβ-Fibrillen, jedoch

nicht Aβ-Oligomere oder das disaggregierte Peptid. Zusätzlich zu Aβ40-Fibrillen bindet B10 eine Vielzahl von Nicht-Aβ-Fibrillen. Allerdings gibt ea auch einige Fibrillen (z. B. PABPN1-(+7)-Fibrillen, Aβ(16-22)-Fibrillen), an die B10 nicht bindet. Darüber hinaus zeigt B10 keine sigifikanten Interaktionen mit β-Faltblatt-reichen globulär gefalteten Proteinen (z. B. Lysozym, Transthyretin) oder intrinsisch ungefalteten Polypeptidketten (z. B. Glukagon, Poly-L-Lysin).

Eine detaillierte Analyse des Bindungsmechanismus von B10 an Fibrillen zeigte, dass elektrostatische Wechselwirkungen, sowie zueinander komplementäre flache Oberflächen entscheidend für die Interaktion sind. Daraus ergibt sich, dass von B10 erkannte Fibrillen die folgenden Eigenschaften aufweisen: eine regelmässige gekreuzte β-Faltblattstruktur, welche verantwortlich für eine relativ flache Fibrillenoberfläche ist, und eine regelmässige Verteilung von anionischen Oberflächenladungen.

KW1 bindet spezifisch an Aβ40-Oligomere, aber nicht an Aβ40-Fibrillen oder an disaggregiertes Aβ40-Peptid. Des Weiteren interagiert KW1, in Abhängigkeit von den jeweiligen Herstellungsbedingungen der Oligomere, nur mit bestimmten Typen von Aβ40-Oligomeren. Dagegen werden Oligomere des Aβ42-Peptides, als auch Oligomere von anderen Polypeptidketten nicht durch KW1 erkannt. Diese Spezifität lässt sich durch keines der untersuchten Merkmale der Oligomere (z. B. Polypeptidsequenz, morphologische Erscheinung, β-Faltblatt-Organisation) erklären. Allerdings deutet die Analyse der Kristallstruktur von KW1 darauf hin, dass die Erkennung von Aβ40-Oligomeren auf hydrophoben Interaktionen basiert.

Die in dieser Dissertation beschriebenen Antikörperdomänen stellen hervorragende Werkzeuge für die strukturelle Untersuchung von Amyloidaggregaten dar. Die hier vorgeschlagenen Erkennungsmechanismen der VHH-Antikörper, basierend auf ionischen (B10-Fibrillen) oder hydrophoben (KW1-Oligomere) Wechselwirkungen, liefern indirekt Informationen über die Oberflächenstruktur der jeweiligen Aggregate. Des Weiteren sind die beschriebenen Antikörper in der Lage verschiedene konformationelle Zustände des Aβ-Peptides zu unterscheiden. Dadurch könnten die Antikörper nützlich für die Untersuchung der pathologischen Eigenschaften von Aβ sein. Darüber hinaus besitzen rekombinante VHH-Domänen durch die selektive Erkennung von verschiedenen Aβ-Aggregaten ein vielversprechendes Potenzial als therapeutische oder diagnostische Werkzeuge.

Literature Cited

Ahmed, M., J. Davis, D. Aucoin, T. Sato, S. Ahuja, S. Aimoto, J. I. Elliott, W. E. Van Nostrand, and S. O. Smith, 2010. Structural conversion of neurotoxic amyloid-β(1–42) oligomers to fibrils. *Nat Struct Mol Biol* **17**:561–567.

Alzheimer, A., 1906. Über einen eigenartigen schweren Erkrankungsprozess der Hirnrinde. *Neurologisches Centralblatt* **23**:1129–36.

Arap, M., 2005. Phage display technology: applications and innovations. *Genet Mol Biol* **28**:1–9.

Bard, F., C. Cannon, R. Barbour, R. L. Burke, D. Games, H. Grajeda, T. Guido, K. Hu, J. Huang, K. Johnson-Wood, K. Khan, D. Kholodenko, M. Lee, I. Lieberburg, R. Motter, M. Nguyen, F. Soriano, N. Vasquez, K. Weiss, B. Welch, P. Seubert, D. Schenk, and T. Yednock, 2000. Peripherally administered antibodies against amyloid β-peptide enter the central nervous system and reduce pathology in a mouse model of Alzheimer disease. *Nat Med* **6**:916–919.

Barghorn, S., V. Nimmrich, A. Striebinger, C. Krantz, P. Keller, B. Janson, M. Bahr, M. Schmidt, R. Bitner, J. Harlan, et al., 2005. Globular amyloid β-peptide1- 42 oligomer-a homogenous and stable neuropathological protein in Alzheimer's disease. *J Neurochem* **95**:834–847.

Basi, G. S., H. Feinberg, F. Oshidari, J. Anderson, R. Barbour, J. Baker, T. A. Comery, L. Diep, D. Gill, K. Johnson-Wood, A. Goel, K. Grantcharova, M. Lee, J. Li, A. Partridge, I. Griswold-Prenner, N. Piot, D. Walker, A. Widom, M. N. Pangalos, P. Seubert, J. S. Jacobsen, D. Schenk, and W. I. Weis, 2010. Structural correlates of antibodies associated with acute reversal of amyloid β-related behavioral deficits in a mouse model of Alzheimer disease. *J Biol Chem* **285**:3417–3427.

Bernstein, S. L., N. F. Dupuis, N. D. Lazo, T. Wyttenbach, M. M. Condron, G. Bitan, D. B. Teplow, J.-E. Shea, B. T. Ruotolo, C. V. Robinson, and M. T. Bowers, 2009. Amyloid-β protein oligomerization and the importance of tetramers and dodecamers in the aetiology of Alzheimer's disease. *Nat Chem* **1**:326–331.

Biancalana, M. and S. Koide, 2010. Molecular mechanism of Thioflavin-T binding to amyloid

fibrils. *Biochim Biophys Acta* **1804**:1405–1412.

Bitan, G., E. A. Fradinger, S. M. Spring, and D. B. Teplow, 2005. Neurotoxic protein oligomers—what you see is not always what you get. *Amyloid* **12**:88–95.

Bitan, G., M. D. Kirkitadze, A. Lomakin, S. S. Vollers, G. B. Benedek, and D. B. Teplow, 2003. Amyloid β-protein (Aβ) assembly: Aβ40 and Aβ42 oligomerize through distinct pathways. *Proc Natl Acad Sci U S A* **100**:330–335.

Bradford, M., 1976. A rapid and sensitive method for the quantitation of microgram quantities of protein utilizing the principle of protein-dye binding. *Anal Biochem* **72**:248–254.

Broersen, K., F. Rousseau, and J. Schymkowitz, 2010. The culprit behind amyloid beta peptide related neurotoxicity in Alzheimer's disease: oligomer size or conformation? *Alzheimers Res Ther* **2**:12.

Caughey, B. and P. T. Lansbury, 2003. Protofibrils, pores, fibrils, and neurodegeneration: separating the responsible protein aggregates from the innocent bystanders. *Annu Rev Neurosci* **26**:267–298.

Cerf, E., R. Sarroukh, S. Tamamizu-Kato, L. Breydo, S. Derclaye, Y. F. Dufrene, V. Narayanaswami, E. Goormaghtigh, J.-M. Ruysschaert, and V. Raussens, 2009. Antiparallel β-sheet: a signature structure of the oligomeric amyloid β-peptide. *Biochem J* **421**:415–423.

Chan, J. C. C., N. A. Oyler, W.-M. Yau, and R. Tycko, 2005. Parallel β-sheets and polar zippers in amyloid fibrils formed by residues 10–39 of the yeast prion protein Ure2p. *Biochemistry* **44**:10669–10680.

Chen, Y.-R. and C. G. Glabe, 2006. Distinct early folding and aggregation properties of Alzheimer amyloid-β peptides Aβ40 and Aβ42: stable trimer or tetramer formation by Aβ42. *J Biol Chem* **281**:24414–24422.

Chimon, S., M. Shaibat, C. Jones, D. Calero, B. Aizezi, and Y. Ishii, 2007. Evidence of fibril-like β-sheet structures in a neurotoxic amyloid intermediate of Alzheimer's β-amyloid. *Nat Struct Mol Biol* **14**:1157–1164.

Chiti, F. and C. M. Dobson, 2006. Protein misfolding, functional amyloid, and human disease. *Annu Rev Biochem* **75**:333–366.

Chiti, F., M. Stefani, N. Taddei, G. Ramponi, and C. M. Dobson, 2003. Rationalization of the effects of mutations on peptide and protein aggregation rates. *Nature* **424**:805–808.

Chromy, B. A., R. J. Nowak, M. P. Lambert, K. L. Viola, L. Chang, P. T. Velasco, B. W. Jones, S. J. Fernandez, P. N. Lacor, P. Horowitz, C. E. Finch, G. A. Krafft, and W. L. Klein, 2003. Self-assembly of Aβ(1-42) into globular neurotoxins. *Biochemistry* **42**:12749–12760.

Citron, M., 2004. Strategies for disease modification in Alzheimer's disease. *Nat Rev Neurosci*

5:677–685.

Dahlgren, K., A. Manelli, W. Stine, L. Baker, G. Krafft, and M. LaDu, 2002. Oligomeric and fibrillar species of amyloid-β peptides differentially affect neuronal viability. *J Biol Chem* **277**:32046–32053.

Dattilo, B. M., G. Fritz, E. Leclerc, C. W. V. Kooi, C. W. Heizmann, and W. J. Chazin, 2007. The extracellular region of the receptor for advanced glycation end products is composed of two independent structural units. *Biochemistry* **46**:6957–6970.

De Genst, E., K. Silence, K. Decanniere, K. Conrath, R. Loris, J. Kinne, S. Muyldermans, and L. Wyns, 2006. Molecular basis for the preferential cleft recognition by dromedary heavy-chain antibodies. *Proc Natl Acad Sci U S A* **103**:4586–4591.

Delrieu, J., P. Ousset, C. Caillaud, and B. Vellas, 2011. 'Clinical trials in Alzheimer's disease': immunotherapy approaches. *J Neurochem* **1**:186–193.

DeMattos, R. B., K. R. Bales, D. J. Cummins, J. C. Dodart, S. M. Paul, and D. M. Holtzman, 2001. Peripheral anti-Aβ antibody alters cns and plasma Aβ clearance and decreases brain Aβ burden in a mouse model of Alzheimer's disease. *Proc Natl Acad Sci U S A* **98**:8850–8855.

DeWeerdt, S., 2011. Prevention: activity is the best medicine. *Nature* **475**:S16–7.

Dobson, C., 2001. The structural basis of protein folding and its links with human disease. *Philos Trans R Soc Lond B Biol Sci* **356**:133.

Donzeau, M. and A. Knappik, 2007. Recombinant monoclonal antibodies. *Methods Mol Biol* **378**:14–31.

Eckert, A., S. Hauptmann, I. Scherping, J. Meinhardt, V. Rhein, S. Drose, U. Brandt, M. Fändrich, W. E. Muller, and J. Götz, 2008. Oligomeric and fibrillar species of β-amyloid (Aβ42) both impair mitochondrial function in P301L tau transgenic mice. *J Mol Med* **86**:1255–1267.

Eisenstein, M., 2011. Genetics: finding risk factors. *Nature* **475**:S20–2.

Ewert, S., C. Cambillau, K. Conrath, and A. Pluckthun, 2002. Biophysical properties of camelid V(HH) domains compared to those of human V(H)3 domains. *Biochemistry* **41**:3628–3636.

Fabian, H., K. Gast, M. Laue, R. Misselwitz, B. Uchanska-Ziegler, A. Ziegler, and D. Naumann, 2008. Early stages of misfolding and association of β2-microglobulin: insights from infrared spectroscopy and dynamic light scattering. *Biochemistry* **47**:6895–6906.

Fändrich, M., 2007. On the structural definition of amyloid fibrils and other polypeptide aggregates. *Cell Mol Life Sci* **64**:2066–2078.

Fändrich, M., 2012. Oligomeric intermediates in amyloid formation: Structure determination

and mechanisms of toxicity. *J Mol Biol* doi: 10.1016/j.jmb.2012.01.006.

Fändrich, M., J. Meinhardt, and N. Grigorieff, 2009. Structural polymorphism of Alzheimer Aβ and other amyloid fibrils. *Prion* **3**:89–93.

Fändrich, M., M. Schmidt, and N. Grigorieff, 2011. Recent progress in understanding Alzheimer's β-amyloid structures. *Trends Biochem Sci* **36**:338–345.

Fändrich, M., G. Zandomeneghi, M. Krebs, M. Kittler, K. Buder, A. Roßner, S. Heinemann, C. Dobson, and S. Diekmann, 2006. Apomyoglobin reveals a random-nucleation mechanism in amyloid protofibril formation. *Acta Histochem* **108**:215–219.

Ferri, C., M. Prince, C. Brayne, H. Brodaty, L. Fratiglioni, M. Ganguli, K. Hall, K. Hasegawa, H. Hendrie, Y. Huang, et al., 2006. Global prevalence of dementia: a Delphi consensus study. *Lancet* **366**:2112–2117.

Frenkel, D., N. Kariv, and B. Solomon, 2001. Generation of auto-antibodies towards Alzheimer's disease vaccination. *Vaccine* **19**:2615–2619.

Frid, P., S. Anisimov, and N. Popovic, 2007. Congo red and protein aggregation in neurodegenerative diseases. *Brain Res Rev* **53**:135–160.

Frisardi, V., V. Solfrizzi, P. B. Imbimbo, C. Capurso, A. D'Introno, A. M. Colacicco, G. Vendemiale, D. Seripa, A. Pilotto, A. Capurso, and F. Panza, 2010. Towards disease-modifying treatment of Alzheimer's disease: drugs targeting β-amyloid. *Curr Alzheimer Res* **7**:40–55.

Gardberg, A. S., L. T. Dice, S. Ou, R. L. Rich, E. Helmbrecht, J. Ko, R. Wetzel, D. G. Myszka, P. H. Patterson, and C. Dealwis, 2007. Molecular basis for passive immunotherapy of Alzheimer's disease. *Proc Natl Acad Sci U S A* **104**:15659–15664.

Gellermann, G., H. Byrnes, A. Striebinger, K. Ullrich, R. Mueller, H. Hillen, and S. Barghorn, 2008. Aβ-globulomers are formed independently of the fibril pathway. *Neurobiology of disease* **30**:212–220.

Geula, C., C. K. Wu, D. Saroff, A. Lorenzo, M. Yuan, and B. A. Yankner, 1998. Aging renders the brain vulnerable to amyloid β-protein neurotoxicity. *Nat Med* **4**:827–831.

Gill, S. and P. von Hippel, 1989. Calculation of protein extinction coefficients from amino acid sequence data. *Anal biochem* **182**:319–326.

Glabe, C. G., 2008. Structural classification of toxic amyloid oligomers. *J Biol Chem* **283**:29639–29643.

Goldsbury, C. S., S. Wirtz, S. A. Muller, S. Sunderji, P. Wicki, U. Aebi, and P. Frey, 2000. Studies on the in vitro assembly of Aβ 1–40: implications for the search for Aβ fibril formation inhibitors. *J Struct Biol* **130**:217–231.

Gong, Y., L. Chang, K. Viola, P. Lacor, M. Lambert, C. Finch, G. Krafft, and W. Klein, 2003.

Alzheimer's disease-affected brain: presence of oligomeric Aβ ligands (ADDLs) suggests a molecular basis for reversible memory loss. *Proc Natl Acad Sci U S A* **100**:10417–10422.

Gunzburg, M., M. Perugini, and G. Howlett, 2007. Structural basis for the recognition and cross-linking of amyloid fibrils by human apolipoprotein E. *J Biol Chem* **282**:35831.

Haass, C. and D. Selkoe, 2007. Soluble protein oligomers in neurodegeneration: lessons from the Alzheimer's amyloid β-peptide. *Nat Rev Mol Cell Biol* **8**:101.

Habicht, G., 2002. Konstruktion einer vollsynthetischen *Camelidae*-VHH-Antikörper-Bibliotek optimierter Qualität und deren Expression in *Escherichia coli*. Master's thesis, Friedrich Schiller Universität, Jena.

Habicht, G., C. Haupt, R. P. Friedrich, P. Hortschansky, C. Sachse, J. Meinhardt, K. Wieligmann, G. P. Gellermann, M. Brodhun, J. Götz, K.-J. Halbhuber, C. Röcken, U. Horn, and M. Fändrich, 2007. Directed selection of a conformational antibody domain that prevents mature amyloid fibril formation by stabilizing Aβ protofibrils. *Proc Natl Acad Sci U S A* **104**:19232–19237.

Haigh, N. G. and R. E. Webster, 1998. The major coat protein of filamentous bacteriophage f1 specifically pairs in the bacterial cytoplasmic membrane. *J Mol Biol* **279**:19–29.

Hamers-Casterman, C., T. Atarhouch, S. Muyldermans, G. Robinson, C. Hamers, E. B. Songa, N. Bendahman, and R. Hamers, 1993. Naturally occurring antibodies devoid of light chains. *Nature* **363**:446–448.

Hanahan, D., 1983. Studies on transformation of Escherichia coli with plasmids. *J Mol Biol* **166**:557–580.

Hanes, J. and A. Plückthun, 1997. In vitro selection and evolution of functional proteins by using ribosome display. *Proc Natl Acad Sci U S A* **94**:4937–4942.

Hardy, J. and D. Allsop, 1991. Amyloid deposition as the central event in the aetiology of Alzheimer's disease. *Trends Pharmacol Sci* **12**:383–388.

Hardy, J. and D. Selkoe, 2002. The amyloid hypothesis of Alzheimer's disease: progress and problems on the road to therapeutics. *Science* **297**:353–356.

Hardy, J. A. and G. A. Higgins, 1992. Alzheimer's disease: the amyloid cascade hypothesis. *Science* **256**:184–185.

Harper, J. D. and P. T. J. Lansbury, 1997. Models of amyloid seeding in Alzheimer's disease and scrapie: mechanistic truths and physiological consequences of the time-dependent solubility of amyloid proteins. *Annu Rev Biochem* **66**:385–407.

Harper, J. D., S. S. Wong, C. M. Lieber, and P. T. Lansbury, 1997. Observation of metastable Aβ amyloid protofibrils by atomic force microscopy. *Chem Biol* **4**:119–125.

Haupt, C., M. Bereza, S. T. Kumar, B. Kieninger, I. Morgado, P. Hortschansky, G. Fritz,

C. Röcken, U. Horn, and M. Fändrich, 2011a. Pattern recognition with a fibril-specific antibody fragment reveals the surface variability of natural amyloid fibrils. *J Mol Biol* **408**:529–540.

Haupt, C., J. Leppert, R. Rönicke, J. Meinhardt, J. K. Yadav, R. Ramachandran, O. Ohlenschlager, K. G. Reymann, M. Görlach, and M. Fändrich, 2012. Structural basis of β-amyloid-dependent synaptic dysfunctions. *Angew Chem Int Ed Engl* **51**:1576–1579.

Haupt, C., I. Morgado, S. T. Kumar, C. Parthier, M. Bereza, P. Hortschansky, M. T. Stubbs, U. Horn, and M. Fändrich, 2011b. Amyloid fibril recognition with the conformational B10 antibody fragment depends on electrostatic interactions. *J Mol Biol* **405**:341–348.

He, M. and F. Khan, 2005. Ribosome display: next-generation display technologies for production of antibodies *in vitro*. *Expert Rev Proteomics* **2**:421–430.

Holliger, P. and P. J. Hudson, 2005. Engineered antibody fragments and the rise of single domains. *Nat Biotechnol* **23**:1126–1136.

Holmes, C., D. Boche, D. Wilkinson, G. Yadegarfar, V. Hopkins, A. Bayer, R. W. Jones, R. Bullock, S. Love, J. W. Neal, E. Zotova, and J. A. R. Nicoll, 2008. Long-term effects of Aβ42 immunisation in Alzheimer's disease: follow-up of a randomised, placebo-controlled phase I trial. *Lancet* **372**:216–223.

Horn, U., W. Strittmatter, A. Krebber, U. Knüpfer, M. Kujau, R. Wenderoth, K. Müller, S. Matzku, A. Plückthun, and D. Riesenberg, 1996. High volumetric yields of functional dimeric miniantibodies in *Escherichia coli*, using an optimized expression vector and high-cell-density fermentation under non-limited growth conditions. *Appl Microbiol Biotechnol* **46**:524–532.

Hortschansky, P., V. Schroeckh, T. Christopeit, G. Zandomeneghi, and M. Fändrich, 2005. The aggregation kinetics of Alzheimer's β-amyloid peptide is controlled by stochastic nucleation. *Protein Sci* **14**:1753–1759.

Hsia, A. Y., E. Masliah, L. McConlogue, G. Q. Yu, G. Tatsuno, K. Hu, D. Kholodenko, R. C. Malenka, R. A. Nicoll, and L. Mucke, 1999. Plaque-independent disruption of neural circuits in Alzheimer's disease mouse models. *Proc Natl Acad Sci U S A* **96**:3228–3233.

Huang, L., S. Muyldermans, and D. Saerens, 2010. Nanobodies ®: proficient tools in diagnostics. *Expert Rev Mol Diagn* **10**:777–785.

Istrin, G., E. Bosis, and B. Solomon, 2006. Intravenous immunoglobulin enhances the clearance of fibrillar amyloid-β peptide. *J Neurosci Res* **84**:434–443.

Iwata, K., T. Fujiwara, Y. Matsuki, H. Akutsu, S. Takahashi, H. Naiki, and Y. Goto, 2006. 3D structure of amyloid protofilaments of β2-microglobulin fragment probed by solid-state NMR. *Proc Natl Acad Sci U S A* **103**:18119.

Jakob-Roetne, R. and H. Jacobsen, 2009. Alzheimer's disease: from pathology to therapeutic approaches. *Angew Chem Int Ed Engl* **48**:3030–3059.

Jones, D. R., W. A. Taylor, C. Bate, M. David, and M. Tayebi, 2010. A camelid anti-PrP antibody abrogates PrP replication in prion-permissive neuroblastoma cell lines. *PLoS One* **5**:e9804.

Kabat, E., T. Te Wu, K. Gottesman, and C. Foeller, 1992. Sequences of Proteins of Immunological Interest. Diane Pub Co.

Kammerer, R., D. Kostrewa, J. Zurdo, A. Detken, C. García-Echeverría, J. Green, S. Müller, B. Meier, F. Winkler, C. Dobson, et al., 2004. Exploring amyloid formation by a de novo design. *Proc Natl Acad Sci U S A* **101**:4435.

Kasturirangan, S., S. Boddapati, and M. R. Sierks, 2010a. Engineered proteolytic nanobodies reduce Aβ burden and ameliorate Aβ-induced cytotoxicity. *Biochemistry* **49**:4501–4508.

Kasturirangan, S., L. Li, S. Emadi, S. Boddapati, P. Schulz, and M. Sierks, 2010b. Nanobody specific for oligomeric β-amyloid stabilizes nontoxic form. *Neurobiol Aging* doi: 10.1016/j.neurobiolaging.2010.09.020.

Kayed, R., I. Canto, L. Breydo, S. Rasool, T. Lukacsovich, J. Wu, R. Albay, A. Pensalfini, S. Yeung, E. Head, et al., 2010. Conformation dependent monoclonal antibodies distinguish different replicating strains or conformers of prefibrillar Aβ oligomers. *Mol Neurodegener* **5**:1–10.

Kayed, R., E. Head, F. Sarsoza, T. Saing, C. W. Cotman, M. Necula, L. Margol, J. Wu, L. Breydo, J. L. Thompson, S. Rasool, T. Gurlo, P. Butler, and C. G. Glabe, 2007. Fibril specific, conformation dependent antibodies recognize a generic epitope common to amyloid fibrils and fibrillar oligomers that is absent in prefibrillar oligomers. *Mol Neurodegener* **2**:18.

Kayed, R., E. Head, J. L. Thompson, T. M. McIntire, S. C. Milton, C. W. Cotman, and C. G. Glabe, 2003. Common structure of soluble amyloid oligomers implies common mechanism of pathogenesis. *Science* **300**:486–489.

Kayed, R., A. Pensalfini, L. Margol, Y. Sokolov, F. Sarsoza, E. Head, J. Hall, and C. Glabe, 2009. Annular protofibrils are a structurally and functionally distinct type of amyloid oligomer. *J Biol Chem* **284**:4230–4237.

Kheterpal, I., M. Chen, K. Cook, and R. Wetzel, 2006. Structural differences in Aβ amyloid protofibrils and fibrils mapped by hydrogen exchange-mass spectrometry with on-line proteolytic fragmentation. *J Mol Biol* **361**:785–795.

Kirkitadze, M., G. Bitan, and D. Teplow, 2002. Paradigm shifts in Alzheimer's disease and other neurodegenerative disorders: the emerging role of oligomeric assemblies. *J Neurosci*

Res **69**:567–577.

Kisilevsky, R., 2000. The relation of proteoglycans, serum amyloid P and apo E to amyloidosis current status, 2000. *Amyloid* **7**:5–23.

Klein, W. L., 2002. Aβ toxicity in Alzheimer's disease: globular oligomers (ADDLs) as new vaccine and drug targets. *Neurochem Int* **41**:345–352.

Krebs, B., R. Rauchenberger, S. Reiffert, C. Rothe, M. Tesar, E. Thomassen, M. Cao, T. Dreier, D. Fischer, A. Hoss, L. Inge, A. Knappik, M. Marget, P. Pack, X. Meng, R. Schier, P. Sohlemann, J. Winter, J. Wolle, and T. Kretzschmar, 2001. High-throughput generation and engineering of recombinant human antibodies. *J Immunol Methods* **254**:67–84.

Lacor, P. N., M. C. Buniel, L. Chang, S. J. Fernandez, Y. Gong, K. L. Viola, M. P. Lambert, P. T. Velasco, E. H. Bigio, C. E. Finch, G. A. Krafft, and W. L. Klein, 2004. Synaptic targeting by Alzheimer's-related amyloid-β oligomers. *J Neurosci* **24**:10191–10200.

Ladiwala, A. R. A., J. S. Dordick, and P. M. Tessier, 2011. Aromatic small molecules remodel toxic soluble oligomers of amyloid-β through three independent pathways. *J Biol Chem* **286**:3209–3218.

Lafaye, P., I. Achour, P. England, C. Duyckaerts, and F. Rougeon, 2009. Single-domain antibodies recognize selectively small oligomeric forms of amyloid β, prevent Aβ-induced neurotoxicity and inhibit fibril formation. *Mol Immunol* **46**:695–704.

Lambert, M. P., A. K. Barlow, B. A. Chromy, C. Edwards, R. Freed, M. Liosatos, T. E. Morgan, I. Rozovsky, B. Trommer, K. L. Viola, P. Wals, C. Zhang, C. E. Finch, G. A. Krafft, and W. L. Klein, 1998. Diffusible, nonfibrillar ligands derived from Aβ1-42 are potent central nervous system neurotoxins. *Proc Natl Acad Sci U S A* **95**:6448–6453.

Lambert, M. P., P. T. Velasco, L. Chang, K. L. Viola, S. Fernandez, P. N. Lacor, D. Khuon, Y. Gong, E. H. Bigio, P. Shaw, F. G. De Felice, G. A. Krafft, and W. L. Klein, 2007. Monoclonal antibodies that target pathological assemblies of Aβ. *J Neurochem* **100**:23–35.

Lasagna-Reeves, C., C. Glabe, and R. Kayed, 2011. Amyloid-β: Annular protofibrils evade fibrillar fate in Alzheimer disease brain. *J Biol Chem* **286**:22122.

Lashuel, H., D. Hartley, B. Petre, T. Walz, and P. Lansbury, 2002. Neurodegenerative disease: amyloid pores from pathogenic mutations. *Nature* **418**:291–291.

Lee, L. L., H. Ha, Y.-T. Chang, and M. P. DeLisa, 2009. Discovery of amyloid-β aggregation inhibitors using an engineered assay for intracellular protein folding and solubility. *Protein Sci* **18**:277–286.

Lemere, C. A., R. Maron, E. T. Spooner, T. J. Grenfell, C. Mori, R. Desai, W. W. Hancock, H. L. Weiner, and D. J. Selkoe, 2000. Nasal Aβ treatment induces anti-Aβ antibody production and decreases cerebral amyloid burden in PD-APP mice. *Ann N Y Acad Sci*

920:328–331.

Lemere, C. A. and E. Masliah, 2010. Can Alzheimer disease be prevented by amyloid-β immunotherapy? *Nat Rev Neurol* **6**:108–119.

Lemere, C. A., E. T. Spooner, J. LaFrancois, B. Malester, C. Mori, J. F. Leverone, Y. Matsuoka, J. W. Taylor, R. B. DeMattos, D. M. Holtzman, J. D. Clements, D. J. Selkoe, and K. E. Duff, 2003. Evidence for peripheral clearance of cerebral Aβ protein following chronic, active Aβ immunization in PSAPP mice. *Neurobiol Dis* **14**:10–18.

Lemkul, J. A. and D. R. Bevan, 2010. Destabilizing Alzheimer's Aβ(42) protofibrils with morin: mechanistic insights from molecular dynamics simulations. *Biochemistry* **49**:3935–3946.

Lesne, S., M. T. Koh, L. Kotilinek, R. Kayed, C. G. Glabe, A. Yang, M. Gallagher, and K. H. Ashe, 2006. A specific amyloid-beta protein assembly in the brain impairs memory. *Nature* **440**:352–357.

Lichtenthaler, S. and C. Haass, 2004. Amyloid at the cutting edge: activation of α-secretase prevents amyloidogenesis in an Alzheimer disease mouse model. *J Clin Invest* **113**:1384–1386.

Lombardo, J. A., E. A. Stern, M. E. McLellan, S. T. Kajdasz, G. A. Hickey, B. J. Bacskai, and B. T. Hyman, 2003. Amyloid-β antibody treatment leads to rapid normalization of plaque-induced neuritic alterations. *J Neurosci* **23**:10879–10883.

Lorenzo, A. and B. Yankner, 1994. β-amyloid neurotoxicity requires fibril formation and is inhibited by congo red. *Proc Natl Acad Sci U S A* **91**:12243.

Lue, L., Y. Kuo, A. Roher, L. Brachova, Y. Shen, L. Sue, T. Beach, J. Kurth, R. Rydel, and J. Rogers, 1999. Soluble amyloid β peptide concentration as a predictor of synaptic change in Alzheimer's disease. *Am J Pathol* **155**:853–862.

Lührs, T., C. Ritter, M. Adrian, D. Riek-Loher, B. Bohrmann, H. Dobeli, D. Schubert, and R. Riek, 2005. 3D structure of Alzheimer's amyloid-β(1-42) fibrils. *Proc Natl Acad Sci U S A* **102**:17342–17347.

Maltsev, A., S. Bystryak, and O. Galzitskaya, 2011. The role of β-amyloid peptide in neurodegenerative diseases. *Ageing Research Reviews* .

Marín-Argany, M., G. Rivera-Hernández, J. Martí, and S. Villegas, 2011. An anti-Aβ (amyloid β) single-chain variable fragment prevents amyloid fibril formation and cytotoxicity by withdrawing Aβ oligomers from the amyloid pathway. *Biochem J* **437**:25–34.

Marshall, K. and L. Serpell, 2009. Insights into the structure of amyloid fibrils. *Open Biol J* **2**:185–192.

Marvin, D. A., 1998. Filamentous phage structure, infection and assembly. *Curr Opin Struct*

Biol **8**:150–158.

Mastrangelo, I. A., M. Ahmed, T. Sato, W. Liu, C. Wang, P. Hough, and S. O. Smith, 2006. High-resolution atomic force microscopy of soluble Aβ42 oligomers. *J Mol Biol* **358**:106–119.

Matulis, D., C. G. Baumann, V. A. Bloomfield, and R. E. Lovrien, 1999. 1-anilino-8-naphthalene sulfonate as a protein conformational tightening agent. *Biopolymers* **49**:451–458.

McLaurin, J., R. Cecal, M. E. Kierstead, X. Tian, A. L. Phinney, M. Manea, J. E. French, M. H. L. Lambermon, A. A. Darabie, M. E. Brown, C. Janus, M. A. Chishti, P. Horne, D. Westaway, P. E. Fraser, H. T. J. Mount, M. Przybylski, and P. St George-Hyslop, 2002. Therapeutically effective antibodies against amyloid-β peptide target amyloid-β residues 4–10 and inhibit cytotoxicity and fibrillogenesis. *Nat Med* **8**:1263–1269.

McLean, C. A., R. A. Cherny, F. W. Fraser, S. J. Fuller, M. J. Smith, K. Beyreuther, A. I. Bush, and C. L. Masters, 1999. Soluble pool of Aβ amyloid as a determinant of severity of neurodegeneration in Alzheimer's disease. *Ann Neurol* **46**:860–866.

Meinhardt, J., 2010. Structural Polymorphism of Alzheimer's Amyloid-β Aggregates. Ph.D. thesis, Friedrich Schiller Universität, Jena.

Meinhardt, J., C. Sachse, P. Hortschansky, N. Grigorieff, and M. Fändrich, 2009. Aβ(1-40) fibril polymorphism implies diverse interaction patterns in amyloid fibrils. *J Mol Biol* **386**:869–877.

Miyazawa, T. and E. Blout, 1961. The infrared spectra of polypeptides in various conformations: Amide I and II bands. *J Am Chem Soc* **83**:712–719.

Morgado, I., K. Wieligmann, M. Bereza, R. Rönicke, K. Meinhardt, K. Annamalai, M. Baumann, J. Wacker, P. Hortschansky, M. Malešević, C. Parthier, C. Mawrin, C. Schiene-Fischer, K. G. Reymann, M. T. Stubbs, J. Balbach, M. Görlach, U. Horn, and M. Fändrich, 2012. Molecular basis of Aβ oligomer recognition with a conformational antibody fragment oligomer recognition with a conformational antibody fragment. *Proc Natl Acad Sci U S A* (in press).

Morgan, D., 2011. Immunotherapy for Alzheimer's disease. *J Intern Med* **269**:54–63.

Morgan, D., D. M. Diamond, P. E. Gottschall, K. E. Ugen, C. Dickey, J. Hardy, K. Duff, P. Jantzen, G. DiCarlo, D. Wilcock, K. Connor, J. Hatcher, C. Hope, M. Gordon, and G. W. Arendash, 2000. Aβ peptide vaccination prevents memory loss in an animal model of Alzheimer's disease. *Nature* **408**:982–985.

Muruganandam, A., J. Tanha, S. Narang, and D. Stanimirovic, 2002. Selection of phage-displayed llama single-domain antibodies that transmigrate across human blood-brain

barrier endothelium. *FASEB J* **16**:240–242.

Muyldermans, S., 2001. Single domain camel antibodies: current status. *J Biotechnol* **74**:277–302.

Myers, A. and A. Goate, 2001. The genetics of late-onset Alzheimer's disease. *Curr Opin Neurol* **14**:433–440.

Natalello, A., V. V. Prokorov, F. Tagliavini, M. Morbin, G. Forloni, M. Beeg, C. Manzoni, L. Colombo, M. Gobbi, M. Salmona, and S. M. Doglia, 2008. Conformational plasticity of the Gerstmann-Straussler-Scheinker disease peptide as indicated by its multiple aggregation pathways. *J Mol Biol* **381**:1349–1361.

Ono, K., M. Condron, and D. Teplow, 2009. Structure–neurotoxicity relationships of amyloid β-protein oligomers. *Proc Natl Acad Sci U S A* **106**:14745–14750.

O'Nuallain, B., D. Freir, A. Nicoll, E. Risse, N. Ferguson, C. Herron, J. Collinge, and D. Walsh, 2010. Amyloid β-protein dimers rapidly form stable synaptotoxic protofibrils. *J Neurosci* **30**:14411–14419.

O'Nuallain, B. and R. Wetzel, 2002. Conformational Abs recognizing a generic amyloid fibril epitope. *Proc Natl Acad Sci U S A* **99**:1485–1490.

Orgogozo, J.-M., S. Gilman, J.-F. Dartigues, B. Laurent, M. Puel, L. C. Kirby, P. Jouanny, B. Dubois, L. Eisner, S. Flitman, B. F. Michel, M. Boada, A. Frank, and C. Hock, 2003. Subacute meningoencephalitis in a subset of patients with AD after Aβ42 immunization. *Neurology* **61**:46–54.

Pedersen, J. S. and D. E. Otzen, 2008. Amyloid-a state in many guises: survival of the fittest fibril fold. *Protein Sci* **17**:2–10.

Petkova, A., R. Leapman, Z. Guo, W. Yau, M. Mattson, and R. Tycko, 2005. Self-propagating, molecular-level polymorphism in Alzheimer's ß-amyloid fibrils. *Science* **307**:262–265.

Petkova, A., W. Yau, and R. Tycko, 2006. Experimental constraints on quaternary structure in Alzheimer's β-amyloid fibrils. *Biochemistry* **45**:498–512.

Plückthun, A., 1992. Mono-and bivalent antibody fragments produced in *Escherichia coli*: Engineering, folding and antigen binding. *Immunol Rev* **130**:151–188.

Plückthun, A., A. Krebber, C. Krebber, U. Horn, U. Knüpfer, R. Wenderoth, L. Nieba, K. Proba, and D. Riesenberg, 1996. Producing antibodies in *Escherichia coli*: from PCR to fermentation. In *Antibody engineering: a practical approach*, pages 203–252. IRL Press, Oxford.

Plückthun, A. and P. Pack, 1997. New protein engineering approaches to multivalent and bispecific antibody fragments. *Immunotechnology* **3**:83–105.

Ponsel, D., J. Neugebauer, K. Ladetzki-Baehs, and K. Tissot, 2011. High affinity, devel-

opability and functional size: the holy grail of combinatorial antibody library generation. *Molecules* **16**:3675–3700.

Reches, M., Y. Porat, and E. Gazit, 2002. Amyloid fibril formation by pentapeptide and tetrapeptide fragments of human calcitonin. *J Biol Chem* **277**:35475–35480.

Roher, A., M. Chaney, Y. Kuo, S. Webster, W. Stine, L. Haverkamp, A. Woods, R. Cotter, J. Tuohy, G. Krafft, et al., 1996. Morphology and toxicity of Aβ(1–42) dimer derived from neuritic and vascular amyloid deposits of Alzheimer's disease. *J Biol Chem* **271**:20631–20635.

Sachse, C., M. Fändrich, and N. Grigorieff, 2008. Paired β-sheet structure of an Aβ(1-40) amyloid fibril revealed by electron microscopy. *Proc Natl Acad Sci U S A* **105**:7462–7466.

Sachse, C., C. Xu, K. Wieligmann, S. Diekmann, N. Grigorieff, and M. Fändrich, 2006. Quaternary structure of a mature amyloid fibril from Alzheimer's Aβ(1–40) peptide. *J Mol Biol* **362**:347–354.

Sackewitz, M., H. A. Scheidt, G. Lodderstedt, A. Schierhorn, E. Schwarz, and D. Huster, 2008. Structural and dynamical characterization of fibrils from a disease-associated alanine expansion domain using proteolysis and solid-state NMR spectroscopy. *J Am Chem Soc* **130**:7172–7173.

Sandberg, A., L. Luheshi, S. Söllvander, T. Pereira de Barros, B. Macao, T. Knowles, H. Biverstål, C. Lendel, F. Ekholm-Petterson, A. Dubnovitsky, et al., 2010. Stabilization of neurotoxic Alzheimer amyloid-β oligomers by protein engineering. *Proc Natl Acad Sci U S A* **107**:15595–15600.

Sarroukh, R., E. Cerf, S. Derclaye, Y. Dufrêne, E. Goormaghtigh, J. Ruysschaert, and V. Raussens, 2010. Transformation of amyloid β (1–40) oligomers into fibrils is characterized by a major change in secondary structure. *Cell Mol Life Sci* **68**:1429–1438.

Sawaya, M., S. Sambashivan, R. Nelson, M. Ivanova, S. Sievers, M. Apostol, M. Thompson, M. Balbirnie, J. Wiltzius, H. McFarlane, et al., 2007. Atomic structures of amyloid cross-β spines reveal varied steric zippers. *Nature* **447**:453–457.

Scheidt, H. A., I. Morgado, S. Rothemund, D. Huster, and M. Fändrich, 2011. Solid-state NMR spectroscopic investigation of Aβ protofibrils: implication of a β-sheet remodeling upon maturation into terminal amyloid fibrils. *Angew Chem Int Ed Engl* **50**:2837–2840.

Schenk, D., 2002. Amyloid-beta immunotherapy for Alzheimer's disease: the end of the beginning. *Nat Rev Neurosci* **3**:824–828.

Schenk, D. B., P. Seubert, M. Grundman, and R. Black, 2005. Aβ immunotherapy: Lessons learned for potential treatment of Alzheimer's disease. *Neurodegener Dis* **2**:255–260.

Schmidt, M., C. Sachse, W. Richter, C. Xu, M. Fändrich, and N. Grigorieff, 2009. Com-

parison of Alzheimer Aβ(1-40) and Aβ(1-42) amyloid fibrils reveals similar protofilament structures. *Proc Natl Acad Sci U S A* **106**:19813–19818.

Schmitz, C., B. P. F. Rutten, A. Pielen, S. Schafer, O. Wirths, G. Tremp, C. Czech, V. Blanchard, G. Multhaup, P. Rezaie, H. Korr, H. W. M. Steinbusch, L. Pradier, and T. A. Bayer, 2004. Hippocampal neuron loss exceeds amyloid plaque load in a transgenic mouse model of Alzheimer's disease. *Am J Pathol* **164**:1495–1502.

Selkoe, D., 2001. Alzheimer's disease: genes, proteins, and therapy. *Physiol Rev* **81**:741–766.

Selkoe, D., 2008. Soluble oligomers of the amyloid β-protein impair synaptic plasticity and behavior. *Behav Brain Res* **192**:106–113.

Sergeeva, A., M. G. Kolonin, J. J. Molldrem, R. Pasqualini, and W. Arap, 2006. Display technologies: application for the discovery of drug and gene delivery agents. *Adv Drug Deliv Rev* **58**:1622–1654.

Shankar, G. and D. Walsh, 2009. Alzheimer's disease: synaptic dysfunction and Aβ. *Mol Neurodegener* **4**:48.

Shankar, G. M., S. Li, T. H. Mehta, A. Garcia-Munoz, N. E. Shepardson, I. Smith, F. M. Brett, M. A. Farrell, M. J. Rowan, C. A. Lemere, C. M. Regan, D. M. Walsh, B. L. Sabatini, and D. J. Selkoe, 2008. Amyloid-β protein dimers isolated directly from Alzheimer's brains impair synaptic plasticity and memory. *Nat Med* **14**:837–842.

Sipe, J. D., M. D. Benson, J. N. Buxbaum, S.-I. Ikeda, G. Merlini, M. J. M. Saraiva, and P. Westermark, 2010. Amyloid fibril protein nomenclature: 2010 recommendations from the nomenclature committee of the International Society of Amyloidosis. *Amyloid* **17**:101–104.

Smith, G. P., 1985. Filamentous fusion phage: novel expression vectors that display cloned antigens on the virion surface. *Science* **228**:1315–1317.

Solomon, B., R. Koppel, D. Frankel, and E. Hanan-Aharon, 1997. Disaggregation of Alzheimer β-amyloid by site-directed mAb. *Proc Natl Acad Sci U S A* **94**:4109–4112.

Solomon, B., R. Koppel, E. Hanan, and T. Katzav, 1996. Monoclonal antibodies inhibit *in vitro* fibrillar aggregation of the Alzheimer β-amyloid peptide. *Proc Natl Acad Sci U S A* **93**:452–455.

Soreghan, B., J. Kosmoski, and C. Glabe, 1994. Surfactant properties of Alzheimer's Aβ peptides and the mechanism of amyloid aggregation. *J Biol Chem* **269**:28551–28554.

Stine Jr, W., K. Dahlgren, G. Krafft, and M. LaDu, 2003. In vitro characterization of conditions for amyloid-β peptide oligomerization and fibrillogenesis. *Journal of Biological Chemistry* **278**:11612–11622.

Streltsov, V. A., J. N. Varghese, C. L. Masters, and S. D. Nuttall, 2011. Crystal structure of the

amyloid-beta p3 fragment provides a model for oligomer formation in Alzheimer's disease. *J Neurosci* **31**:1419–1426.

Suh, Y. and F. Checler, 2002. Amyloid precursor protein, presenilins, and α-synuclein: molecular pathogenesis and pharmacological applications in Alzheimer's Disease. *Pharmacol Rev* **54**:469.

Sunde, M. and C. Blake, 1998. From the globular to the fibrous state: protein structure and structural conversion in amyloid formation. *Q Rev Biophys* **31**:1–39.

Sunde, M., L. Serpell, M. Bartlam, P. Fraser, M. Pepys, and C. Blake, 1997. Common core structure of amyloid fibrils by synchrotron X-ray diffraction. *J Mol Biol* **273**:729–739.

Thompson, D., M. Pepys, I. Tickle, and S. Wood, 2002. The structures of crystalline complexes of human serum amyloid P component with its carbohydrate ligand, the cyclic pyruvate acetal of galactose. *J Mol Biol* **320**:1081–1086.

Turnell, W. and J. Finch, 1992. Binding of the dye congo red to the amyloid protein pig insulin reveals a novel homology amongst amyloid-forming peptide sequences. *J Mol Biol* **227**:1205–1223.

Upadhaya, A., I. Lungrin, H. Yamaguchi, M. Fändrich, and D. Thal, 2011. High-molecular weight Aβ-oligomers and protofibrils are the predominant Aβ-species in the native soluble protein fraction of the AD brain. *J Cell Mol Med* .

Van der Linden, R., L. Frenken, B. De Geus, M. Harmsen, R. Ruuls, W. Stok, L. De Ron, S. Wilson, P. Davis, and C. Verrips, 1999. Comparison of physical chemical properties of llama VHH antibody fragments and mouse monoclonal antibodies. *Biochim Biophys Acta* **1431**:37–46.

Vasilevko, V., F. Xu, M. L. Previti, W. E. Van Nostrand, and D. H. Cribbs, 2007. Experimental investigation of antibody-mediated clearance mechanisms of amyloid-β in CNS of Tg-SwDI transgenic mice. *J Neurosci* **27**:13376–13383.

Vaughan, T. J., A. J. Williams, K. Pritchard, J. K. Osbourn, A. R. Pope, J. C. Earnshaw, J. McCafferty, R. A. Hodits, J. Wilton, and K. S. Johnson, 1996. Human antibodies with sub-nanomolar affinities isolated from a large non-immunized phage display library. *Nat Biotechnol* **14**:309–314.

Wagner, S. D. and M. S. Neuberger, 1996. Somatic hypermutation of immunoglobulin genes. *Annu Rev Immunol* **14**:441–457.

Walsh, D., A. Lomakin, G. Benedek, M. Condron, and D. Teplow, 1997. Amyloid β-protein fibrillogenesis. *J Biol Chem* **272**:22364–22372.

Walsh, D. and D. Selkoe, 2004. Oligomers on the brain: the emerging role of soluble protein aggregates in neurodegeneration. *Protein Pept Lett* **11**:213–228.

Walsh, D. M., D. M. Hartley, Y. Kusumoto, Y. Fezoui, M. M. Condron, A. Lomakin, G. B. Benedek, D. J. Selkoe, and D. B. Teplow, 1999. Amyloid β-protein fibrillogenesis. structure and biological activity of protofibrillar intermediates. *J Biol Chem* **274**:25945–25952.

Walsh, D. M., I. Klyubin, J. V. Fadeeva, W. K. Cullen, R. Anwyl, M. S. Wolfe, M. J. Rowan, and D. J. Selkoe, 2002. Naturally secreted oligomers of amyloid β protein potently inhibit hippocampal long-term potentiation in vivo. *Nature* **416**:535–539.

Wasmer, C., A. Lange, H. Van Melckebeke, A. B. Siemer, R. Riek, and B. H. Meier, 2008. Amyloid fibrils of the HET-s(218-289) prion form Aβ solenoid with a triangular hydrophobic core. *Science* **319**:1523–1526.

Weiner, H. L., C. A. Lemere, R. Maron, E. T. Spooner, T. J. Grenfell, C. Mori, S. Issazadeh, W. W. Hancock, and D. J. Selkoe, 2000. Nasal administration of Aβ peptide decreases cerebral amyloid burden in a mouse model of Alzheimer's disease. *Ann Neurol* **48**:567–579.

Westermark, P., M. Benson, J. Buxbaum, A. Cohen, B. Frangione, S. Ikeda, C. Masters, G. Merlini, M. Saraiva, and J. Sipe, 2005. Amyloid: toward terminology clarification report from the Nomenclature Committee of the International Society of Amyloidosis. *Amyloid* **12**:1–4.

Westermark, P., M. Benson, J. Buxbaum, A. Cohen, B. Frangione, S. Ikeda, C. Masters, G. Merlini, M. Saraiva, and J. Sipe, 2007. A primer of amyloid nomenclature. *Amyloid* **14**:179–183.

Wilcock, D., A. Rojiani, A. Rosenthal, S. Subbarao, M. Freeman, M. Gordon, and D. Morgan, 2004. Passive immunotherapy against Aβ in aged APP-transgenic mice reverses cognitive deficits and depletes parenchymal amyloid deposits in spite of increased vascular amyloid and microhemorrhage. *J Neuroinflammation* **1**:24.

Williams, A. D., M. Sega, M. Chen, I. Kheterpal, M. Geva, V. Berthelier, D. T. Kaleta, K. D. Cook, and R. Wetzel, 2005. Structural properties of Aβ protofibrils stabilized by a small molecule. *Proc Natl Acad Sci U S A* **102**:7115–7120.

Williams, R., 2011. Biomarkers: warning signs. *Nature* **475**:S5–7.

Williams, T. and L. Serpell, 2011. Membrane and surface interactions of Alzheimer's Aβ peptide—insights into the mechanism of cytotoxicity. *FEBS J* .

Xie, J., S. Reverdatto, A. Frolov, R. Hoffmann, D. S. Burz, and A. Shekhtman, 2008. Structural basis for pattern recognition by the receptor for advanced glycation end products (RAGE). *J Biol Chem* **283**:27255–27269.

Zheng, H. and E. Koo, 2011. Biology and pathophysiology of the amyloid precursor protein. *Mol Neurodegener* **6**:27.

Curriculum Vitae

Personal data

Name	Magdalena Bereza
Address	Wenigenjenaer Ufer 5, D-07749 Jena
Date of birth	August 7th, 1980 in Warsaw, Poland
Phone	+49 17649006876
E-mail	magda.bereza@gmail.com

Education

06/2012	Submission of PhD dissertation at Friedrich Schiller University, Jena, Germany
09/2007 — present	Doctoral candidate at Friedrich Schiller University. Project carried out at Hans Knöll Institute, Bio Pilot Plant Department. Title: 'Assessment of structural diversity of β-amyloid with genetically engineered antibody fragments' Supervisors: Dr. M. Fändrich, Dr. U. Horn, Prof. S. Diekmann
10/1999 — 06/2004	Studies at the Faculty of Biology, Warsaw University. Specialization: Biology of Cell and Organism. Academic degree: Master of Science (M. Sc.)
09/1987 — 06/1999	Schooling in Warsaw

Employment

01/2008 — 12/2011	Scientific coworker at Hans Knöll Institute, Departament of Bio Pilot Plant (Jena, Germany) in cooperation with Max Planck Research Unit for Enzymology of Protein Folding, Halle, Germany
09/2007 — 12/2007	Scientific coworker at Fritz Lipmann Institute, Jena, Germany
07/2007 — 08/2007	Sales Executive, BASF Poland Ltd, Warsaw, Poland
11/2004 — 02/2007	Medical Coordinator at Merck Poland Ltd, Warsaw, Poland

Conference talks

Presentations at the annual workshop 'Amyloid Fibril Structure and Amyloid Formation':

Assessment of the Aβ structural diversity with genetically engineered antibody fragments. March 24th–25th, 2011, Jena, Germany

Discrimination of Aβ aggregation states with antibody domains. May 10th–12th, 2010, Wernigerode, Germany

Selection and characterisation of the anti-Aβ antibody by phage display technique. May 7th–8th, 2009, Weimar, Germany

Selection of B10 ligands by phage display technique. April 14th–15th, 2008, Weimar, Germany

Camelid antibody library: from PCR to fermentation. Colloquium at Hans Knöll Institute June 2nd, 2009, Jena, Germany.

Conference posters

Bereza, M., Haupt, C., Morgado, I., Kumar, S., Hortschansky, P., Fändrich, M., Horn, U. Molecular basis of the β-amyloid recognition with the conformation-specific B10 antibody fragment. International Conference AD/PD, March 9th–14st, 2011, Barcelona, Spain.

Bereza, M., Morgado, I., Haupt, C., Kumar, S., Parthier, C., Stubbs, M. T., Hortschansky, P., Fändrich, M., Horn, U. Structural recognition of amyloid fibrils with an antibody fragment from phage display. 21. Faltertage, October 15th–17th, 2010, Regensburg, Germany.

Publications

Morgado, I., Wieligmann, K., Bereza, M., Rönicke, R., Meinhardt, K., Annamalai, K., Baumann, M., Wacker, J., Hortschansky, P., Malešević, M., Parthier, C., Mawrin, C., Schiene-Fischer, C., Reymann, K. G., Stubbs, M. T., Balbach, J., Görlach, M., Horn, U., Fändrich, M. (2012) Molecular basis of Aβ oligomer recognition with a conformational antibody fragment. Proc Natl Acad Sci U S A *(in press)*.

Haupt, C., Bereza, M., Kumar, S. T., Kieninger, B., Hortschansky, P., Fritz. G., Röcken, C., Horn, U., Fändrich, M. (2011) Pattern recognition with a fibril-specific antibody fragment reveals the surface variability of natural amyloid fibrils. J Mol Biol 408(3):529–540.

Haupt, C., Morgado, I., Kumar, S. T., Parthier, C., Bereza, M., Hortschansky, P., Stubbs, M. T., Horn, U., Fändrich, M. (2011) Amyloid fibril recognition with the conformational B10 antibody fragment depends on electrostatic interactions. J Mol Biol 405(2):341-348.

Ehrenwörtliche Erklärung

Hiermit erkläre ich, Magdalena Bereza, geboren am 07. August 1980 in Warschau (Polen) an Eides statt,

- dass mir die geltende Promotionsordnung der Biologisch-Pharmazeutischen Fakultät bekannt ist;
- dass ich die vorliegende Dissertation mit dem Titel 'Assessment of structural diversity of β-amyloid with genetically engineered antibody fragments' selbst angefertigt habe, keine Textabschnitte eines Dritten ohne Kennzeichnung übernommen habe und alle von mir benutzten Hilfsmittel, persönlichen Mitteilungen und Quellen in meiner Arbeit angegeben habe;
- dass die Hilfe eines Promotionsberaters nicht in Anspruch genommen wurde und dass Dritte weder unmittelbar noch mittelbar geldwerte Leistungen von mir für Arbeiten erhalten haben, die im Zusammenhang mit dem Inhalt der vorgelegten Dissertation stehen;
- dass ich die Dissertation noch nicht als Prüfungsarbeit für eine staatliche oder andere wissenschaftliche Prüfung eingereicht habe;
- dass ich nicht die gleiche, oder eine in wesentlichen Teilen ähnliche oder eine andere Abhandlung bei einer anderen Hochschule als Dissertation eingereicht habe;
- dass ich weder während meiner Zeit an der Friedrich-Schiller-Universität Jena, noch davor ein anderes Promotionsverfahren beantragt oder durchlaufen habe.

Jena, Juni 2012 .....

Magdalena Bereza

Abbreviations

3D	Three-dimensional
Aβ	amyloid β peptide
AβPP	β-amyloid precursor protein
AD	Alzheimer's disease
ADDL	Aβ-derived diffusible ligand
AFM	Atomic force microscopy
ANS	1-anilino-8-naphthalene sulfonate
AP	Alkaline phosphatase
ATR-FTIR	Attenuated total reflectance Fourier transform infrared spectroscopy
BSA	Bovine serum albumin
CD	Circular dichroism
CDR	Complementarity determining region
CNS	Central nervous system
CR	Congo red
cryo-EM	Cryo-electron microscopy
DMSO	Dimethyl sulfoxide
ELISA	Enzyme-linked immunosorbent assay
EM	Electron microscopy
HCAb	Camelid heavy chain antibodies
HFIP	1,1,1,3,3,3-hexafluoro-2-propanol
HMW	High molecular weight
HRP	Horseradish peroxidase
IEC	Ion exchange chromatography
Ig	Immunoglobulin
IMAC	Immobilised metal ion affinity chromatography
IPTG	Isopropyl β-D-1-thiogalactopyranoside
IUPC	Intrinsically unfolded polypeptide chain
aK_D	Apparent dissociation constant

LMW	Low molecular weight
LTP	Long-term potentiation
NMR	Nuclear magnetic resonance
OD	Optical density
PBS	Phosphate-buffered saline
PCR	Polymerase chain reaction
PS1	Presenilin 1
PS2	Presenilin 2
PVDF	Polyvinylidene fluoride membrane
RAGE	Receptors for advanced glycation end products
RPC	Reversed phase chromatography
SDS-PAGE	Sodium dodecyl sulphate polyacrylamide gel electrophoresis
SD	Standard deviation
SEC	Size exclusion chromatography
SPR	Surface plasmon resonance
ssNMR	Solid state nuclear magnetic resonance
TBS	Tris-buffered saline
TEM	Transmission electron microscopy
TFA	Trifluoroacetic acid
TFE	Trifluoroethanol
ThT	Thioflavin T
VHH	Camelid variable heavy chain domain
WB	Western blot